Eur. Phys. J. C (2010) 67: 637–686
DOI 10.1140/epjc/s10052-010-1314-6

THE EUROPEAN PHYSICAL JOURNAL C

Review

Towards jetography

Gavin P. Salam[a]

LPTHE, UPMC Univ. Paris 6, CNRS UMR 7589, 75252 Paris 05, France

Received: 28 September 2009 / Revised: 28 February 2010 / Published online: 8 May 2010
© Springer-Verlag / Società Italiana di Fisica 2010

Abstract As the LHC prepares to start taking data, this review is intended to provide a QCD theorist's understanding and views on jet finding at hadron colliders, including recent developments. My hope is that it will serve both as a primer for the newcomer to jets and as a quick reference for those with some experience of the subject. It is devoted to the questions of how one defines jets, how jets relate to partons, and to the emerging subject of how best to use jets at the LHC.

Contents

[a] e-mail: salam@lpthe.jussieu.fr

1 Introduction

It is common to discuss high-energy phenomena involving quantum chromodynamics (QCD) in terms of quarks and gluons. Yet quarks and gluons are never visible in their own right. Almost immediately after being produced, a quark or gluon fragments and hadronises, leading to a collimated spray of energetic hadrons—a jet. Jets are obvious structures when one looks at an event display, and by measuring their energy and direction one can get close to the idea of the original "parton". The concept of a parton is, however, ambiguous: the fact that partons have divergent branching probabilities in perturbative QCD means that one must introduce a prescription for defining what exactly one means by the term. Similarly, jets also need to be defined—this is generally done through a jet definition, a set of rules for how to group particles into jets and how to assign a momentum to the resulting jet. A good jet definition can be applied to experimental measurements, to the output of parton-showering Monte Carlos and to partonic calculations, and the resulting jets provide a common representation of all these different kinds of events.

Jets are used for a wide range of physics analyses. One way of classifying their uses is according to the different possible origins for the partons that give rise to the jets. At hadron colliders (and in photoproduction), one of the best studied jet observables is the inclusive jet spectrum, related to the high-momentum-transfer $2 \to 2$ scattering of partons inside the colliding (anti)protons. In this kind of process the energy of the jet (in the partonic centre-of-mass frame) is closely related to that of the parton in the proton that underwent a hard scattering and the inclusive jet spectrum therefore contains information on the distributions of partons inside the proton (e.g. [1–4]), and also on the strength of their interaction.

Another origin for the partons that lead to jets is that they come from the hadronic decay of a heavy particle, for example a top quark, a Higgs boson, or some other yet-to-be discovered resonance. If, at tree-level, the heavy particle decays to many partons (e.g. through a cascade of decays) then

a high multiplicity of corresponding jets may be a sign of the presence of that particle (as used for example in SUSY searches, such as [5]); and the sum of the momenta of the jets (or of the jets, leptons and missing transverse energy information) should have an invariant mass that is close to that of the heavy particle, a feature used for example in measurements of the top-quark mass [6, 7].

Jets may also originate radiatively, for example from the emission of a gluon off some other parton in the event. The rate of production of such jets provides information on the value of strong coupling (for example [8–12]) and is related also to the colour structure of events. One use of this is, for example, to help discriminate between Higgs-boson production through electroweak vector-boson fusion (which radiates less) and through gluon-fusion (which radiates more). Radiative emission of partons is also one of the main backgrounds to multi-jet signals of new physics; consistently predicting such backgrounds involves matching tree-level matrix-element calculations with Monte Carlo parton showers, for which jet definitions provide a powerful way of avoiding double counting, by prescribing which emissions should be the responsibility of the matrix element (those that lead to extra jets) and which ones should come from the parton showers (those that do not) [13, 14].

Though most uses of jets essentially identify a jet as coming from a single parton, one should never forget how ambiguous this association really is, and not just because partons are an ill-defined concept. For example, when a highly boosted W or Z boson decays to two partons, those partons may be so collimated by the boost that they will lead to a single jet, albeit it one with substructure. And QCD radiative corrections also inevitably give substructure to jets. Much as the number of jets and their kinematics can be used to learn about the properties of the event, so can the structure within the jets.

Given the variety of these and other related possible uses of jets, it should not be surprising that there is no single optimal way of defining jets and, over the 30 years that have passed since the first detailed proposal for measuring jets [15], many jet definitions have been developed and used. The ideas behind jet definitions are rather varied. One of the aims of this review (Sect. 2) is to provide an overview of the different kinds of jet definition that exist. Given that the main use of jets in the coming years will be at the Large Hadron Collider at CERN (LHC), the emphasis here and throughout the review will be on hadron-collider jets, though a number of the ideas in jet finding actually have their origins in studies of e^+e^- and ep collisions.

One of the characteristics of the LHC is that its particle multiplicity is expected to be much higher than in preceding colliders. Some part of the increase is due to the LHC's higher energy, but most of it will be a consequence of the multiple minimum-bias interactions (pileup) that will occur in each bunch crossing. High multiplicities pose practical challenges for the computer codes that carry out jet finding, because the computing time that is required usually scales as some power of the multiplicity, N. Until a few years ago, this was often a limiting factor in experimental choices of jet-finding methodology. Recent years' work (described in Sect. 3) has shown how these practical issues can be resolved by exploiting their relation to problems in computational geometry. This makes it easier for LHC's jet-finding choices to be based on physics considerations rather than practical ones.

Given a set of practical jet algorithms, the next question is to establish their similarities and differences. Any jet algorithm will form a jet from a single hard isolated particle. However, different jet definitions may do different things when two hard particles are close by, when a parton radiates a soft gluon, or when the jet is immersed in noise from pileup. Section 4 examines standard and recent results on these issues, for the most important of the current jet algorithms.

Once one has understood how jets behave, the final question that needs to be addressed is that of determining the jet definitions and methods that are optimal for specific physics analysis tasks. One might call this subject "jetography", in analogy with photography, where an understanding of optics, of one's light sensor, and of properties of the subject help guide the choice of focus, aperture and length of exposure. Ultimately, it is neither the photons in photography, nor the jets in jetography that are of interest; rather it is the objects (new particles, PDFs, etc.) that they help you visualise or discover. In the context of the LHC, it is probably fair to say that jetography is still in its infancy, hence the title of the review. Nevertheless some first results have emerged in the past couple of years, notably (as discussed in Sect. 5) with respect to simple dijet mass reconstructions, hadronic decays of boosted heavy particles, and the question of limiting the effect of pileup.

One thing that this review does not do is examine the wide range of uses of jets in LHC and other experiments' analyses, aside from the brief discussion given above. This is a vast subject, and to obtain a full overview probably requires that one consult the main ATLAS and CMS physics analysis programme documents [16, 17] and the "LHC primer" [18], as well as recent work by the Tevatron and HERA, summarised for example in [19, 20]. Other reviews of jets in recent years include [21, 22]. Finally a topic that is barely touched upon here is the nascent field of jet finding in heavy-ion collisions, for which the reader is referred to [23, 24].

2 Jet algorithms

Jet algorithms provide a set of rules for grouping particles into jets. They usually involve one or more parameters that indicate how close two particles must be for them to belong to the same jet. Additionally they are always associated with a recombination scheme, which indicates what momentum to assign to the combination of two particles (the simplest is the 4-vector sum). Taken together, a jet algorithm with its parameters and a recombination scheme form a "jet definition".

An accord as to some general properties of jet definitions, the "Snowmass accord", was set out in 1990 [25] by a group of influential theorists and experimenters, and reads as follows:

Several important properties that should be met by a jet definition are [3]:

1. Simple to implement in an experimental analysis;
2. Simple to implement in the theoretical calculation;
3. Defined at any order of perturbation theory;
4. Yields finite cross sections at any order of perturbation theory;
5. Yields a cross section that is relatively insensitive to hadronisation;

where [3] is given below as [26]. It is revelatory that [25] is entitled "*Toward* a standardisation of jet definitions" (my italics). If one reads the rest of the article, one realises that it was not evident at the time what the standard jet definition should actually be, nor was there a clear path towards satisfying the Snowmass accords, at least for hadron colliders.

When the next major community-wide discussion on jets took place, in 2000, in preparation for Run II of the Tevatron [21], new jet algorithms had been invented [27–32], old algorithms had been patched [33–36] and it is probably fair to say that the community had *almost* satisfied the Snowmass requirements. Nevertheless, the recommendations of the Run II workshop were followed in only part of subsequent Tevatron work and, until recently, had also been ignored in much of the preparatory work towards LHC.

This means that there are currently very many hadron-collider jet algorithms in use—some dating from the 80s, others from the 90s. The situation is further confused by the fact that different algorithms share the same name (notably "iterative cone"), and that there is no single source of information on all the different algorithms. Additionally, it has not always been clear how any given algorithm fared on the Snowmass requirements.

The purpose of this section is to give an overview of all the main different algorithms, including some of the most recently developed ones, so as to provide the background for anyone reading current jet work from both the theory and experimental communities.

The section's organisation reflects the split of jet algorithms into two broad categories. Firstly those based in one form or another on "cones". They can be thought of as "top-down" algorithms, relying on the idea that QCD branching and hadronisation leaves the bulk features of an event's energy flow unchanged (specifically, energy flow into a cone). Secondly, sequential recombination algorithms, "bottom-up" algorithms that repeatedly recombine the closest pair of particles according to some distance measure, usually related to the divergent structure of QCD matrix elements.

The nomenclature used to distinguish the types of jet algorithm (notably cones) is currently not always uniform across the field. That used here follows the lines set out in [37, 38].

Before continuing, a note is due concerning the completeness of this section. Its aim is to communicate the essential ideas about many of the main jet algorithms (a more concise overview is given in [38]). It will not describe every detail of every single jet algorithm. Where possible, references will be supplied to more complete descriptions. In some cases, no such reference exists, and the interested reader is then advised to consult computer code for the given jet algorithm.

2.1 Cone algorithms

The first-ever jet algorithm was developed by Sterman and Weinberg in the 1970s [15]. It was intended for e^+e^- collisions and classified an event as having two jets if at least a fraction $1-\epsilon$ of the event's energy was contained in two cones of opening half-angle δ (and hence is known as a "cone" algorithm). This definition made it possible to have a fully consistent perturbative QCD calculation of the probability of having two jets in an event.

The two parameters δ and ϵ reflect the arbitrariness in deciding whether an event has two or more jets. Typically one would avoid taking extreme values (ϵ too close to 0 or 1, δ too close to zero), but apart from that the optimal choice of δ and ϵ would depend on the specific physics analysis being carried out. The presence of separate angular and energy parameters to dictate the characteristics of the jet finding is typical of cone algorithms, as we shall see below.

Cone algorithms have evolved substantially since [15] and are today mostly used at hadron colliders. The changes reflect the fact that in hadron collisions it does not make sense to discuss the total energy (since most of it is not involved in the hard reaction, and goes down the beam pipe), that it is not always obvious, physically or computationally, *where* to place the cones, and that issues arise when trying to define events with more than two jets (with the associated problem of "overlapping" cones).

2.1.1 Iteration

Let us first examine the question of where to place the cones. Most of today's widely used cone algorithms are "iterative cones" (IC). In such algorithms, a seed particle i sets some initial direction, and one sums the momenta of all particles j within a circle ("cone") of radius R around i in azimuthal angle ϕ and rapidity y (or pseudorapidity η),[1] i.e. taking all j such that

$$\Delta R_{ij}^2 = (y_i - y_j)^2 + (\phi_i - \phi_j)^2 < R^2, \tag{1}$$

where y_i and ϕ_i are respectively the rapidity and azimuth of particle i. The direction of the resulting sum is then used as a new seed direction, and one iterates the procedure until the direction of the resulting cone is stable. The dimensionless parameter R here, known as the jet radius, replaces the angular scale δ that was present in the original Sterman–Weinberg proposal. The Sterman–Weinberg ϵ parameter is less-directly mirrored in hadron-collider cone algorithms. Rather, most physics analyses will use a cone algorithm to obtain jets without any specific energy cut, but then will consider only those jets that are above a certain transverse-momentum threshold.

To be fully specified, seeded iterative jet algorithms must deal with two issues:

- What should one take as the seeds?
- What should one do when the cones obtained by iterating two distinct seeds "overlap" (i.e. share particles)?

Different approaches to these issues lead to two broad classes of cone algorithm.

2.1.2 Overlapping cones: the progressive removal approach

One approach is to take as one's first seed the particle (or calorimeter tower) with the largest transverse momentum. Once one has found the corresponding stable cone, one calls it a jet and removes from the event all particles contained in that jet. One then takes as a new seed the hardest particle/tower among those that remain, and uses that to find the next jet, repeating the procedure until no particles are left (above some optional threshold). This avoids any issue of overlapping cones. A possible name for such algorithms is iterative cone with progressive removal (IC-PR) of particles.

IC-PR algorithms' use of the hardest particle in an event gives them the drawback that they are collinear unsafe: the splitting of the hardest particle (say p_1) into a nearly collinear pair (p_{1a}, p_{1b}) can have the consequence that another, less hard particle, p_2, pointing in a different direction and with $p_{t,1a}$, $p_{t,1b} < p_{t,2} < p_{t,1}$, suddenly becomes the hardest particle in the event, thus leading to a different final set of jets. We will return to this in Sect. 2.1.4.

Fixed cones A widespread, simpler variant of IC-PR cone algorithms is one that does not iterate the cone direction, but rather identifies a fixed cone (FC)[2] around the seed direction and calls that a jet. It starts from the hardest seed and progressively removes particles as the jets are identified (thus FC-PR). It suffers from the same collinear unsafety issue as the IC-PR algorithms.

IC-PR and FC-PR algorithms are often referred to as UA1-type cone algorithms, even though the algorithm described in the original UA1 reference [39] is somewhat different.[3] This may be due to different versions of the UA1 algorithm having been presented at conferences prior to its final publication [39].[4]

2.1.3 Overlapping cones: the split–merge approach

Another approach to the issue of the same particle appearing in many cones applies if one chooses, as a first stage, to find all the stable cones obtained by iterating from all particles or calorimeter towers (or those for example above some seed threshold ∼1–2 GeV).[5] One may then run a split–merge (SM) procedure, which merges a pair of cones if more than a fraction f of the softer cone's transverse momentum is in particles shared with the harder cone; otherwise the shared particles are assigned to the cone to which they are closer. A possible generic name for such algorithms is IC-SM. The exact behaviour of SM procedures depends on the precise

[1] These are standard hadron-collider variables. Given a beam along the z-direction, a particle with longitudinal momentum p_z, energy E and angle θ with respect to the beam (longitudinal) direction has rapidity $y \equiv \frac{1}{2}\ln\frac{E+p_z}{E-p_z}$ and pseudorapidity $\eta \equiv -\ln\tan\theta/2$. Massless particles have $y = \eta$. Differences in rapidity are invariant under longitudinal boosts, whereas differences in pseudorapidity are invariant only for massless particles. Where an analysis in e^+e^- will use particles' energies and the angles between the particles, an analysis in a pp collider will often use p_t (or E_t) and ΔR_{ij}^2 (defined either with rapidities or pseudorapidities).

[2] "Fixed cone" can be an ambiguous term. In particular, in some contexts it is used to refer to cones whose shape is fixed rather than cones whose position is fixed.

[3] The UA1 algorithm [39] proceeds as follows: the particle (or cell) with highest E_t starts a jet; working through the list of particles in decreasing E_t, each one is added to the jet to which it is closest, as long as it is within $\Delta R < R$ ($\Delta R^2 = \Delta\eta^2 + \Delta\phi^2$, R taken to be 1); otherwise, the particle initiates a new jet. Finally, once all remaining particles have $E_t < 2.5$ GeV, each particle is simply added to the jet nearest in η, ϕ if its transverse momentum relative to the jet axis is less than 1 GeV and it is no further than 45° in direction from the jet axis.

[4] I am grateful to Torbjörn Sjöstrand for comments on this point.

[5] In one variant, CDF's JetClu [40], "ratcheting" is included, which means that during iteration of cone, all particles included in previous iterations are retained even if they are no longer within the geometrical cone, see also Sect. 2.1.6.

ordering of split and merge steps and a fairly widespread procedure is described in detail in [21]. It essentially works as follows, acting on an initial list of "protojets", which is just the full list of stable cones:

1. Take the protojet with the largest p_t (the 'hardest' protojet), label it a.
2. Find the next hardest protojet that shares particles with the a (i.e. overlaps), label it b. If no such protojet exists, then remove a from the list of protojets and add it to the list of final jets.
3. Determine the total p_t of the particles shared between the two protojets, $p_{t,\text{shared}}$.
   - If $p_{t,\text{shared}}/p_{t,b} > f$, where f is a free parameter known as the overlap threshold, replace protojets a and b with a single merged protojet.
   - Otherwise "split" the protojets, for example assigning the shared particles just to the protojet whose axis is closer (in angle).
4. Then repeat from step 1 as long as there are protojets left.

Generally the overlap threshold f is chosen to be 0.5 or 0.75 (the latter is probably to be preferred [41]). An alternative to SM is to have a "split–drop" (SD) procedure, where the non-shared particles that belong to the softer of two overlapping cones are simply dropped, i.e. are left out of jets altogether. The main example of an algorithm with a SD procedure is PxCone (described for example in [42]).

The outcome of split–merge and split–drop procedures depends on the initial set of stable cones. One of the main issues with IC-SM and IC-SD algorithms is that the addition of a new soft seed particle can lead to new stable cones being found, altering the final set of jets. This is infrared unsafety and we will discuss it in detail in the next section.

2.1.4 Infrared and collinear safety, midpoint cones

Infrared and collinear (IRC) safety is the property that if one modifies an event by a collinear splitting or the addition of a soft emission, the set of hard jets that are found in the event should remain unchanged. IRC safety is an important property for a range of reasons:

- A hard parton undergoes many collinear splittings as part of the fragmentation process; and the non-perturbative dynamics also lead to collinear splittings, for example in the decay of energetic hadrons. Additionally there is always some emission of soft particles in QCD events, both through perturbative and non-perturbative effects. Collinear splittings and soft emissions effectively occur randomly and even their average properties are hard to predict because of the way they involve non-perturbative effects. The motivation for constructing jets is precisely that one wants to establish a way of viewing events that is insensitive to all these effects (this is also connected with point 5 of the Snowmass conditions).
- In fixed-order perturbative QCD calculations, one of the main tools involved in making accurate standard-model predictions at high-energy colliders, soft emissions and collinear splittings are associated with divergent tree-level matrix elements. There are also corresponding divergent loop matrix elements that enter with the opposite sign. Normally the two sources of divergence should cancel, but for IRC unsafe jet algorithms the tree-level splittings may lead to one set of jets, while the loop diagrams may lead to another, breaking the cancellation and leading to infinite cross sections in perturbation theory (point 4 of the Snowmass conditions). Below, we shall illustrate this point in more detail.
- Experimental detectors provide some regularisation of any collinear and infrared unsafety (because of their finite resolution and non-zero momentum thresholds), but the extent to which this happens depends on the particular combination of tracking, electromagnetic calorimetry and hadronic calorimetry that is used by the experiment. This can make it quite difficult to connect experimental results for IRC unsafe algorithms to the expectations at hadron level.

Cone-type jet algorithms have, historically, been plagued by issues related to IRC safety, and a significant amount of the work on them has been directed towards understanding and eliminating these problems. Let us therefore examine the question for the two classes of algorithm we have seen so far.

The IC-PR case IC-PR algorithms suffer from collinear unsafety, as illustrated in Fig. 1. With a collinear safe jet algorithm, if configuration (a) (with an optional virtual loop also drawn in) leads to one jet, then the same configuration with one particle split collinearly, (b), also leads to a single jet. In perturbative QCD, after integrating over loop variables in (a) and the splitting angle in (b), both diagrams have infinite weights, but with opposite signs, so that the total weight for the 1-jet configuration is finite.

Diagrams (c) and (d) are similar, but for an IC-PR algorithm. In configuration (c), the central particle is hardest and provides the first seed. The stable cone obtained by iterating from this seed contains all the particles, and one obtains a single jet. In configuration (d), the fact that the central particle has split collinearly means that it is now the leftmost particle that is hardest and so provides the first seed. Iteration from that seed leads to a jet (jet 1) that does not contain the rightmost particle. That rightmost particle therefore remains, provides a new seed, and goes on to form a jet in its own right (for full details, see the appendix of [37]). As we have discussed above, it is problematic for the result of the jet finding to depend on a collinear splitting. The formal

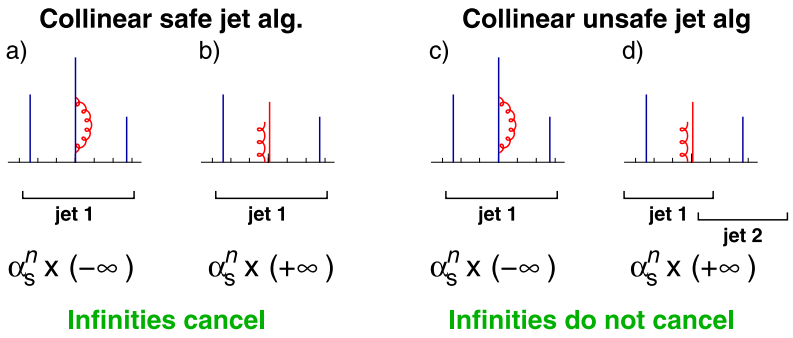

Fig. 1 Illustration of collinear safety (*left*) and collinear unsafety in an IC-PR type algorithm (*right*) together with its implication for perturbative calculations (taken from the appendix of [37]). Partons are *vertical lines*, their height is proportional to their transverse momentum, and the *horizontal axis* indicates rapidity

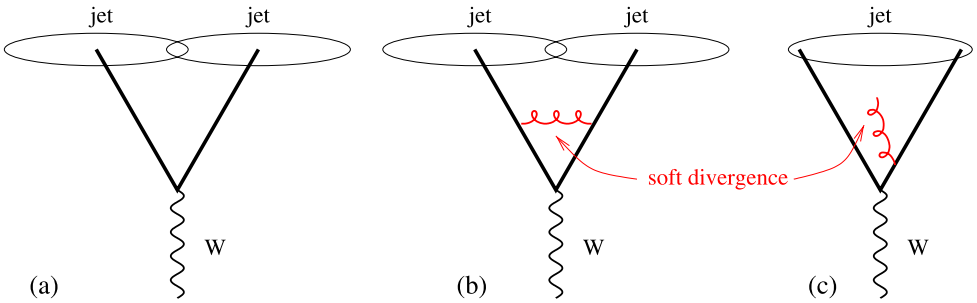

Fig. 2 Configurations illustrating IR unsafety of IC-SM algorithms in events with a W and two hard partons. The addition of a soft gluon converts the event from having two jets to just one jet. In contrast to Fig. 1, here the explicit angular structure is shown (rather than p_t as a function of rapidity)

perturbative QCD consequence of this here is that the infinities in diagrams (c) and (d) contribute separately to the 1-jet and 2-jet cross sections. Thus both the 1-jet and 2-jet cross sections are divergent.

The IC-SM case IC-SM (and IC-SD) type algorithms have the drawback that the addition of an extra soft particle, acting as a new seed, can cause the iterative process to find a new stable cone. Once passed through the split–merge step this can lead to the modification of the final jets, thus making the algorithm *infrared* unsafe. This is illustrated in Fig. 2: in an event (a) with just two hard partons (and a W, which balances momentum), both partons act as seeds, there are two stable cones and two jets. The same occurs in the (negative) infinite loop diagram (b). However, in diagram (c) where an extra soft gluon has been emitted, the gluon provides a new seed and causes a new stable cone to be found containing both hard partons (as long as they have similar momenta and are separated by less than $2R$). This stable cone overlaps with the two original ones and the result of the split–merge procedure is that only one jet is found. So the number of jets depends on the presence or absence of a soft gluon and after integration over the virtual/real soft-gluon momentum the 2-jet and 1-jet cross sections each get non-cancelling infinite contributions. This is a serious problem, just like collinear unsafety. A good discussion of it was given in [43].

The midpoint "fix" for IC-SM algorithms A partial solution [33–36] (described also in [43]), which was recommended in [21], is to additionally search for new stable cones by iterating from midpoints between each pair of stable cones found in the initial seeded iterations (IC_{mp}-SM). This resolves the problem shown in Fig. 2 and the resulting "midpoint" algorithm has often been presented as a cone algorithm that was free of IR safety issues. However, for configurations with three hard particles in a common neighbourhood (rather than two for the IC-SM algorithms) the IR safety reappears, as illustrated in Fig. 3.

The "midpoint algorithm" has been widely used in Run II of the Tevatron within CDF (midpoint cone algorithm) and DØ (Run II Cone algorithm, or improved legacy cone algorithm). The two experiments have separate implementations, with slightly different treatment of seeds (CDF imposes a threshold, DØ does not), cone iteration (DØ eliminates cones below a p_t threshold, CDF does not) and the split–merge stage. In practice both algorithms incorporate a number of further technical subtleties (for example an upper limit on the number of iterations, or split–merge steps) and the best reference is probably the actual code (available both within FastJet [45] v2.4 and SpartyJet [46]).

Impact of IRC unsafety The impact of infrared and collinear (IRC) unsafety depends on the observable in which one is interested. For example for the IC-SM type algorithms, the configuration on the right of Fig. 2 is a NNLO contribution to the W + jet cross section, i.e. a contribution $\alpha_s^3 \alpha_{\text{EW}} \times \infty$. Physically, the infinity gets regularised by non-perturbative effects and so is replaced by a factor of order $\ln p_t/\Lambda$, giving an overall contribution $\alpha_s^3 \alpha_{\text{EW}} \ln p_t/\Lambda$. Since $\alpha_s \sim 1/\ln(p_t/\Lambda)$, this can be rewritten as $\sim \alpha_s^2 \alpha_{\text{EW}}$, i.e. the NNLO diagrams will give a contribution that is as large as the NLO diagrams. Thus the perturbative series

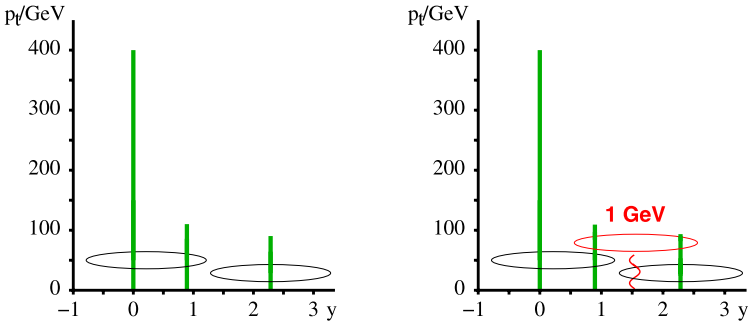

Fig. 3 Configuration that is the source of IR unsafety in the midpoint (IC_{mp}-SM) algorithm, with the diagram on the right illustrating the extra stable cone that can appear with the addition of a new soft seed. Taken from [44]

Table 1 Summary of the last meaningful order for various measurements with jet algorithms having different levels of IR and collinear unsafety. Adapted from [44]

Observable	IR_{2+1}	IR_{3+1}, $Coll_{3+1}$
Inclusive jet cross section	LO	NLO
$W/Z/H$ + 1-jet cross section	LO	NLO
3-jet cross section	none	LO
$W/Z/H$ + 2-jet cross section	none	LO
jet masses in 3-jet and $W/Z/H$ + 2-jet events	none	none

looks like:

$$\underbrace{\alpha_s\alpha_{\mathrm{EW}}}_{\mathrm{LO}}+\underbrace{\alpha_s^2\alpha_{\mathrm{EW}}}_{\mathrm{NLO}}+\underbrace{\alpha_s^3\alpha_{\mathrm{EW}}\ln\frac{p_t}{\Lambda}}_{\mathrm{NNLO}}+\underbrace{\alpha_s^4\alpha_{\mathrm{EW}}\ln^2\frac{p_t}{\Lambda}}_{\mathrm{NNNLO}}+\cdots$$
$$\sim\underbrace{\alpha_s\alpha_{\mathrm{EW}}}_{\mathrm{LO}}+\underbrace{\alpha_s^2\alpha_{\mathrm{EW}}}_{\mathrm{NLO}}+\underbrace{\alpha_s^2\alpha_{\mathrm{EW}}}_{\mathrm{NNLO}}+\underbrace{\alpha_s^2\alpha_{\mathrm{EW}}}_{\mathrm{NNNLO}}+\cdots, \quad (2)$$

and it is meaningful to calculate the LO term, but no advantage is to be had by calculating terms beyond, because the neglected pieces will always be as large as the NLO term. If one instead examines the W + 2-jet cross section then the LO term is $\alpha_s^2\alpha_{\mathrm{EW}}$. The NLO term, $\alpha_s^3\alpha_{\mathrm{EW}}\ln p_t/\Lambda \sim \alpha_s^2\alpha_{\mathrm{EW}}$ is of the same size, so even the LO prediction makes no sense.

The unsafety of the IC-SM algorithm can be labelled IR_{2+1}: its IR unsafety is manifest for configurations with two hard particles in a common neighbourhood plus one soft one. The midpoint algorithm is IR_{3+1}, while the IC-PR and FC-PR algorithms are $Coll_{3+1}$ (the collinear unsafety is manifest when there are 3 hard particles in a common neighbourhood, of which one splits collinearly).

For an algorithm labelled as IR_{n+1} or $Coll_{n+1}$, the last meaningful order for the W + jet or the 2-jet cross section is $N^{n-2}LO$. The last meaningful order for the W + 2-jet or the 3-jet cross section is $N^{n-3}LO$. The situation is summarised for various process in Table 1.

One way of visualising infrared and collinear unsafety (especially for IR_{2+1} algorithms) is that they lead to an ambiguity in the effective jet radius R—a soft emission or collinear splitting affects how far the jet algorithm will reach for particles. For the IR_{2+1} algorithms that ambiguity is of $\mathcal{O}(R)$ in the reach (i.e. the jet radius is devoid of meaning). For the IR_{3+1} and $Coll_{3+1}$ algorithms this analogy is less useful.

What to do with IRC unsafe measurements Many IRC-unsafe jet measurements exist in the experimental literature.[6] Some of these cases are like [47], where the measurement for the $W + n$-jet cross section is carried out with JetClu, an IR_{2+1} unsafe algorithm for which no order of perturbation theory is meaningful when $n > 1$.

The question then arises of how one can compare NLO theory predictions like [48–53] with the experimental results. One approach, specific to the IC-SM case, is to carry out the NLO prediction with two somewhat different jet algorithms (for example SISCone and anti-k_t, both discussed below), and use the difference between the NLO calculations with the two algorithms as a measure of the uncertainty in the prediction due to IR safety issues. The logic behind this is that SISCone behaves as would an IC-SM algorithm when there are soft particles everywhere (combining hard partons into a common jet when they are as far as $2R$ apart in some cases), while anti-k_t behaves somewhat similarly to an IC-SM algorithm when there are no soft particles present (hard partons separated by more than R usually do not end up in the same jet). These differences are discussed in more detail in Sect. 4.1.

[6] Strictly speaking, many algorithms incorporate a seed threshold, e.g. $p_t > 1$ GeV. This means that they are not truly infrared unsafe, in that they do not lead to infrared infinities in perturbative calculations (though they are then collinear unsafe if applied to particles rather than to calorimeter towers). However a 1 GeV seed threshold fails to remove the large logarithms in (2) or to eliminate the non-perturbative uncertainties associated with IR unsafety. So the seed threshold does not make these algorithms any better than a formally IR unsafe one.

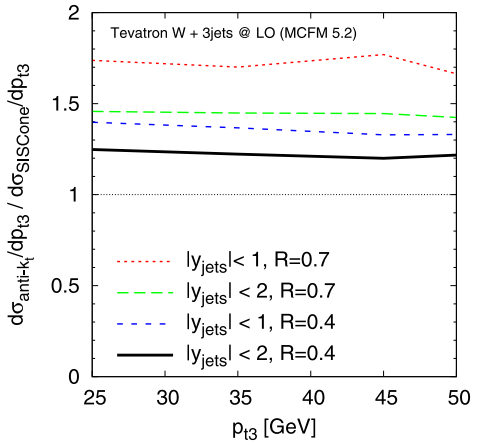

Fig. 4 The ratio of the anti-k_t and SISCone results for the $W + 3$ jet cross section, shown as a function of the transverse momentum of the third hardest jet, for two different R values and rapidity acceptances for the jets, as calculated with MCFM [48]. This ratio provides a measure of the ambiguity in perturbative predictions for an IR unsafe IC-SM jet algorithm such as JetClu

A comparison of SISCone and anti-k_t was performed for example in [53]. It examined the $W + 3$ jets cross section at the Tevatron (measured with JetClu, $R = 0.4$ for jets with $|y| < 2$ [47]) and found that the SISCone prediction was about 20% smaller than the anti-k_t prediction at LO (the difference is reduced at NLO), because in the SISCone case there is a higher likelihood that two of the three LO partons will be combined into a single jet, giving $W + 2$ jets rather than $W + 3$ jets. This may not seem like an enormous effect compared to typical experimental systematic uncertainties, however one should remember that the size of the difference depends also on the cuts and the choice of R. For example, with a larger R value (e.g. $R = 0.7$) or a smaller rapidity range, the differences between the algorithms increase noticeably, as illustrated in Fig. 4.

In the long-run, an alternative approach might be to use tools like MC@NLO [54] and POWHEG [55], which may eventually include a range of jet processes and thus provide both the NLO terms and an acceptable estimate of the large higher-order logarithms and the non-perturbative effects (with IRC jet safe algorithms another advantage of tools like MC@NLO and POWHEG is that they provide a way of consistently including both NLO corrections and non-perturbative hadronisation effects within a single calculation).

2.1.5 *Exact seedless cones*

One full solution to the IRC safety issue avoids the use of seeds and iterations, and instead finds *all* stable cones through some exact procedure. This type of algorithm is often called a seedless cone (SC, thus SC-SM with a split–merge procedure).

In a seedless cone algorithm, the addition of a soft particle may lead to the presence of new stable cones, however none of those new cones will involve hard particles (a soft particle does not affect the stability of a cone involving much larger momenta), and therefore the set of hard stable cones is infrared safe. As long as the presence of new soft stable cones (or of new soft particles inside hard stable cones) does not change the outcome of the split–merge procedure (a non-trivial requirement), then a seedless cone will lead to an infrared safe collection of hard jets.

A computational strategy for identifying all cones was outlined in [21]: one takes all subsets of particles and establishes for each one whether it corresponds to a stable cone—i.e. one calculates its total momentum, draws a circle around the resulting axis, and if the points contained in the circle are exactly as those in the initial subset, then one has found a stable cone. This is guaranteed to find all stable cones.

The above seedless procedure was intended for fixed-order calculations, with a very limited number of particles. It becomes impractical for larger numbers of particles because there are $\mathcal{O}(2^N)$ possible subsets (think of an N-bit binary number where each bit corresponds to a particle, and the subset consists of all particles whose bit is turned on). Testing the stable-cone property takes $\mathcal{O}(N)$ time for each subset and so the total time is $\mathcal{O}(N2^N)$. This exponential-time behaviour made seedless cones impractical for use on events with realistic numbers of particles (the $N2^N$ approach would take about 10^{17} years to cluster 100 particles). However in 2007 a polynomial-time geometrically-based solution was found to the problem of identifying all stable cones [44]. The corresponding algorithm is known as SISCone and it is described in Sect. 3.2. An explicit test of the IR safety of SISCone is shown in Fig. 5.

Seedless cone algorithms are also programmed into NLO codes like NLOJET++ [49, 50] and MCFM [48]. Users should however be aware that there is some degree of confusion in nomenclature—for example the cone algorithm in MCFM v. 5.2 is referred to as the midpoint algorithm, but is actually a seedless implementation; in NLOJET++ v. 3 the algorithm is referred to as seedless, but has a midpoint option. Users of NLO codes are therefore advised to make sure they know *exactly* what is implemented in the NLO code's native jet finder (i.e. they should carefully inspect the portion of code devoted to the jet finder). Alternatively they may use appropriately documented 3rd party libraries for their jet finding.

2.1.6 *Dark towers*

The xC-SM class of algorithms collectively suffers from a problem known as dark towers [56]: regions of hard energy flow that are not clustered into any jet. Dark towers arise because there exist configurations in which some particles

will never end up in a stable cone. The stages of an iteration in which this is the case are shown in Fig. 6, for which the rightmost particle cannot be in a stable cone: even when one uses it as a starting point for iteration, it is not contained in the final stable cone (nor is it contained in any stable cone in a seedless algorithm).

One solution to this problem in iterative algorithms is "ratcheting": a particle that was included at any stage of the iteration is manually included in all subsequent stages of the iteration even if it is not within the cone boundary. This is used in CDF's JetClu algorithm (though it is not actually described in the reference usually quoted by CDF for JetClu [40]).

Another fix to dark towers was proposed in [56], and referred to as the "searchcone". It eliminates a large fraction of the dark towers by using a smaller radius to find stable cones and then expands the cones to their full radius, without further iteration, before passing them to the SM procedure. Unfortunately, when applied together with the midpoint procedure ($IC_{se,mp}$-SM) it worsens its IR unsafety status from IR_{3+1} back to IR_{2+1} [57].

Perhaps the simplest solution [57] to dark towers is to identify any remainder energy flow that was not clustered by the xC-SM algorithm and run an extra pass of the algorithm on that remainder. This is the approach used in SISCone (which by default runs multiple passes until no energy is left).

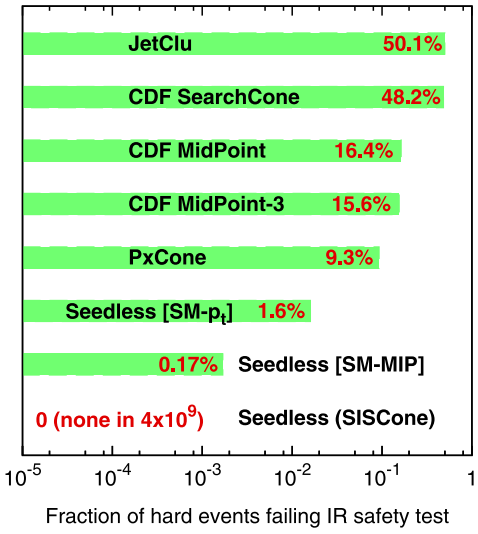

Fig. 5 Failure rates for IR safety tests [44] with various algorithms, including a midpoint variant with 3-way midpoints and some seedless algorithms with commonly used, but improper, split–merge procedures. See Table 2, p. 651, for the classification of the main different algorithms and [44] for a description of the different seedless variants. CDF MidPoint-3 is like the standard MidPoint algorithm except that it also uses midpoints between triplets of stable cones. Briefly, the IR safety test proceeds as follows: first one generates an event with between 2 and 10 hard particles, and applies a jet finder to the event; then one generates some number of random very soft particles ($p_t \sim 10^{-100}$ GeV), and applies the jet finder to the event consisting of soft and hard particles. If the hard jets (those with $p_t \gg 10^{-100}$ GeV) are the same in the two cases, then the jet finder passes the IR safety test for that event. One repeats the exercise for many events. SISCone passed the test for all 4×10^9 events used. Other algorithms failed the test for some fraction of events, as given in the figure

2.2 Sequential recombination jet algorithms

Sequential recombination algorithms have their roots in e^+e^- experiments. A detailed overview of their history in e^+e^- studies is given in the introduction of [58]. The intention here is not to repeat that history, but rather to walk through the most widely used of the e^+e^- algorithms and then see how they lead to corresponding hadron-collider algorithms. It should be said that many of the ideas underlying today's sequential recombination algorithms (including a momentum-related parameter to decide jet resolution and the use of relative transverse momenta) actually appeared first in the LUCLUS algorithm of Sjöstrand [59] (earlier work includes [60–63]). However computational constraints at the time led to the algorithm including a preclustering phase, and it also involved a non-trivial procedure of reassignment of particles between clusters at each recombination. These two characteristics made it somewhat more complicated than its successors.

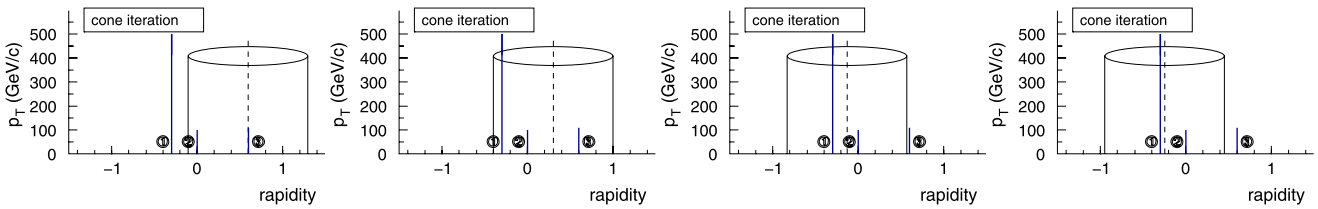

Fig. 6 Some of the stages of a stable-cone iteration that leads to dark towers. In the *first panel*, one starts the stable-cone iteration with the rightmost particle (3) as a seed. The cone contains particles 2 and 3 and its momentum points roughly midway between them. The direction of the momentum is then used as the centre of a cone for the next iteration (*second panel*). The cone in the *2nd panel* contains all three particles. The resulting momentum direction provides the cone centre in the *3rd panel* and now particle 3 is no longer contained in the cone. One further iteration leads to the stable cone in *panel 4*, which does not contain particle 3 even though it provided the initial seed direction. For this event, therefore, particle 3 will never appear in any stable cone

Today's sequential recombination algorithms are all rather simple to state (far more so than the cone algorithms). Additionally they go beyond just finding jets and implicitly assign a "clustering sequence to an event", which is often closely connected with approximate probabilistic pictures that one may have for parton branching.

2.2.1 Jade algorithm

The first simple sequential recombination algorithm was introduced by the JADE collaboration in the middle of the 1980s [64, 65]. It is formulated as follows:

1. For each pair of particles i, j work out the distance
$$y_{ij} = \frac{2E_iE_j(1-\cos\theta_{ij})}{Q^2} \tag{3}$$
where Q is the total energy in the event,[7] E_i is the energy of particle i and θ_{ij} the angle between particles i and j. For massless particles, y_{ij} is the just the (normalised) squared invariant mass of the pair.
2. Find the minimum $y_{\min}$ of all the y_{ij}.
3. If $y_{\min}$ is below some *jet resolution threshold* y_{cut}, then recombine i and j into a single new particle (or "pseudo-jet") and repeat from step 1.
4. Otherwise, declare all remaining particles to be jets and terminate the iteration.

The number of jets that one obtains depends on the value of y_{cut}, and as one reduces y_{cut}, softer and/or more collinear emissions get resolved into jets in their own right. Thus here the number of jets is controlled by a single parameter rather than the two parameters (energy and angle) of cone algorithms.

Quite often in e^+e^- analyses one examines the value of y_{cut} that marks the transition between (say) an event being labelled as having n and $n+1$ jets, $y_{n(n+1)}$. Thus if y_{23} is small, the event is 2-jet like, while if it large then the event clearly has three (or more) jets.

The JADE algorithm is infrared and collinear safe, because any soft particle will get recombined right at the start of the clustering, as do collinear particles. It was widely used up to the beginning of the 1990s (and still somewhat beyond then), however the presence of E_iE_j in the distance measure means that two very soft particles moving in opposite directions often get recombined into a single particle in the early stages of the clustering, which runs counter to the intuitive idea that one has of a jet being restricted in its angular reach. As well as being physically disturbing, this leads to very non-trivial structure (non-exponentiated double logarithms) in higher-order calculations of the distribution of y_{23} [66–68] (later, this was also discussed in terms of a violation of something called recursive infrared and collinear safety [69]).

2.2.2 The k_t algorithm in e^+e^-

The e^+e^- k_t algorithm [27] is identical to the JADE algorithm except as concerns the distance measure, which is

$$y_{ij} = \frac{2\min(E_i^2, E_j^2)(1-\cos\theta_{ij})}{Q^2}. \tag{4}$$

In the collinear limit, $\theta_{ij} \ll 1$, the numerator just reduces to $(\min(E_i, E_j)\theta_{ij})^2$ which is nothing but the squared transverse momentum of i relative to j (if i is the softer particle)—this is the origin of the name k_t-algorithm.[8] The use of the minimal energy ensures that the distance between two soft, back-to-back particles is larger than that between a soft particle and a hard one that is nearby in angle.

Another way of thinking about (4) is that the distance measure is essentially proportional to the squared inverse of the splitting probability for one parton k to go into two, i and j, in the limit where either i or j is soft and they are collinear to each other,

$$\frac{dP_{k\to ij}}{dE_i\,d\theta_{ij}} \sim \frac{\alpha_s}{\min(E_i, E_j)\theta_{ij}}. \tag{5}$$

There is a certain arbitrariness in this statement, because of the freedom to change variables in the measure on the left-hand side of (5). However the presence of a power of just the minimum of the energy in the denominator (rather than some function of both energies as in the JADE distance measure) is robust.

The k_t algorithm's closer relation to the structure of QCD divergences made it possible to carry out all-order resummed calculations of the distribution of $y_{n(n+1)}$ [27, 70, 71] and of the mean number of jets as a function of y_{cut} [72]. This helped encourage its widespread use at LEP. The relation to QCD divergences also means that the clustering sequence retains useful approximate information about the sequence of QCD splittings that occurred during the showering that led to the jet. This is of interest both in certain theoretical studies (for example CKKW matching of parton showers and matrix elements [13]) and also for identifying the origin of a given jet (for example quark versus gluon discrimination [73]).

[7] In experimental uses, it is often the total *visible* energy in the event.

[8] As mentioned above, the distance measured used in the earlier LUCLUS algorithm [59], $y_{ij} = 2\frac{|\vec{p}_i|^2|\vec{p}_j|^2}{(|\vec{p}_i|+|\vec{p}_j|)^2Q^2}(1-\cos\theta_{ij})$ (in the version given in [58]), was also a relative transverse-momentum type variable.

2.2.3 The k_t algorithm with incoming hadrons

In experiments with incoming hadrons two issues arise. Firstly (as mentioned already for cone algorithms) the total energy is no longer well defined. So instead of the dimensionless distance y_{ij}, one might choose to use a dimensionful distance

$$d_{ij} = 2\min\bigl(E_i^2, E_j^2\bigr)(1-\cos\theta_{ij}), \tag{6}$$

together with a dimensionful jet-resolution parameter d_{cut} (alternatively, one might maintain a dimensionless measure by choosing some convention for the normalisation scale). Secondly, the divergences in the QCD branching probability are not just between pairs of outgoing particles, but also between an outgoing particle and the incoming beam direction.

The first attempt at formulating a k_t algorithm in such cases was [74]. It introduced the idea of an additional *particle–beam* distance,

$$d_{iB} = 2E_i^2(1-\cos\theta_{iB}), \tag{7}$$

which, for small θ_{iB}, is just the squared transverse momentum of particle i with respect to the beam. The algorithm then remains the same as in e^+e^-, except that if a d_{iB} is the smallest, then the particle is recombined with the beam, to form part of the "beam-jet". If there are two beams, then one just introduces a measure for each beam.

In pp collisions it is standard to use variables that are invariant under longitudinal boosts, however the d_{ij} and d_{iB} given above only satisfy this property approximately. Thus [28] introduced versions of the distance measures that were exactly longitudinally invariant

$$d_{ij} = \min\bigl(p_{ti}^2, p_{tj}^2\bigr)\Delta R_{ij}^2, \tag{8a}$$

$$d_{iB} = p_{ti}^2, \tag{8b}$$

where

$$\Delta R_{ij}^2 = (y_i - y_j)^2 + (\phi_i - \phi_j)^2,$$

(this variant does not distinguish between the two beam jets).[9] It is straightforward to verify that in the relevant collinear limits, these measures just reduce to relative transverse momenta, like those in (6, 7). Furthermore, since $(y_i - y_j)$, the ϕ_i and p_{ti} are all invariant under longitudinal boosts, the d_{ij} and d_{iB} are too. Nowadays the procedure of Sect. 2.2.1, with the distance measures of (8), is referred to as the *exclusive* k_t algorithm, in that every particle is assigned either to a beam-jet or to a final-state jet.

[9]Reference [28] also proposes a variant where $\Delta R_{ij}^2 \equiv 2(\cosh(y_i - y_j) - \cos(\phi_i - \phi_j))$, more closely related to the precise structure of the QCD matrix elements; however, to the author's knowledge, it has not seen extensive use.

Inclusive k_t algorithm At about the same time that [28] appeared, a separate formulation was proposed in [29], which has almost the same distance measures as (8),

$$d_{ij} = \min\bigl(p_{ti}^2, p_{tj}^2\bigr)\frac{\Delta R_{ij}^2}{R^2}, \tag{9a}$$

$$d_{iB} = p_{ti}^2, \tag{9b}$$

where the difference lies in the presence of a new parameter R (also called D) in the d_{ij}, whose role is similar to R in a cone algorithm (see below). The other difference in this version of the algorithm is in how the d_{ij} get used:

1. Work out all the d_{ij} and d_{iB} according to (8).
2. Find the minimum of the d_{ij} and d_{iB}.
3. If it is a d_{ij}, recombine i and j into a single new particle and return to step 1.
4. Otherwise, if it is a d_{iB}, declare i to be a [final-state] jet, and remove it from the list of particles. Return to step 1.
5. Stop when no particles remain.

Here, all particles are included in final-state jets, there is no concept of a beam jet, and there is no d_{cut} parameter—the question of what gets called a jet is determined by R: if a particle i has no other particles within a distance R then the d_{iB} will be smaller than the d_{ij} for any j and the particle will then become a jet. One consequence of this is that arbitrarily soft particles can becomes jets in their own right and therefore (just as for cone algorithms), one should additionally specify a minimum transverse momentum that a jet should have for it to be of interest.

The above algorithm is most unambiguously referred to as the *inclusive* k_t algorithm, though when people mention the "k_t algorithm" in a collider context, it is nearly always the inclusive variant that they have in mind. It so happens that the exclusive and inclusive variants have identical clustering sequences—it is only the interpretation of those clustering sequences that differs.

The k_t algorithm has long been advocated by theorists because it is free of any infrared and collinear safety issues. On the other hand it had been criticised by experimenters on the grounds (a) that it was computationally slow, insofar as the two public implementations that were available in 2005, `KtClus` (Fortran) [75] and `KtJet` (C++) [76], both took times $\sim N^3$ to cluster N particles; and (b) that it produces geometrically irregular jets, which complicates certain detector and non-perturbative corrections.[10] We will return to

[10]For example, if jets are circular with radius R in the $y-\phi$ plane, then any jet whose momentum points at least a distance R away from the edge of the central part of the detector will always be fully contained in that central part. If jets can be irregular, with boundaries that sometimes extend beyond a distance R from the jet momentum, then there is no such simple way of identifying the region of the detector in which all jets will be fully contained.

the speed issue in Sect. 3.1, while the irregularity is visible as the jagged boundaries of the jets in Fig. 7, p. 652 (related issues will be discussed in Sect. 4.4).

Given the number of experimental objections that have been raised in the past regarding the k_t algorithm in a pp environment, it is worth commenting briefly on the two sets of hadron-collider measurements that have been carried out with the k_t algorithm. One, from DØ [77, 78], had to go to considerable lengths (introducing preclustering) to get around the speed issue (DØ's fine calorimeter meant that it had many input towers) and found rather large non-perturbative corrections from the underlying event (UE); the latter issue perhaps discouraged further use of the k_t algorithm until CDF performed a similar measurement in 2005 [1, 79]. CDF did not suffer particularly from the speed issue, largely because their coarser calorimeter segmentation ensured modest input multiplicities. Also, crucially, they showed that DØ's large UE corrections were probably a consequence of taking the jet radius parameter $R = 1$. When CDF instead took $R = 0.7$ (as is common for cone algorithms), they found UE corrections that were commensurate with those for cone algorithms.

It should also be added that the longitudinally invariant k_t algorithm was the main jet algorithm used at HERA, both in photoproduction (e.g. [3, 80]), the first (published) experimental context in which it was used [81], and deep inelastic scattering (e.g. [82, 83]). Compared to Tevatron this was probably facilitated by the lower particle multiplicities in DIS and photoproduction and also by the quieter underlying event.

2.2.4 *The Cambridge and Aachen algorithms*

The Cambridge algorithm [30] is a sequential recombination algorithm for e^+e^- collisions that introduces *two* distance measures between pairs of particles. It has $v_{ij} = 2(1 - \cos\theta_{ij})$ (i.e. the squared angle) as well as the y_{ij} of (3). It reads as follows

1. If only one particle is left, call it a jet and stop.
2. Otherwise find the pair of particles with smallest v_{ij}.
3. If the corresponding $y_{ij} < y_{\text{cut}}$, replace i and j with the recombined one and go to step 1.
4. Otherwise: take the less energetic of i and j, remove it from the list of particles, call it a jet, and go to step 1.

The idea here was to combine the y_{cut} jet resolution of the k_t algorithm with a clustering sequence dictated by angular ordering, i.e. one that relates closely to the powerful concept of angular ordering that arises when considering multiple gluon emission [84–88].

Cambridge/Aachen The most widely discussed extension (and simplification) of the Cambridge algorithm to hadron colliders was actually originally given in the context of DIS studies [31, 32] (another one [89] has seen less study). It is like the inclusive k_t algorithm in that it uses longitudinally invariant variables, introduces an R parameter, and does away with the y_{ij} cut on jets. It proceeds by recombining the pair of particles with the smallest ΔR_{ij}, and repeating the procedure until all objects are separated by a $\Delta R_{ij} > R$. The final objects are then the jets.[11]

This algorithm was originally named the Aachen algorithm, though it is often now called the Cambridge/Aachen (C/A) algorithm, reflecting its angular-ordered Cambridge roots.

Like the k_t algorithm, the C/A algorithm gives somewhat irregular jets, and its original implementations took a time that scales as N^3. The latter problem is now solved (as for the k_t algorithm) and the fact that the C/A has a clustering hierarchy in angle makes it possible to consistently view a specific jet on many different angular scales, a feature whose usefulness will become apparent in Sect. 5.3 and is also relevant for a "filtering" method discussed below.

2.2.5 *The anti-k_t algorithm*

One can generalise the k_t and Cambridge/Aachen distance measures to [37]

$$d_{ij} = \min\left(p_{ti}^{2p}, p_{tj}^{2p}\right)\frac{\Delta R_{ij}^2}{R^2}, \tag{10a}$$

$$d_{iB} = p_{ti}^{2p}, \tag{10b}$$

where p is a parameter that is 1 for the k_t algorithm, and 0 for C/A. It was observed in [37] that if one takes $p = -1$, dubbed the "anti-k_t" algorithm, then this favours clusterings that involve hard particles rather than clusterings that involve soft particles (k_t algorithm) or energy-independent clusterings (C/A). This ultimately means that the jets grow outwards around hard "seeds". However since the algorithm still involves a combination of energy and angle in its distance measure, this is a collinear-safe growth (a collinear branching automatically gets clustered right at the beginning of the sequence).[12] The result is an IRC safe algorithm that gives circular hard jets, making it an attractive replacement for certain cone-type algorithms (notably IC-PR algorithms).

[11] Alternatively, one can formulate it like the inclusive k_t algorithm, but with $d_{ij} = \Delta R_{ij}^2/R^2$ and $d_{iB} = 1$.

[12] If one takes $p \to -\infty$ then energy is privileged at the expense of angle and the algorithm then becomes collinear unsafe, and somewhat like an IC-PR algorithm.

One should be aware that, unlike for the k_t and C/A algorithms, the substructure classification that derives from the clustering-sequence inside an anti-k_t jet cannot be usefully related to QCD branching (essentially the anti-k_t recombination sequence will gradually expand through a soft subjet, rather than first constructing the soft subjet and then recombining it with the hard subjet).

2.2.6 Other sequential recombination ideas

The flexibility inherent in the sequential recombination procedure means that a number of variants have been considered in both past and recent work. Some of the main ones are listed below.

Flavour-k_t algorithms If one is interested in maintaining a meaningful flavour for jets (for example in purely partonic studies, or when discussing heavy-flavour jets), then one may use a distance measure that takes into account the different divergences for quark and gluon branching, as in [90, 91]. The essential idea is to replace (4) with

$$y_{ij}^{(F)} = \frac{2(1-\cos\theta_{ij})}{Q^2} \times \begin{cases} \max(E_i^2, E_j^2), & \text{softer of } i,j \text{ is flavoured,} \\ \min(E_i^2, E_j^2), & \text{softer of } i,j \text{ is flavourless,} \end{cases} \quad (11)$$

where gluonic (or non-heavy-quark) objects are considered flavourless. This reflects the fact that there is no divergence for producing a lone soft quark, and correctly ensures that soft quarks are recombined with soft antiquarks. In normal algorithms, in contrast, a soft quark and anti-quark may end up in different jets, polluting the flavour of each one. Full details, and the hadron-collider variants, are given in [90], while an application to b-jets was given [91], where it led to a much more accurate NLO prediction for the inclusive b-jet spectrum. Related ideas have also been used in a sequential-recombination jet algorithm designed for combining QCD matrix elements and parton showers [92].

Variable-R algorithms A recent proposal in [93] suggests a class of hadron-collider distance measures of the following form

$$d_{ij} = \min\bigl(p_{ti}^{2p}, p_{tj}^{2p}\bigr)\Delta R_{ij}^2, \qquad d_{iB} = p_{ti}^{2p} R_{\text{eff}}\bigl(p_{ti}^2\bigr), \quad (12)$$

where the radius of the jet (now placed in the d_{iB} term rather than d_{ij}) becomes a function of the jet's transverse momentum $R_{\text{eff}}(p_{ti}^2)$. This provides an original way of having a jet radius that depends on the event structure, a feature which in general can be useful (cf. Sect. 5.1). In [93] it was applied specifically to the question of dijet resonance reconstruction, with the aim of producing larger jets, $R_{\text{eff}} \sim 1/p_t$, (appropriate with $p \leq 0$) for resonances that decay along the beam direction, and it led to improved resolution on the reconstructed mass peak.

Filtering, pruning and trimming As we shall see in Sect. 5, contamination from non-perturbative effects associated with beam-remnants (underlying event) in hadron colliders is a major cause of degradation of resolution on jets' energies. One way of reducing this [94] is to first find the jets (with some given R) and then reconsider each jet on a smaller angular scale, $R_{\text{filt}} < R$ (either by reclustering, or by making use of the hierarchical angular information in the C/A algorithm). On that smaller angular scale one then takes (say) the two hardest subjets, corresponding physically to a hard parton and its hardest gluon emission, while rejecting the junk that comes from the underlying event. A variant of this, referred to as "trimming" in [95], is to retain all subjets above some threshold in transverse momentum. Initial studies [94–96] indicate that these can provide non-negligible advantages in kinematic reconstructions.

A related idea, "pruning," was suggested in [97, 98]. During the (re)clustering of the jet, if two objects i, j are separated by $\Delta R_{ij} > R_{\text{filt}}$ and the softer one has $z = \min(p_{ti}, p_{tj}) < p_{t,i+j} < z_{\text{cut}}$ (with $z_{\text{cut}} = 0.1$ say), then that softer one is simply discarded.

One issue with filtering, pruning and the variable-R approach discussed above, is that they all introduce extra degrees of freedom in the jet finding. Thus the gains that they may provide come at the expense of having to tune those choices to the specific physics analysis that is being carried out.

$3 \to 2$ recombination Most sequential recombination algorithms are related to the idea of inverting successive $1 \to 2$ perturbative branchings (as used in many parton-shower Monte Carlo programs). When simulating QCD branching it can also be useful to consider "dipole" branchings, i.e. $2 \to 3$ splittings, as in Ariadne [99]. Correspondingly one can imagine a sequential-recombination jet algorithm that inverts these branchings by carrying out $3 \to 2$ clusterings. This is the principle of the ARCLUS algorithm [100] for e^+e^- collisions. In practice its performance is similar to that of other e^+e^- algorithms (as discussed in [58]).

2.3 Jet finding as a minimisation problem

Several groups have considered jet finding as a minimisation problem. Though not the main subject of this review, for completeness it is worth devoting a few lines to describe these ideas, which fit into the top-down approach to jet finding, and have been explored by several groups over the past decade.

One approach [101] relates to a method known as k-means in the more general computer science field of clustering [102]. It introduces a partition of particles i into n

clusters L_k ($k = 1 \ldots n$, with n chosen a priori). For a given partition, each cluster has a centroid C_k and one can evaluate a measure

$$S = \sum_k \sum_{i \in L_k} d(p_i, C_k) \tag{13}$$

where $d(p_i, C_k)$ is some measure of the distance between particle i and the centroid k. One then chooses the assignment of particles into clusters that minimises S. Part of the motivation given for the approach of [101] is that it allows one to also include a range of physical constraints (such as the W-mass in top reconstruction) when carrying out the minimisation. However there are open questions as to how it may fare in analyses where one does not actually know what the number of jets should be (for example because of background contamination).

Two other approaches, "deterministic annealing" (DA) [103, 104] and the "optimal jet finder" (OJF) [105, 106] do away with the idea that a particle belongs to any single jet. Essentially (and in a language closer to [105, 106]), they argue that each particle i is associated with jet k with a weight w_{ik} such that $\sum_k w_{ik} = 1$ (or alternatively also allowing for particles to be associated with no jet [105, 106]). The momentum P_k of jet k is then given by $P_k = \sum_i w_{ik} p_i$. In the OJF approach, one makes an a-priori choice for the number of jets, and then a minimisation is carried out over all the entries of the w_{ik} matrix, so as to find the lowest value of some cost function, corresponding for example to some combination of the jet masses; one can then repeat the minimisation for a different number of jets and introduce some criterion for one's choice of the number n of jets, based on the value of the cost function for each n.

In the DA approach, roughly speaking, given some initial weights, one calculates the jet momenta P_k, and then one recalculates the weights according to

$$w_{ik} = \frac{P_{t,k} e^{-\beta d(p_i, P_k)}}{\sum_m P_{t,m} e^{-\beta d(p_i, P_m)}}, \tag{14}$$

where β is an inverse temperature and $d(p_i, P_k)$ is some distance measure (for example ΔR_{ik}^2). One iterates until the weights converge. This is accompanied by the observation that for $\beta = 0$, whatever the starting conditions, the w_{ik} will be independent of i, which implies that whatever the initial conditions and value of n, all jets will have identical directions (i.e. there is only one jet); as one increases β, the system will then tend to develop a larger number of distinct jets. Thus β plays the role of $1/d_{\text{cut}}$ in sequential recombination algorithms.

Finally, just as this review was about to be made public, it was brought to the author's attention that a code FFTJet had just been released [107] which is a further approach involving minimisation (using fast Fourier transforms) as well as weighted assignment of individual particles to multiple jets (the method is discussed in detail in [108]).

The ideas behind the OJF, DA and FFTJet algorithms are certainly interesting, especially the concept that a particle may be associated with more than one jet, though it is perhaps not obvious that the extra conceptual complexity that stems from this is offset by any particular benefits. In the corresponding initial studies of OJF and DA [103–106] physics performances were found to be comparable to that of the k_t algorithm, though a practical advantage at the time that OJF and DA were proposed (no longer relevant nowadays) was a better scaling of the computational speed with particle multiplicity, $\sim N$ for OJF, $\sim N^2$ for DA. The study performed with FFTJet in [108] suggests that it might be more resilient than other algorithms with respect to the effects of magnetic fields, however the study was lacking a number of important physical effects such as the underlying event, which might well affect the conclusions. A further point is that FFTJet's timing scales not as the number of particles in the event but as $k \ln k$ where k is the number of cells used in the fast Fourier transform procedure used for the minimisation. This is an advantage in very busy events, but can be a drawback for parton-level calculations or other situations with low multiplicity, because one still needs to use a large number of cells in order to accurately carry out the minimisation.

The relation between minimisation and jet finding has also been investigated in [56], where stable-cone finding (and cone iteration) has been interpreted in terms of the search for the local minima of the potential

$$F(\hat{n}) = \frac{1}{2} \sum_i E_{ti} \Delta R_{i\hat{n}}^2 \Theta\left(R^2 - \Delta R_{i\hat{n}}^2\right), \tag{15}$$

which is a function of the particle momenta and of a cone direction $\hat{n}$ (a coordinate in η, ϕ). Each stable cone corresponds to a local minimum of the potential as a function of n. Investigations have also been carried out [109, 110] into whether one can directly use "potential" approaches as a replacement for jet finding altogether.

For completeness, it should be stated that the above approaches are infrared and collinear safe, as an almost direct consequence of the way in which they are constructed.

2.4 Recombination schemes

The most widespread recombination scheme nowadays is the E-scheme, or 4-vector recombination scheme. To merge two particles, it just adds their 4-vectors (and it produces massive jets). This is the current recommendation according to [21].

A scheme that was widely used in the past at hadron colliders was the E_t weighted recombination scheme, which

had been put forward also in the Snowmass accord. To recombine a set of particles into a jet, it uses the following procedure:

$$E_{t,\text{jet}} = \sum_i E_{ti}, \tag{16a}$$

$$\eta_{\text{jet}} = \frac{1}{E_{t,\text{jet}}} \sum_i E_{ti}\eta_i, \tag{16b}$$

$$\phi_{\text{jet}} = \frac{1}{E_{t,\text{jet}}} \sum_i E_{ti}\phi_i, \tag{16c}$$

where the sum runs over the particles contained in the jet, and the jet is taken to be massless. This procedure has the drawback that it is not invariant under longitudinal boosts if the component particles are massive (though one can formulate boost-invariant alternatives in terms of rapidity y_i and transverse momentum p_{ti}).

When other recombination schemes are used, this is usually stated explicitly in the corresponding publication. One should be aware that in some cases the recombination scheme used during the clustering (e.g. in the iteration of stable cones) differs from the recombination scheme that is used to obtain the final jet momenta once the particle assignments to the jets are known.

2.5 Summary

We have seen many different jet algorithms in this section. A summary of the main ones in common use in hadron-collider studies is given in Table 2. Many of the algorithms (and all the IRC safe ones) are available from the FastJet [45] or SpartyJet [46] packages (the latter provides access to the IRC safe algorithms via FastJet).

A general recommendation is that hadron-collider algorithms that are IR or collinear unsafe should in future work be replaced by IRC safe ones, of which the inclusive k_t, C/A (possibly with "filtering"), anti-k_t and SISCone are good choices. Specifically the xC-PR class of algorithms is naturally replaced by the anti-k_t algorithm (which produces circular jets, as illustrated in Fig. 7, and has similar low-order perturbative properties), while SISCone is very much like the IC-SM algorithms, but ensures that the stable-cone finding is IRC safe.

Table 2 Overview of some jet algorithms used in experimental or theoretical work in hadronic collisions in the past few years. $\text{SR}_{p=x}$ = sequential recombination, with $p = -1, 0, 1$ characterising the exponent of the transverse-momentum scale, (10); SC = seedless cone (finds all cones); IC = iterative cone (with midpoints *mp*, ratcheting *r*, search-cone *se*), using either split–merge (SM), split–drop (SD) or progressive removal (PR) in order to address issues with overlapping stable cones; FC = fixed-cone. In the characterisation of infrared and collinear (IRC) safety properties (for the algorithm as applied to particles), IR_{n+1} indicates that given n hard particles in a common neighbourhood, the addition of 1 extra soft particle can modify the number of final hard jets; Coll_{n+1} indicates that given n hard particles in a common neighbourhood, the collinear splitting of one of the particles can modify the number of final hard jets. Where an algorithm is labelled with the name of an experiment, this does not imply that it is the only or favoured one of the above algorithms used within that experiment. Note that some of the corresponding computer codes for jet finding first project particles onto modelled calorimeters

Algorithm	Type	IRC safe?	Ref.	Notes
inclusive k_t	$\text{SR}_{p=1}$	OK	[27–29]	Also has exclusive variant
Cambridge/Aachen	$\text{SR}_{p=0}$	OK	[30–32]	
anti-k_t	$\text{SR}_{p=-1}$	OK	[37]	
SISCone	SC-SM	OK	[44]	Multipass, with optional cut on stable cone p_t
CDF JetClu	IC_r-SM	IR_{2+1}	[40]	
CDF MidPoint cone	IC_{mp}-SM	IR_{3+1}	[21]	
CDF MidPoint searchcone	$\text{IC}_{\text{se,mp}}$-SM	IR_{2+1}	[56]	
DØ Run II cone	IC_{mp}-SM	IR_{3+1}	[21]	No seed threshold, but cut on cone p_t
ATLAS Cone	IC-SM	IR_{2+1}	[16]	
PxCone	IC_{mp}-SD	IR_{3+1}	[42]	No seed threshold, but cut on cone p_t
CMS Iterative Cone	IC-PR	Coll_{3+1}	[17]	
PyCell/CellJet (from Pythia)	FC-PR	Coll_{3+1}	[111]	
GetJet (from ISAJET)	FC-PR	Coll_{3+1}		

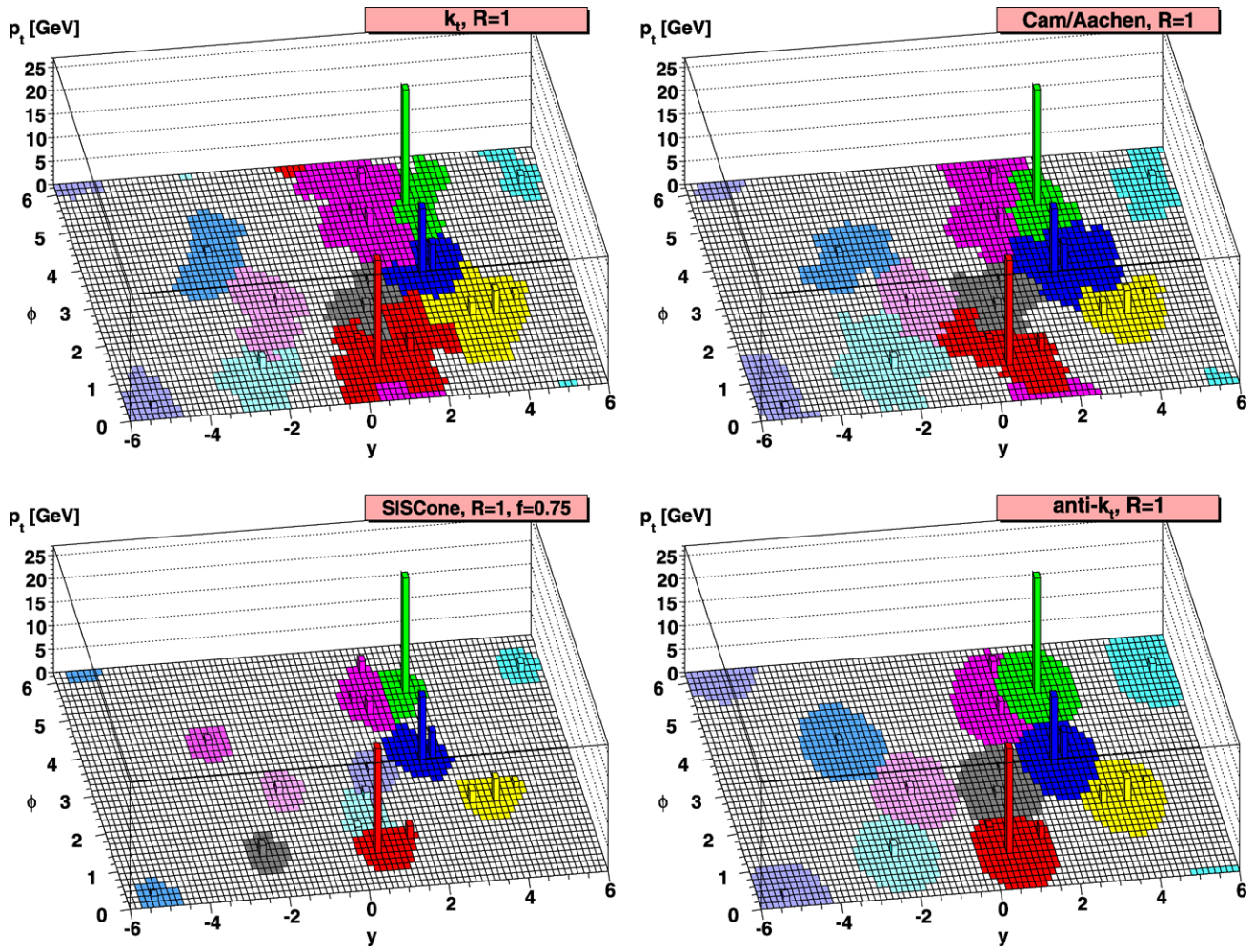

Fig. 7 A sample parton-level event (generated with Herwig [112, 113]), together with many random soft "ghosts", clustered with four different jet algorithms, illustrating the "active" catchment areas of the resulting hard jets (cf. Sect. 4.4). For k_t and Cam/Aachen the detailed shapes are in part determined by the specific set of ghosts used, and change when the ghosts are modified

Figure 7 illustrates the jets that are produced with the four "choice" IRC-safe algorithms in a simple, parton-level event (generated with Herwig), showing among other things, the degree of regularity (or not) of the boundaries of the resulting jets and their extents in the rapidity-azimuth place.

3 Computational geometry and jet finding

It takes the human eye and brain a fraction of a second to identify the main regions of energy flow in a calorimetric event such as Fig. 7. A good few seconds might be needed to quantify that energy flow, and to come to a conclusion as to how many jets it contains. Those are timescales that usefully serve as a reference when considering the speed of jet finders—if a jet finder takes a few seconds to classify an event it will seem somewhat tedious, whereas a few milliseconds will seem fast. One can reach similar conclusions by comparing to the time for a Monte Carlo event generator to produce an event (from tens of milliseconds to a fraction of a second), or for a fast detector simulation to process it. Or by considering the number of CPU hours needed to process a typical event sample, which might consist of $\mathcal{O}(10^7)$ events.

The time taken for jet finding by computer codes depends strongly on the number of input particles (or towers, etc.), N. We do not yet know the exact average multiplicities of LHC events, but rough estimates are given in Table 3. With the k_t algorithm's "standard" N^3 timing, assuming about 10^9 computer operations per second, one expects a time for clustering a low-luminosity LHC event of 1 s (this is also what one finds in practice). So this is close to being "tedious," and becomes dissuasive for high-luminosity LHC and heavy-ion collisions, or if one wishes to try out many distinct jet definitions (e.g. several different R values to see which is best). A more extreme example is the exact seedless cone algorithm following the method in [21], which

Table 3 Orders of magnitude of the event multiplicities N (charged + neutral) for various kinds of event. The e^+e^-, photoproduction, DIS and pp results have been estimated with Pythia 6.4 [111, 114], LHC PbPb with Pythia + Hydjet [115, 116] and RHIC has been deduced from [117]. Note that experimentally, algorithms may run on calorimeter towers or cells, which may be more or less numerous than the particle multiplicity

Type of event	N
$e^+e^- \to$ hadrons event on the Z peak	40
HERA direct photoproduction (dijet) or DIS	40
HERA resolved photoproduction (dijet)	60
Tevatron ($\sqrt{s} = 1.96$ TeV) dijet event	200
LHC ($\sqrt{s} = 14$ TeV) dijet event	400
LHC low-luminosity event (5 pileup collisions)	1000
RHIC Au Au event ($\sqrt{s} = 200$ GeV/nucleon)	3000
LHC high-luminosity event (20 pileup collisions)	4000
LHC Pb Pb event ($\sqrt{s} = 5.5$ TeV/nucleon)	30000

has a timing of $N2^N$. In practice (NLOJET++ implementation [49, 50]), an event with ~ 20 particles takes about a second, so one can extrapolate that even just 100 particles will take 10^{17} years. This is beyond prohibitive.

To speed up jet finders one may consider the general class of computational algorithm that the jet finder belongs to. For instance, all the SR jet finders are examples of "hierarchical clustering", with a range of different distance measures. General solutions to the problem were discussed long ago in the computer science literature by Anderberg [118], with a set of rather good solutions proposed by Cardinal and Eppstein more recently in [119, 120], which scale roughly as N^2.

Generic hierarchical clustering is, however, a broad problem. For example, given three "points", A, B and C, generic distances are not 'transitive': if A is close to B and B is close to C, this does *not* imply that A is close to C (the reader is encouraged to think up a concrete example for the k_t distance measure). On the other hand, jet finding often has a geometrical component (since, at hadron colliders, the rapidity and azimuth coordinates represent the surface of a cylinder). In geometry, if A is close to B and B to C, then A and C are necessarily also close. This is of significant help, and a whole research field exists for such geometric proximity problems, computational geometry. Section 3.1 will show how we can make use of this to obtain $N \ln N$ scalings for the k_t algorithm rather than the N^2 of generic hierarchical clustering, or N^3 of the older k_t-clustering codes. Then in Sect. 3.2 we will examine how to apply computational geometry to cone algorithms.

3.1 Sequential recombination algorithms

The original implementations of the k_t algorithm [75, 76] set up a two-dimensional array of the d_{ij}, and at each stage of the clustering run through all entries of it in order to find the minimum, and then update the array with the entries for the newly created particle. Since the d_{ij} array is of size $\mathcal{O}(N^2)$ and the minimum is searched for $\mathcal{O}(N)$ times in total (i.e. $\mathcal{O}(N)$ clusterings), these implementations take a time $\sim N^3$.

We have seen briefly above that there exist generic methods for hierarchical clustering, i.e. repeated recombination of the closest pair of objects, that take N^2 time. In general N^2 time is a lower bound because, at the very least, one has to consider all entries of the d_{ij} distance matrix in order to find the smallest. One may then be clever in keeping track of distance information as points are recombined, so as to side-step the N^3 growth of some k_t algorithm implementations,[13] but the initial search for the minimum among all pairs of points seems unavoidable.

3.1.1 k_t algorithm

To see whether we can evade the N^2 bound, let us examine the k_t algorithm's distance measure in more detail

$$d_{ij} = \min\bigl(p_{ti}^2, p_{tj}^2\bigr)\Delta R_{ij}^2. \tag{17}$$

We could equally well have considered a distance measure

$$D_{ij} = p_{ti}^2 \Delta R_{ij}^2. \tag{18}$$

The smallest of the D_{ij} across all i, j coincides with the smallest of all the d_{ij}, since $\min(D_{ij}, D_{ji}) = d_{ij}$. So it is irrelevant whether we use (17) or (18) in the k_t algorithm.

Equation (18) has the important property that the transverse-momentum part depends on just one of the two particles, so we can write

$$\min_j\{D_{ij}\} = p_{ti}^2 \min_j\bigl\{\Delta R_{ij}^2\bigr\}, \tag{19}$$

i.e. fixing i, the smallest of the D_{ij} involves i's geometrical nearest neighbour (let us refer to it as $\mathcal{G}_i$). So if we can find some efficient way of establishing and tracking that geometrical information, then rather than finding the minimum of N^2 D_{ij} values, the sequential recombination problem involves only finding the minimum of N $D_{i\mathcal{G}_i}$ values. This was the key observation of [121].

One is then left with the question of how to find the minimum of the ΔR_{ij}^2 for each i, since this still seems to involve a total of N^2 points. Technically, the problem is that of establishing and maintaining a nearest-neighbour graph on the 2-dimensional surface of a cylinder. A rule of thumb when faced with such problems is to first ask how one might deal

[13] Essentially, observing that at most $\mathcal{O}(N)$ distances change at every pair recombination.

with them in 1 dimension, say rapidity y. That is easy: one sorts the points according to their y coordinate, and the nearest neighbour of a point is the one that immediately precedes or follows it.

Let us do the bookkeeping for this case with just a rapidity coordinate:

Initialisation:

- Sort points according to y coordinate (with a balanced binary tree), find nearest neighbours, and find all $d_{i\mathcal{G}_i}$. [N ln N]
- Place the $d_{i\mathcal{G}_i}$ in a "priority queue" (a structure for efficient minimum-finding and updates; often simply a balanced binary tree). [N ln N]

Iteration:

- Recombine the pair with smallest $d_{i\mathcal{G}_i}$, remove the corresponding two points from the rapidity-sorted tree, add the new one, establish the new point's nearest neighbours and establish if it has become the nearest neighbour of any of the existing points. [ln N per recomb.]
- Update the priority queue of $d_{i\mathcal{G}_i}$ values and find the new minimum (only a finite number of $d_{i\mathcal{G}_i}$ will change per round). [ln N per recomb.]

This gives a total time of $\mathcal{O}(N \ln N)$. To understand the origin of the $\ln N$ factor, observe, for example, that if you organise N objects into a binary tree structure, then the depth of the tree will be $\ln_2 N$ (equivalently, given k levels to the tree, it can contain up to $\sum_{\ell=0}^{k-1} 2^\ell = 2^k - 1$ objects). Any operation such as adding or removing an entry in the tree involves working through the depth of the tree, and so paying a price $\mathcal{O}(\ln N)$. Since building the tree can be seen as adding N objects this costs $\mathcal{O}(N \ln N)$ time.

With two geometrical dimensions, nearest-neighbour finding is more complex, however it has been the subject of research by the computational geometry community. One structure that can help is the Voronoi diagram [122–125], or its dual, the Delaunay triangulation. A Voronoi diagram divides the plane into cells (one per vertex), such that every point in the cell surrounding a vertex i has i as its nearest vertex. The structure is useful for nearest-neighbour location because the vertex $\mathcal{G}_i$ nearest to vertex to i is always in one of the (few, *expected*[14] $\mathcal{O}(1)$) cells that share an edge with the cell of vertex i. An example is shown in Fig. 8.

Voronoi diagrams for N points can be constructed with $\mathcal{O}(N \ln N)$ operations [126]. Maintaining dynamic point sets is more complicated, however there exists an approach [127, 128] that takes $\mathcal{O}(N \ln N)$ for the initial construction and expected $\ln N$ per insertion/deletion and it is available as a public code, CGAL [129, 130].

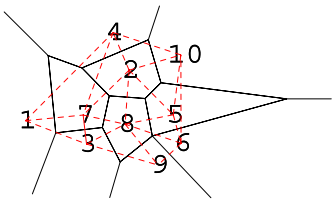

Fig. 8 The Voronoi diagram for ten random points. The Delaunay triangulation (*dashed*, *red*) connecting the ten points is also shown. In this example the points 1, 4, 2, 8 and 3 are the 'Voronoi' neighbours of 7, and 3 is its nearest neighbour. Adapted from [121]

A complete expected $N \ln N$ implementation that makes use of CGAL is available in the FastJet program [45]. In practice, $\ln N$ terms in computational geometry come with a large coefficient—typically a $\ln N$ term might be smaller than a term linear in N only for $N \gtrsim 10^3$. Therefore for moderate N it is useful to include alternative computational strategies. One particularly successful one (optimal in the range $50 \lesssim N \lesssim 10^4$) makes use of the fact that only for $\Delta R_{ij} < R$ will a d_{ij} distance be smaller than d_{iB}, d_{jB} in (6)— therefore one can restrict one's search for i's geometric nearest neighbours to the region within R of i. Denoting by n the typical number of points in such a region, one then has a $\mathcal{O}(Nn)$ algorithm.

Further details are available in the FastJet documentation (from the web site [45]) and from an unpublished preprint [131].

3.1.2 *Special cases*

The above approaches can be used for the whole class of generalised (longitudinally invariant) k_t algorithms, however some special cases deserve comment.

Cambridge/Aachen For the C/A jet finder, there is no momentum scale, so rather than having a dynamic planar nearest-neighbour problem, one has a dynamic planar closest pair problem, $d_{ij} \equiv \Delta R_{ij}$. This is simpler—essentially one can maintain a nearest neighbour candidate for each point, but it only need be correct for the closest pair. One remarkable solution to this problem[15] was given by Chan in [132]. It is included natively in FastJet, and is slightly faster than the CGAL based solution (as well as avoiding the need for a separate package).

Note: Chan's solution relies on the use of integer arithmetic (part of its cleverness lies in its implicit use of the binary representation of integers). However since rapidities and azimuths do not extend to large values, one can safely rescale them by some large constant and represent them as integers.

[14] "Expected" means that there can be special cases where the number is parametrically larger.

[15] Which can be stated in a paragraph, though this does not mean that it is simple to understand!

Anti-k_t The generalised k_t algorithm with $p < 0$ (and specifically anti-k_t, with $p = -1$) has the property that it effectively produces jets that grow outwards in a circular pattern around a high-p_t seed. This leads to configurations with one particle at the centre of a circle and many on the edge (the first layer of points on the edge contains $\mathcal{O}(\sqrt{n})$ particles).

This is precisely the configuration in which the 'expected' $N \ln N$ behaviour of the clustering breaks down: the central point has many Voronoi neighbours, and, furthermore, is involved in each clustering (so it is removed, reinserted, and then one must go around all the points on the edge to see which now is its nearest neighbour). This means that for very large N, n, the timing for anti-k_t type algorithms is closer to $N\sqrt{n}$ than to $N \ln N$.

According to [133] there exist approaches to the planar nearest-neighbour problem that have worst-case behaviour N^ϵ with arbitrarily small ϵ, however these have not been investigated in the context of jet finding.

3.2 A polynomial-time seedless cone

We saw in Sect. 2.1.4 that the use of particles as seeds, i.e. starting points for cone iterations, gets us into trouble with IRC safety: if one finds jets based on the ordering of the seeds in p_t, then one is sensitive to collinear splittings; if one uses the stable cones obtained from iterating all seeds, then one becomes sensitive to the addition of new soft seeds.

We also saw an exact seedless approach that takes all subsets of particles and establishes for each one whether it corresponds to a stable cone—i.e. for each subset one calculates its total momentum, draws a circle around the resulting axis, and if the points contained in the circle are exactly those in the initial subset, then one has found a stable cone. This is guaranteed to find all stable cones.

For large multiplicities, this is inherently wasteful insofar as most of the 2^N subsets of particles do not fit into a circle of radius R on the rapidity-azimuth plane, so there is no way for them to form a stable cone.

The obvious corollary of that observation is that one should only consider subsets of points in which the members of the subset are contained within a circle of radius R, and any point not in the subset is outside the circle. It is only these subsets that can ever form a stable cone. Therefore rather than considering all subsets of points, one can restrict one's attention to all distinct ways of separating points on the surface of a cylinder (or plane) into two subsets, those points inside a circle of radius R, all others outside—a "planar all distinct circular enclosures" problem.

This problem is a clear example of a computational geometry problem. Let us first see how we would deal with it in one dimension, for which a "circular enclosure" just reduces to a line segment enclosure (cf. Fig. 9). Given points

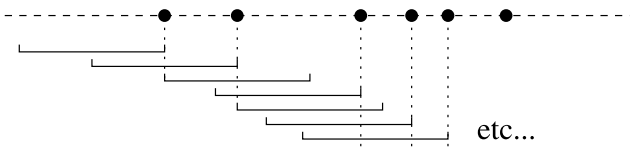

Fig. 9 Representation of points on a line and the places where a sliding segment has a change in its set of enclosed points

on a line and a segment of length $2R$, we can order the points, place the segment to the left of the leftmost point, and then slide it sideways. Each time the left or right edge of the segment touches a point, the contents of the enclosure change. The cost of finding all enclosures is just that of ordering the points ($N \ln N$).

How do we extend this to two dimensions? The central idea is that the enclosed point set changes when a point touches the enclosure. In 1d we can always shift the enclosure, without changing its contents, until its edge touches a point (either in or out of the enclosure). In 2d we can first shift the circular enclosure until one point touches the edge, then pivot the circle around that point until its circumference touches a second point (Fig. 10). Conversely if we consider all pairs of points (within $2R$ of each other) and draw all possible circles that go through those pairs, then we will have found all possible enclosures (one should remember that edge points can be either in or out of the enclosure; special treatment is also needed for points that are alone, i.e. further than $2R$ from the nearest other point).

There are $\mathcal{O}(Nn)$ relevant pairs of points (recall, cf. the end of Sect. 3.1.1, that n is the number of objects in a region of area $\sim R^2$).[16] One could directly check the stability of the cones defined by each pair as follows: one sums the $\mathcal{O}(n)$ momenta contained within a given cone and then checks to see whether a new cone centred on the direction of the resulting momentum contains the same set of points. This would give an $\mathcal{O}(Nn^2)$ algorithm. Alternatively one can establish a traversal order in which the circle contents change by one point at a time, avoiding (with the help of a few other tricks) the need to pay a price of $\mathcal{O}(n)$ for the stable-cone check for each distinct enclosure. This is the basis of the (expected) $Nn \ln n$ algorithm that is known as SISCone (Seedless Infrared Safe Cone) [44].[17]

[16] There is a correspondingly large number of distinct cones, and this has implications for proposal [108, 134] to use a fast Fourier transform for the stable-cone search (cf. also the FFTJet package [107], which was released just as this review was being finalised), essentially because it implies the need for a fast Fourier transform grid of size $\mathcal{O}(Nn)$.

[17] It has been pointed out by Sjöstrand [135] that SISCone's use of all pairs of points to provide the full list of distinct circular enclosures bears a close relation to a technique used in the N^3 computation of the Thrust [136]. There, all pairs of particles are used to generate all relevant separations of the surface of a sphere into two hemispheres.

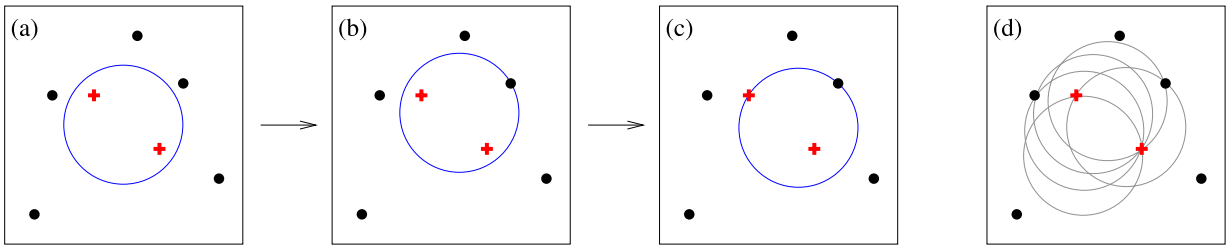

Fig. 10 (**a**) Some initial circular enclosure; (**b**) moving the circle in a random direction until some enclosed or external point touches the edge of the circle; (**c**) pivoting the circle around the edge point until a second point touches the edge; (**d**) all circles defined by pairs of edge points leading to the same circular enclosure

Some comments are due concerning SISCone's timing. There are usually only $\mathcal{O}(N)$ stable cones, parametrically fewer than the number of distinct enclosures. Might there be a way of somehow skipping all the unstable enclosures? It is not clear, because the upper bound on the number of stable cones is actually $\mathcal{O}(Nn)$ (the much lower expected value holds for random point sets [44]). This worst case can actually occur (for example with regular sets of "ghosts," cf. Sect. 4.4), with implications then for the split–merge procedure. Normally the split–merge procedure is significantly faster than the stable-cone search, in that it takes time $\mathcal{O}(N^2)$ ($\ll Nn\ln n$ in practice)[18] in SISCone's fairly straightforward implementation. However if the number of stable cones is $\mathcal{O}(Nn)$, then the split–merge step becomes $\mathcal{O}(N^2 n)$ unless one applies additional dedicated techniques (such as quad-trees or k-d trees, as discussed in [44] and also suggested in [134]).

A further comment is due on memory usage: SISCone maintains a hash of circular enclosures that it has already seen (and whether they are candidates for stable cones or not). That hash has as many entries as distinct enclosures, $\mathcal{O}(Nn)$, and this can become problematic for very large multiplicities.[19] In such cases one could in principle reduce the memory use to $\mathcal{O}(N)$, at the expense of a slower run-time $\mathcal{O}(Nn^{3/2})$, but this has not been implemented.

A corollary of this observation is that SISCone's idea of a traversal order could also be used in the context of the thrust, to reduce its computation time to $N^2 \ln N$.

[18] In QCD events and with typical values of the jet-finding radius $R = 0.4 - 1.0$, N/n is usually between 10 and 100; in 2-dimensional problems, for the multiplicities that are of relevance here, a rule of thumb seems to be that $\ln n$ is very roughly equivalent to a factor of order 10^3.

[19] If we suppose $n \sim 0.1N$, and that each entry needs 12 bytes for the hash, two double-precision numbers (8 bytes each) to describe the centre of the cone, and a pointer to the next hash element, plus various overheads, then we get a memory usage of about $4N^2$ bytes, i.e. nearly 4 GB for $N \sim 30\,000$, which is a typical expected LHC heavy-ion multiplicity.

3.3 Speed summaries

Statements of timings in terms of their scaling with N can hide large coefficients and significant preasymptotic corrections. Another issue is that as N increases so does memory usage, requiring (slower) access to the main memory rather than the CPU cache, and this too can affect practical timing results.

Timings for a subset of commonly used algorithms are shown in Fig. 11. One conclusion from that figure is that SISCone, the slowest of the IRC safe algorithms, is still competitive in speed with the main public Midpoint-cone code and is acceptably fast unless one goes to N larger than several thousand. FastJet's implementation of the k_t algorithm (and C/A and anti-k_t) is much faster, with clearly healthier scaling at large N, and it beats even the fast IRC unsafe cone codes, like CDF's JetClu.

The FastJet curve has a clear kink at $N \sim 15000$. This is the point where FastJet switches from an Nn (tiled) algorithm to the $N \ln N$ CGAL-based one. One can explicitly verify that the CGAL-based algorithm does have an $N \ln N$ behaviour, by dividing the run times by N and plotting the result. This is shown in Fig. 12.

To conclude this part, we have seen how the computational geometry aspect of jet-related problems can be exploited to help resolve many of the practical computational issues that arise if one is to carry out infrared-safe hadron-collider jet finding. It is probably fair to say that this is playing a crucial role in encouraging the LHC experiments to switch to QCD-compatible jet finders. In particular, all the LHC experiments now incorporate FastJet and its SISCone plugin in their software frameworks (and ATLAS also has its own $\sim N^2$ implementation of the sequential recombination algorithms) [16, 137].

4 Understanding jets

Ideally, one would really like to be able to measure partons in experiments. Jets are the closest, physically, that we get to partons. How close are they exactly? And what about the

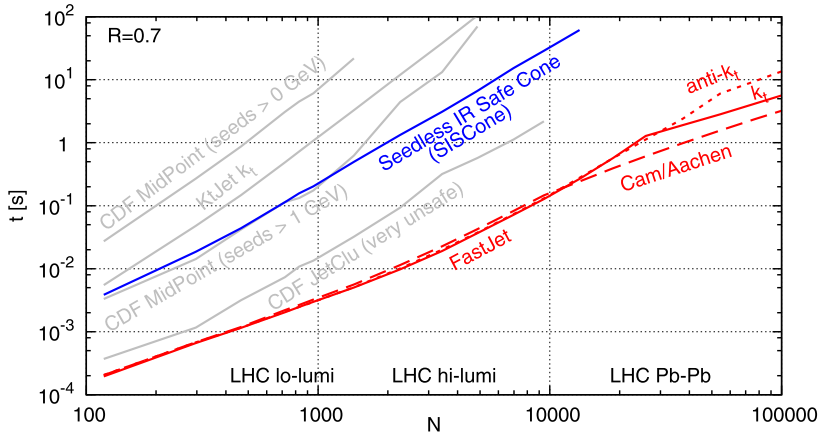

Fig. 11 Timings for the clustering of a simulated ∼50 GeV dijet event, to which increasing numbers of simulated minimum-bias events have been added (both simulated with Pythia). In *dark colours* one sees SISCone and the FastJet k_t, anti-k_t and Cambridge/Aachen implementations. For k_t (anti-k_t), the kink at $N \simeq 25000$ ($N \simeq 50000$) signals the point where FastJet switches between Nn and $N \ln N$ ($Nn^{1/2}$) strategies. In *grey* one sees results for the KtJet implementation [76] of the k_t algorithm, the Midpoint cone ($\mathrm{IC}_{\mathrm{mp}}$-SM) in CDF's implementation (with and without a 1 GeV cutoff on seeds) and the JetClu iterative cone (IC_r-SM, with a 1 GeV seed threshold). All non-FastJet algorithms (except KtJet) have been accessed through FastJet plugins

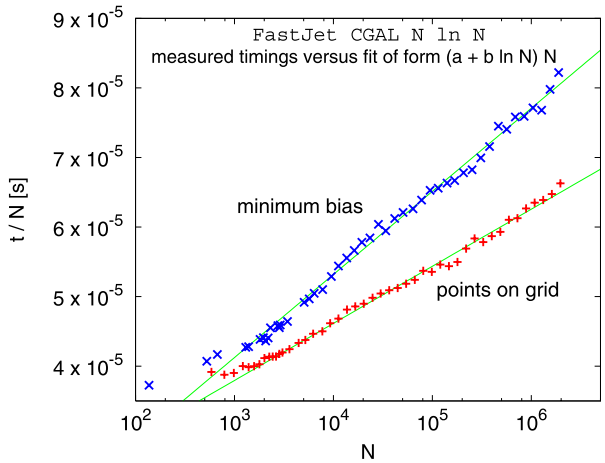

Fig. 12 Verification of the $N \ln N$ timing behaviour of the CGAL-based implementation of the k_t algorithm in FastJet. The timings are divided by N so as to highlight the remaining $\ln N$ dependence. Taken from [131]

fact that a "parton" is not actually a well-defined concept in the first place? An understanding of these questions is part of the key to knowing how best to use jet algorithms at colliders, both in terms of choosing which algorithm to use and setting its parameters.

The precise issues that one might investigate fall into various categories. For example, how broadly will a jet reach for its constituents (Sect. 4.1)? This information is important in terms of one's ability to disentangle different partons in heavy-particle decays (for example hadronic $t\bar{t}$ events, which decay to six hard partons). Often, one will use jets to reconstruct the kinematics of some 'parent object' (again, a heavy particle that decayed; or, in inclusive-jet measurements, a scattered parton from the incoming proton). How does the jet's energy relate to that of the 'parent object'? This is affected both by perturbative (Sect. 4.2) and non-perturbative (Sect. 4.3) radiation. Finally LHC is special in that it will have significant underlying-event activity (maybe 15 GeV per unit rapidity) and even larger pileup (easily 100 GeV per unit rapidity). How do jets react to this (Sect. 4.4)?

It is probably fair to say that our understanding of all these questions is still incomplete. But the material below outlines some of what we do know.

4.1 Reach

4.1.1 Two-particle case

Given just two massless particles, separated by a distance ΔR on the $y - \phi$ cylinder, will they be recombined into a single jet? This is the simplest of the questions one might ask about a jet-definition's reach. It was discussed in [29] for the inclusive k_t algorithm and for a partially specified cone, which behaves somewhat like SISCone.

It is convenient to take the transverse momenta of the two particles, p_{t1}, p_{t2} (defined as the softer one) to be related by

$$p_{t2} = x p_{t1}, \quad x < 1. \tag{20}$$

Writing the sum of the two particles' momentum as p_J, with $p_{tJ} = p_{t1} + p_{t2}$,[20] and imagining the two partons as coming

[20] In the widespread 4-vector (E-scheme) recombination scheme, this is exact only if the particles are very close in angle. However it remains a good approximation even for $\Delta R_{12} \sim 1$ and so it is an approximation that will recur in this section.

from a common ancestor, we can also write

$$p_{t1} = (1-z)\,p_{tJ}, \quad p_{t2} = z p_{tJ} \quad \left(z = \frac{x}{1+x} < \frac{1}{2}\right). \tag{21}$$

According to the context, results are more simply expressed either in terms of x or z, which is why it is useful to introduce both.

In the k_t algorithm, the two particles will form a single jet if $d_{12} < d_{1B}, d_{2B}$ (as defined in (9)), or equivalently if

$$\Delta R_{12} < R. \tag{22}$$

In the case of an algorithm like SISCone, based on stable cones, the question is whether particles 1 and 2 can both belong to a single cone. This happens if both are within R of p_J,

$$\left.\begin{aligned} \Delta R_{1J} &= z\Delta R_{12} \\ \Delta R_{2J} &= (1-z)\Delta R_{12} \end{aligned}\right\} < R, \tag{23}$$

where the relations between ΔR_{iJ} and ΔR_{12} follow from $y_J = (1-z)y_1 + z y_2$, $\phi_J = (1-z)\phi_1 + z\phi_2$. Since we have defined $z < 1/2$, it is the lower condition of (23) that is more constraining and it leads to

$$\Delta R_{12} < (1+x)R, \tag{24}$$

i.e. the same as the k_t algorithm condition, (22), when p_2 is soft, $x \ll 1$, but reaching twice as far when $p_{t2} \simeq p_{t1}$.

The conditions (22, 24) basically account for the behaviours of nearly all jet algorithms:

- (22) holds for the k_t algorithm, as well as Cambridge/Aachen, anti-k_t, and the xC-PR cone algorithms;
- (24) holds for $\mathrm{IC_{mp}}$-SM ("midpoint"), $\mathrm{IC_{mp}}$-SD (PxCone) and SC-SM (SISCone) algorithms;
- IC-SM algorithms without midpoint seeds (JetClu, Atlas Cones) have ill-defined behaviour. For just two particles, they lead to a single jet based on (22), but if additional soft seeds are present then this transforms into (24). This is a manifestation of their infrared unsafety.

4.1.2 General case

The complexity of tracing the behaviour of a jet algorithm precludes general results about the reach of different jet algorithms for multi-particle configurations. One question that has however seen some attention is that of how the results of Sect. 4.1.1 get modified in the presence of parton showering and hadronisation.

This is a delicate question because to answer it one has to know something about the *environment* that created the two partons: did they come from the branching of a single parent quark, or a parent gluon, or even the decay of a colour-singlet particle? And what was the parent parton colour-connected to? All of these issues relate to the fact that there is no rigorous way of defining partons in the first place. Furthermore, even in a probabilistic Monte-Carlo type approximation, the way partons shower and hadronise depends on the environment.

One approach [40, 138] to the question involved superposing pairs of events and establishing under what conditions jets that had been identified in the individual events became a single jet if one applied the jet finder to the two events combined together. This study was performed for IC-SM type algorithms and came to the conclusion that the individual jets were merged if there were within $1.3R$ of each other.[21] This corresponds roughly to expectations based on (24), if one performs some reasonable averaging over the jet momenta, i.e. x (indeed we will see the value 1.3 appear again below in Sect. 4.2.1). However it fails to provide a direct link with the x-dependence of (24).

Another approach to testing (22, 24) was taken in [44]. There, jets were initially found with a "reference," $R = 1$ hierarchical-clustering algorithm. The hierarchy was used to identify the two main subjets, S_1 and S_2, within the jet. Each event was also clustered with a test algorithm T, with $R_T = 0.4$. The test algorithm is the one whose clustering behaviour one wishes to probe and need not be the same as the reference algorithm (and in our tests will often not be). One then looked to see if there was a jet with algorithm T that contained at least half of the p_t of each of S_1 and S_2. If there was, the conclusion was that the two subjets had ended up (dominantly) in a single jet from the test algorithm. The procedure was repeated for many events and one could then plot the fraction of k_t-algorithm jets for which this occurs, $P_{2\to1}(\Delta R, x)$, as a function of the distance $\Delta R \equiv \Delta R_{S_1 S_2}$ and the momentum ratio $x \equiv p_{t,S_2}/p_{t,S_2}$.

In [44] it was the k_t algorithm that was used as a reference. Here we shall instead use the C/A algorithm as a reference and the subjets are the two objects whose merging in the reference jet's clustering sequence involves the largest k_t distance (i.e. the hardest merging).[22] The results will be based on dijet events simulated with Herwig 6.5 [112, 113], both at parton and hadron levels (the latter including Herwig's default soft UE). Reference jets were required to have $p_t > 50$ GeV.

[21] The value 1.3 has also inspired a practice in NLO calculations, still current within the CDF collaboration (e.g. [139]), that involves placing an artificial cut on the separation between partons within a jet at $\Delta R = R_{\mathrm{sep}} \times R$, with $R_{\mathrm{sep}} = 1.3$. Such ad-hoc modifications of the jet algorithm used in a theory prediction defeat the purpose of a NLO calculation. It is probably fair to say, however, that in most contexts where R_{sep} has been used, its impact is smaller than the dominant theory and experimental uncertainties.

[22] This is inspired by the use of a k_t and an angular distance measure in the original Cambridge algorithm, and gives clearer results than the k_t algorithm's subjets.

Results are shown in Fig. 13, for various jet algorithms T, with parton-level results on the left and hadron level on the right. In the regions in black, the two C/A subjets always end up in a common T-jet, while in the region in white this does not occur. For the IR-safe algorithms one sees rough agreement with the expectations from (22, 24), though for SISCone the boundary is quite broad and shifted to the left of $\Delta R/R_T = 2$ at $x = 1$. This is probably partly a consequence of the showering and hadronisation, which limit the stability of configurations in which the two subjets are near opposing edges of a cone, as has been extensively discussed in [56]. The dependence of the effect also on the split–merge overlap threshold f suggests that the split–merge dynamics have a non-trivial impact as well. Figure 13 also shows results two very IR unsafe algorithms, a plain IC-SM variant (CDF's Midpoint algorithm with the midpoint option turned off) and JetClu. Among the relevant features, one notes the somewhat different shape for the IC-SM algorithm at parton and hadron level, most visible if one examines the contours (dashed lines), especially at higher x values. This is a consequence of the IR unsafety. JetClu bears little resemblance to the plain IC-SM algorithm, even though it is IC-SM based. More detailed study reveals that this is only partially due to its use of ratcheting.

4.2 Perturbative properties, p_t and mass

Gluon radiation is inevitable from fast-moving partons. How does it affect the properties of a jet? Basically the gluon may be radiated beyond the reach of the jet definition ("splash-out") and thus reduce the jet's energy compared to that of the parton. Alternatively it may be radiated within the reach of the jet definition and then generate a mass for the jet (assuming a 4-vector-addition recombination scheme). The aim of this section is to give some simple analytical understanding of the effect of perturbative radiation on a jet's transverse momentum and mass—rules of thumb—as well as references to the literature for more detailed analyses.

For the reader who is interested principally in the results, the two main ones can be summarised as follows. For small jet radii, $R \ll 1$, the average fractional difference between a jet's transverse momentum and that of the original parton is

$$\frac{\langle p_{t,\text{jet}} - p_{t,\text{parton}}\rangle_{\text{pert}}}{p_t} \simeq \left.\begin{matrix}\text{quarks: } -0.43\\ \text{gluons: } -1.02\end{matrix}\right\} \times \alpha_s \ln\frac{1}{R} + \mathcal{O}(\alpha_s), \tag{25}$$

where the $\mathcal{O}(\alpha_s)$ term depends both on the jet algorithm and the global environment in which the parton is to be found (e.g. colour connections to other partons) and is often ill-defined because of the ambiguities in talking about partons in the first place. Ignoring these important caveats, the above result implies that an $R = 0.4$ quark (gluon) jet has about 5% (11%) less momentum on average that the original parton (for $\alpha_s = 0.12$).

The second result is that the average squared jet mass for all non-cone algorithms is

$$\langle M^2\rangle \simeq \left.\begin{matrix}\text{quarks: } 0.16\\ \text{gluons: } 0.37\end{matrix}\right\} \times \alpha_s p_t^2 R^2. \tag{26}$$

For both the p_t loss and the squared jet mass, SISCone results are similar to k_t, anti-k_t and C/A results when $R_{\text{SISCone}} \simeq 0.75 R_{k_t}$.

4.2.1 *Jet p_t*

In many uses of jets, one needs to know how a jet's energy (or p_t) relates to the underlying hard scale of the process—for example to the mass of a decaying heavy particle (top quark, Higgs boson, new particle), or to the momentum fraction carried by a scattered parton in an inclusive jet cross section.

One approach to this is to take a Monte Carlo event generator, let it shower a parton from some source and then compare the jet's p_t to that of the parton. This often gives a reasonable estimate of what has happened, even if the Monte Carlo basically acts as a black box, and brings a somewhat arbitrary definition of what is meant by the initial "parton" (or of the mass of the top quark).

Another approach is to take a program for carrying out NLO predictions, like MCFM [48] or NLOJET++ [49, 50], and for example determine the relation between the jet p_t-spectrum and the parton distribution functions. NLO calculations are perhaps even blacker boxes than Monte Carlo generators, on the other hand they do have the advantage of giving predictions of well-defined precision; however, one loses all relation to the intermediate (ill-defined) "parton" (this holds also for tools like MC@NLO [54] and POWHEG [55]).

Some insight can be obtained from analytical NLO calculations of jet cross sections, such as [140–145]. A feature that is common to them is that at the first non-trivial order, cross sections acquire a $\ln R$ dependence in the small-R limit. The small-R limit is one case where one *can* say something meaningful the relation between a jet's p_t and that of the original parton (another is the threshold limit, for example [145–149]), because the emitting parton decouples from its environment, a consequence of angular ordering. Working in a collinear approximation and considering an initial quark, with a gluon emission matrix element proportional to the real $P_{qq}(z)$ splitting function ($P_{qq}(z) = C_F(1+z^2)/(1-z)$), one can simply write the average dif-

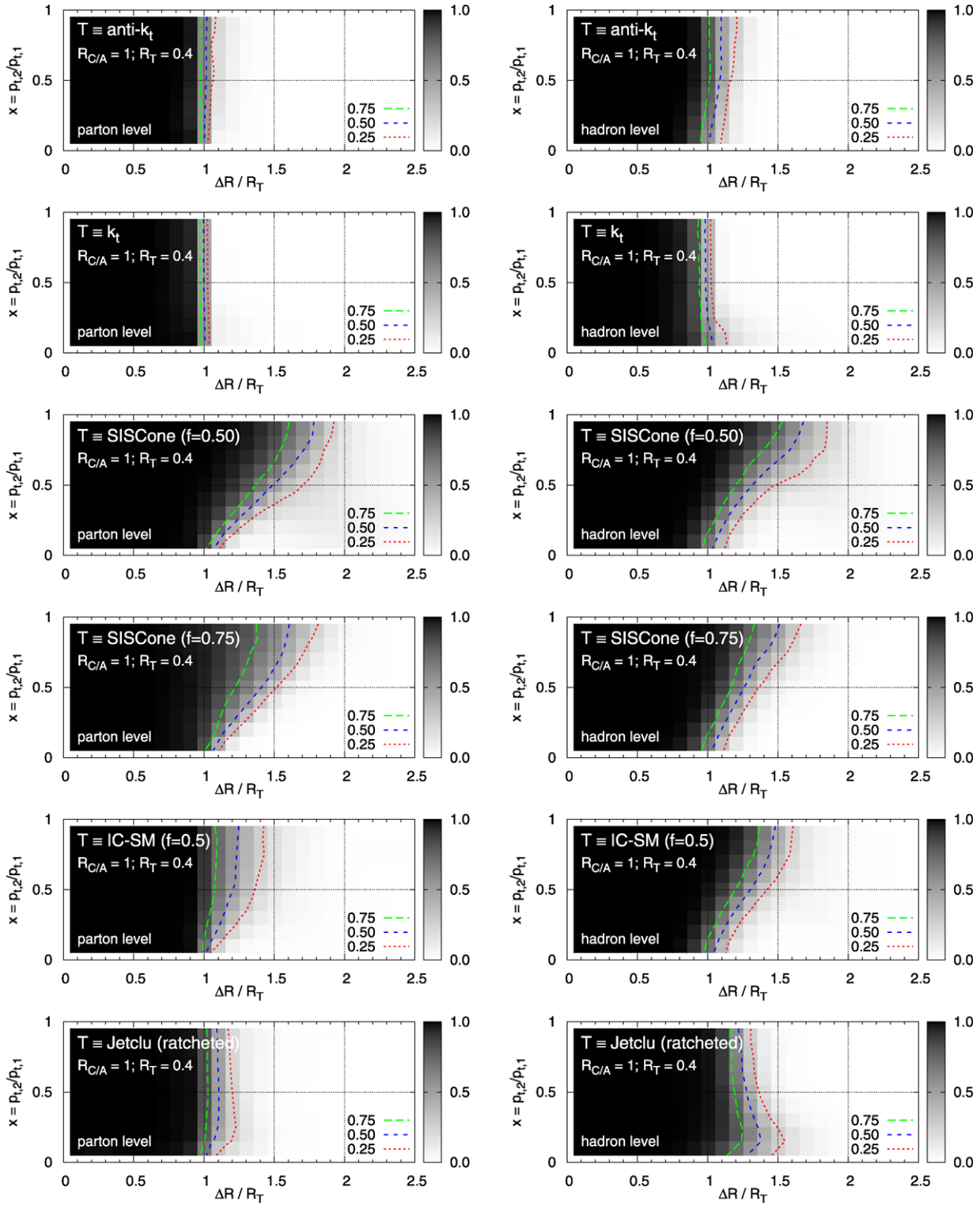

Fig. 13 *Shade/contour plot* of the probability for two C/A subjets to each have at least 50% (*blue*, *short-dashed contour*; 25% and 75%: *red dotted*, *green long-dashed contours*) of their transverse momentum within a single test-algorithm (T) jet. Shown based on a sample of dijet events simulated with Herwig 6.5 at parton-level and at hadron level (with Herwig's default soft UE), using all C/A jets with $p_t > 50$ GeV. Carried out for Tevatron Run II conditions, $p\bar{p}$ at $\sqrt{s} = 1.96$ TeV

ference $\delta p_t = p_{t,\text{jet}} - p_{t,\text{quark}}$ as

$$\langle \delta p_t \rangle_{\text{pert}} = \int \frac{d\theta^2}{\theta^2} \int dz \underbrace{p_t\big(\max[z, 1-z] - 1\big)}_{\delta p_t} \times \frac{\alpha_s(\theta(1-z)p_t)}{2\pi} P_{qq}(z) \Theta\big(\theta - f_{\text{alg}}(z)R\big), \quad (27)$$

where one integrates over the angle θ between the quark and an emitted gluon and over the momentum fraction z that is kept by the quark, weighting the matrix element with the loss of momentum from the leading jet, $p_t(\max[z, 1-z] - 1)$, when the gluon and quark form two separate jets, $\theta > f_{\text{alg}}(z)R$ (throughout this section, θ is to be understood as a boost-invariant angle, $\theta \equiv \Delta R_{qg}$). The quantity $f_{\text{alg}}(z)$ reflects the algorithm's reach, cf. (22, 24) and is given by

$$f(z) = \begin{cases} 1 & k_t, \text{C/A, anti-}k_t, \\ 1 + \min(\frac{z}{1-z}, \frac{1-z}{z}) & \text{SISCone.} \end{cases} \quad (28)$$

Carrying out the integration in a fixed-coupling approximation gives

$$\frac{\langle \delta p_t \rangle_{\text{pert}}}{p_t} = \frac{\alpha_s}{\pi} L_i \ln R + \mathcal{O}(\alpha_s), \quad R \ll 1, \quad (29)$$

with L_i a coefficient that depends on whether it is a quark or a gluon that is the initiating parton (cf. [150]):

$$L_q = C_F\left(2\ln 2 - \frac{3}{8}\right) \simeq 1.01 C_F, \quad (30a)$$

$$L_g = C_A\left(2\ln 2 - \frac{43}{96}\right) + n_f T_R \frac{7}{48} \simeq 0.94 C_A + 0.15 T_R n_f. \quad (30b)$$

One notes that for small R the result of (29) is negative. The unspecified pure $\mathcal{O}(\alpha_s)$ term reflects the result's dependence on the large-angle environment. It can be defined unambiguously only in the threshold limit. Neglecting it, one comes to the conclusion that with $R = 0.4$, a quark-induced jet has, on average, a p_t that is about 4–5% smaller than the initiating parton, while a gluon jet's p_t is 8–10% smaller.

One can also evaluate the small-R limit of the average difference between the p_t of a SISCone jet and (say) a k_t jet (again following [150])

$$\frac{\langle \delta p_t^{\text{SISCone}} \rangle_{\text{pert}} - \langle \delta p_t^{k_t} \rangle_{\text{pert}}}{p_t} = \frac{\alpha_s}{\pi} K_i \quad (31)$$

with

$$K_q = \left(-\frac{15}{16} + \frac{9}{8}\ln 2 + \ln^2 2\right) C_F \simeq 0.323 C_F, \quad (32a)$$

$$K_g = \left(-\frac{1321}{1152} + \frac{133}{96}\ln 2 + \ln^2 2\right) C_A + \left(\frac{241}{576} - \frac{25}{48}\ln 2\right) n_f T_R \simeq 0.294 C_A + 0.057 n_f T_R. \quad (32b)$$

Numerically, $K_i \sim 0.3 L_i$, or equivalently the average behaviour of SISCone and the k_t (and related) algorithms are similar perturbatively when $\ln R_{k_t} \simeq 0.3 + \ln R_{\text{SISCone}}$, that is $R_{k_t} \simeq 1.35 R_{\text{SISCone}}$. This feature was originally observed for a generic cone algorithm in [29].

4.2.2 Jet mass

Partons (except for heavy quarks) are essentially massless. Jets, in particular those with significant substructure, are not. Jet masses are interesting in part because hadronic decays of very high-p_t top quarks and electroweak bosons will be collimated by the Lorentz boost factor and so form a single jet, whose invariant mass might provide a means to identify the origin of the jet (cf. Sect. 5.3).

The simplest quantity to examine is the mean squared invariant mass of a jet. This was studied in a hadron-collider context in [22] and it was pointed out that to first non-trivial order,

$$\langle M^2 \rangle \simeq C \cdot \frac{\alpha_s}{\pi} p_t^2 R^2, \quad (33)$$

where C is a coefficient that depends on the relative fraction of quarks and gluons and on the type of jet algorithm.[23] This is easily derived in the small-R limit, e.g. for a quark-induced jet:

$$\langle M^2 \rangle_{\text{pert}} \simeq \int \frac{d\theta^2}{\theta^2} \int dz \cdot \underbrace{p_t^2 z(1-z)\theta^2}_{M^2} \frac{\alpha_s(\theta(1-z)p_t)}{2\pi} \times P_{qq}(z) \Theta\big(f_{\text{alg}}(z)R - \theta\big). \quad (34)$$

In a fixed-coupling approximation, the results can be summarised as

$$C_q^{k_t} = \frac{3}{8} C_F, \qquad C_g^{k_t} = \frac{7}{20} C_A + \frac{1}{20} n_f T_R, \quad (35)$$

for k_t-like algorithms and

$$C_q^{\text{SIS}} = C_F\left(\frac{7}{4} - \frac{3}{2}\ln 2\right) \simeq 0.71 C_F, \quad (36a)$$

[23] Results for jet masses at $\mathcal{O}(\alpha_s)$ are sometimes quoted as being NLO. It would be more accurate to state that they are LO results, since $\mathcal{O}(\alpha_s)$ is the first order at which the mass is non-zero. True NLO results would go up to $\mathcal{O}(\alpha_s^2)$. Jet masses can be calculated to NLO in dijet events using the 3-jet NLO component of a program like NLOJET++ [49, 50].

$$C_g^{\mathrm{SIS}} = C_A\left(\frac{49}{24} - 2\ln 2\right) + n_f T_R\left(\ln 2 - \frac{7}{12}\right)$$
$$\simeq 0.66 C_A + 0.11 n_f T_R, \tag{36b}$$

for SISCone type algorithms (consistent with the observation that k_t and SISCone type algorithms behave similarly for $R_{k_t} \simeq 1.35 R_{\mathrm{SISCone}}$). These results coincide roughly with the rule of thumb given in [22] that to within 25%, $\sqrt{\langle M^2\rangle} \simeq 0.2 R p_t$, with the exact value depending on the mix of quarks and gluons, and subject also to finite-R effects as well as threshold modifications for high jet transverse momenta. Reference [22] also emphasises that (36) will be subject to significant higher-order corrections, associated with the fact that SISCone's effective clustering reach is somewhat smaller for $z \simeq 1/2$ than the two-parton reach $f(z = 1/2) \simeq 2$, cf. Fig. 13. This is a point of some importance, and one should never lose sight of the fact that *all* the results given above are based on LO perturbation theory and can be quite noticeably affected by higher-order terms.

When using jet masses for tagging hadronically-decaying boosted heavy objects, it is also of interest to know the distribution of the jet mass. At leading order, $d\sigma/dM^2$ diverges with a logarithmic enhancement $\sim \frac{\alpha_s}{M^2} \ln \frac{R^2 p_t^2}{M^2}$ for small masses (cf. the analytical result in [151, 152]). Higher-order terms are enhanced by further powers of $\ln R p_t/M$ and can in principle be resummed. Analytical results exist however only for certain specific cases in e^+e^- [153–155] and DIS [156] and have not been extended to hadron-collider jets, in part because of issues such as the non-trivial process dependence [157, 158] and jet-algorithm dependence [159, 160] of soft logarithms associated with delimited ("non-global" [155, 161, 162]) regions of phase-space.

4.2.3 *Other properties*

Many other properties of jets can be predicted perturbatively. Among them one may mention the scale associated with subjets within a jet [27, 70, 163], multiplicities of subjets [164, 165] and of particles (see e.g. [166] and references therein) and jet shapes [43] (radial moments and the fraction of energy that is within a certain central core of the jet). As well as providing important handles on our understanding of the QCD dynamics within jets, these observables can also be useful for example in discriminating quark and gluon jets. One such application is given in [73].

4.3 Hadronisation

The properties of jets are affected not just by perturbative radiation, but also by low-p_t, non-perturbative effects. It is useful to divide such effects into two classes: hadronisation and the underlying event. Hadronisation corresponds to the transition between partons and hadrons, and occurs in all high-energy QCD processes (e^+e^-, DIS and pp). The underlying event (UE) consists of the multiple low-p_t interactions that occur between the two hadron remnants in a pp or a resolved γp collision. Physically, in a pp collision, hadronisation and the UE cannot be unambiguously separated (the question of what hadronises depends on what has interacted). Nevertheless it is useful to consider them separately, because they affect jets in rather different ways. Hadronisation is discussed here, and the UE in Sect. 4.4.

With current techniques, the impact of hadronisation cannot be calculated (or even easily defined) from first principles. However, in the mid 1990s, methods were developed [167–172] (reviewed in [173]) that allowed one to predict the main features of hadronisation, based on ambiguities that arise in perturbative calculations related to the Landau pole.

A somewhat oversimplified statement of the idea is that if a perturbative calculation involves an integral over $\alpha_s(\mu)$, then one can estimate the size of the non-perturbative contribution by replacing $\alpha_s(\mu)$ with a purely non-perturbative piece $\alpha_s^{\mathrm{NP}}(\mu) = \Lambda\delta(\mu - \Lambda)$ where Λ is commensurate with the Landau scale. So, for example, to estimate the non-perturbative correction to a quark jet's transverse momentum in the small-R limit one takes (27) and writes

$$\langle \delta p_t\rangle_{\mathrm{NP}} \sim p_t \int \frac{d\theta^2}{\theta^2} \int dz \big(\max[z, 1-z] - 1\big) \times \frac{\alpha_s^{\mathrm{NP}}(\theta(1-z)p_t)}{2\pi} P_{qq}(z)\Theta\big(\theta - f_{\mathrm{alg}}(z)R\big) \tag{37a}$$
$$\sim p_t \int_{R^2} \frac{d\theta^2}{\theta^2} \int dz (z-1) \frac{\alpha_s^{\mathrm{NP}}(\theta(1-z)p_t)}{2\pi} \frac{2C_F}{1-z} \tag{37b}$$
$$\sim -\frac{2C_F\Lambda}{\pi R}, \tag{37c}$$

where in the second line one makes use of the knowledge that the δ-function will select $1 - z = \Lambda/(\theta p_t) \ll R$. For gluon jets the result is the same except for the replacement $C_F \to C_A$. A crucial idea in calculations such as (37) is that one can apply the same procedure to a wide range of observables and the same value of Λ should hold for each.[24] This is known as "universality". Universality has been investigated in some detail for event shapes in e^+e^- and DIS collisions and there is some debate as to just how well it works (e.g. [174] as compared to [175]). However for the purpose of understanding the essentials of the hadronisation of jets it is probably an adequate assumption, and one can take $\Lambda \simeq 0.6$ GeV.

[24] As long as they all share the same p_t-dependence in the infrared—a less oversimplified formulation of the idea in (37) is that observables with the same IR p_t-dependence are all sensitive to a common moment of the coupling in the infrared.

The basic result that hadronisation removes transverse momentum $\mathcal{O}(\Lambda/R)$ from a jet was presented in [167] (and could be deduced from the results of [43]; hadronisation as a shift in p_t was also discussed in [176]). Aside from the quark/gluon jet difference it is a process-independent result, as long as R is much smaller than the angle between jets. It seems, however, that this result had largely been forgotten until the advent of a more recent calculation [150], which goes beyond the small R limit (in a threshold approximation for dijet production). As an example, the result for the case of the $qq' \to qq'$ subprocess of dijet production is

$$\langle \delta p_t \rangle_{\mathrm{NP}}^{qq'\to qq'} = \frac{\Lambda}{\pi}\left[-\frac{2}{R}C_F + \frac{1}{8}R\left(5C_F - \frac{9}{N_c}\right) + \mathcal{O}(R^2)\right]. \tag{38}$$

A feature of (38) is that the first correction to the $1/R$ term is fairly small even for $R = 1$ (less than 20%). Consequently for most purposes it is adequate to take just the $1/R$ piece. This is what is done in Fig. 14, whose lower set of curves in each quadrant compares the hadronisation correction as deduced from Herwig (solid lines) and from Pythia (dashed lines) with the $1/R$ part of the analytical expectation given above (dot-dashed lines). Generally speaking the agreement is good, even in the large-R region where the $1/R$ approximation might be expected to break down.

To obtain a closer relation to studies of hadronisation for e^+e^- and DIS event shapes (for a review see e.g. [178]), one may replace

$$\frac{\Lambda}{\pi} \to \frac{2}{\pi}\mathcal{M}\mathcal{A}(\mu_I). \tag{39}$$

Here $\mathcal{A}(\mu_I)$ is defined as the integral over a non-perturbative contribution to α_s, $\delta\alpha_s$, up to some infrared matching scale μ_I (usually 2 GeV), $\mathcal{A}(\mu_I) = \frac{1}{\pi}\int_0^{\mu_I} d\kappa_t \delta\alpha_s(\kappa_t)$. Following [168], it is often written in terms of yet another parameter $\alpha_0(\mu_I)$, the integral of the full coupling in the infrared $\alpha_0(\mu_I) = \int_0^{\mu_I} d\kappa \alpha_s(\kappa)$, via

$$\mathcal{A}(\mu_I) = \frac{1}{\pi}\mu_I\left[\alpha_0(\mu_I) - \alpha_s(p_t) - \frac{\beta_0}{2\pi}\left(\ln\frac{p_t}{\mu_I} + \frac{K}{\beta_0} + 1\right)\alpha_s^2(p_t)\right], \tag{40}$$

where $K = C_A(\frac{67}{18} - \frac{\pi^2}{6}) - \frac{5}{9}n_f$, and the subtracted terms in (40) remove double counting with contributions already included in NLO calculations. Fits to data in DIS and e^+e^- usually give $\alpha_0(2\ \mathrm{GeV}) \simeq 0.5$.

The factor $\mathcal{M}$ in (39) is known as the Milan factor [179–183]. It accounts for the corrections that arise when one considers two non-perturbative "gluons" rather than a single one. For all known event shapes, $\mathcal{M}$ has been calculated to be $\mathcal{M} = 1.49$—this "universality" of the Milan factor is due to the fact that event-shape observables are effectively linear in the momenta of soft gluons [180]. For jets it had been argued that only the anti-k_t algorithm satisfied this linearity property [37]. This was recently confirmed in an explicit calculation by Dasgupta and Delenda [184], who showed that the k_t algorithm instead has $\mathcal{M}_{k_t} = 1.01$. This smaller value is consistent with the somewhat reduced hadronisation corrections observed for the k_t algorithm compared to anti-k_t in Fig. 14, though a detailed quantitative comparison has not yet been performed. Future calculations of the Milan factor for C/A and SISCone will

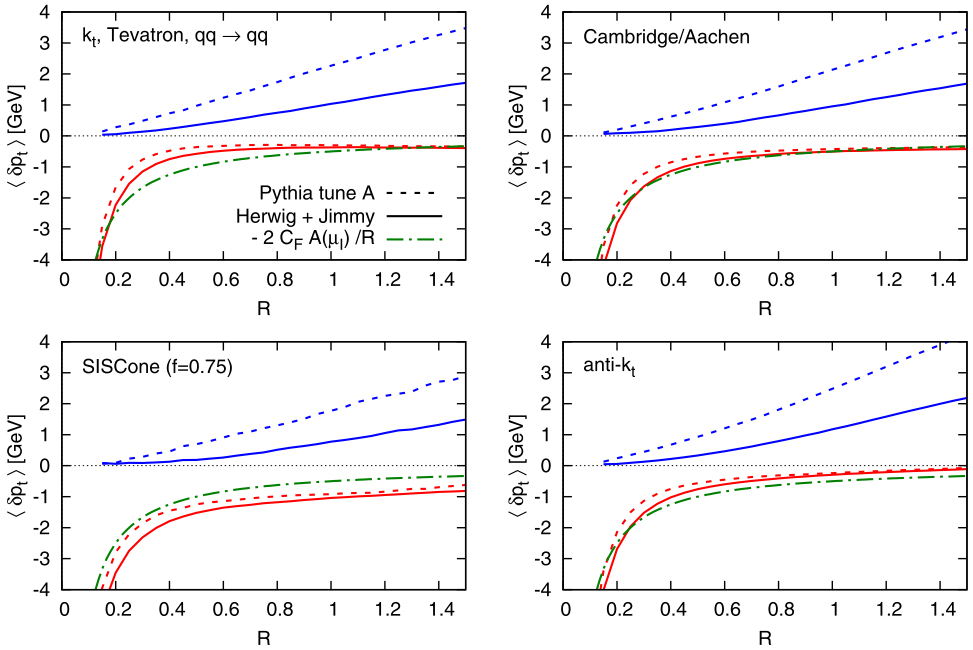

Fig. 14 Modification of the p_t of jets due to the underlying event (*upper curves* in each plot) and hadronisation (*lower curves*), for $qq \to qq$ scattering at the Tevatron Run II ($p\bar{p}$, $\sqrt{s} = 1.96$ TeV), comparing `Pythia` 6.412 [111] (tune A, *dashed lines*) and `Herwig` 6.510 [112, 113] with `Jimmy` 4.3 [177] (*solid lines*). In the case of hadronisation, the Monte Carlo outputs are compared to the $1/R$ part of the analytical result, (38) (*dot-dashed lines*). Dijet events are selected containing an underlying $qq \to qq$ scattering, and with the requirement that at parton-shower level the hardest jet has 55 GeV $< p_t <$ 70 GeV. The non-perturbative corrections shown correspond to the average for the two hardest jets. Taken from [150]

hopefully also fit in with the pattern of slight differences that are observed in Fig. 14 with respect to the algorithm-independent behaviour that is given by (37c, 38).

A point emphasised in [176] is that even if the non-perturbative modification of a jet's p_t is rather modest, $\mathcal{O}(1\ \text{GeV})$, it can nevertheless have a significant impact on steeply falling cross sections. Given a jet p_t spectrum that falls as p_t^{-n}, the full result for the jet spectrum can be expressed in terms of the perturbative spectrum and the non-perturbative shift as

$$\frac{d\sigma_{\text{full}}}{dp_t}(p_t) \to \frac{d\sigma_{\text{PT}}}{dp_t}\big(p_t - \langle \delta p_t \rangle_{\text{NP}}\big) \simeq \frac{d\sigma}{dp_t}(p_t) \cdot \left(1 - n\frac{\langle \delta p_t \rangle_{\text{NP}}}{p_t}\right). \tag{41}$$

Thus for typical values of n in an inclusive-jet spectrum, a 2% change in p_t can lead to a 10–15% change in the cross section (this observation holds also for p_t shifts due to the underlying event, which are discussed below). These are the order of magnitudes often seen in experiments' Monte Carlo studies of hadronisation, whose results also cast light on the R-dependence of non-perturbative effects [79] and on the differences between jet algorithms [3, 31, 32, 77, 185].

A final point is that the above methods can also be used to calculate the non-perturbative corrections to the squared jet mass,

$$\langle \delta M^2 \rangle_{\text{NP}} \simeq \frac{2C_F}{\pi} \Lambda p_t \big(R + \mathcal{O}\big(R^3\big)\big) \equiv \frac{4C_F}{\pi} \mathcal{MA}(\mu_I)\, p_t \big(R + \mathcal{O}\big(R^3\big)\big), \tag{42}$$

where the R^3 terms have small coefficients [150]. Note that for jet algorithms other than anti-k_t, the Milan factors for $\langle \delta p_t \rangle_{\text{NP}}$ and $\langle \delta M^2 \rangle_{\text{NP}}$ will not be the same.

4.4 UE, pileup, jet areas

While the process of hadronisation may well be reasonably universal between e^+e^-, DIS and pp collisions, the latter have the additional feature of the "underlying event" (UE), which can be thought of as the semi- or non-perturbative interactions that occur between hadron remnants in a pp collision. Our understanding of the UE is somewhat less developed than that of hadronisation. One way that one can model it is by saying that it induces an extra amount of transverse momentum per unit rapidity, Λ_{UE}.[25] In this case a jet should receive a position contribution to its p_t from the UE that is proportional to the region of the rapidity-azimuth region that it covers, i.e. $\sim R^2$:

$$\langle \delta p_t \rangle_{\text{UE}} \simeq \Lambda_{\text{UE}} R J_1(R) = \Lambda_{\text{UE}} \left(\frac{R^2}{2} - \frac{R^4}{8} + \cdots\right), \tag{43}$$

where terms at R^4 and beyond [150] hold for the a 4-vector (E) recombination scheme. The corresponding formula for the change to the squared jet mass is

$$\langle \delta M^2 \rangle_{\text{UE}} \simeq \Lambda_{\text{UE}} p_t \left(\frac{R^4}{4} + \frac{R^8}{4608} + \cdots\right). \tag{44}$$

In Fig. 14, the upper curves represent the UE contributions to the p_t of Tevatron jets, as determined from the UE models in Pythia [111] (tune A [57]) and Jimmy [177] (with the ATLAS tune [57]). Three features are worth commenting on: (a) the curves agree with a rough R^2 dependence, (b) the two models disagree by a factor of two even though they have both been tuned to Tevatron data and (c) the value that one extracts for Λ_{UE}, in the range 2–4 GeV, is quite a bit larger than the p_t per unit rapidity that would be generated by normal hadronisation for a quark or gluon dipole stretched between the two beams (respectively 0.5 GeV and 1 GeV).

For the LHC, the models predict an even larger contribution from the UE, cf. Fig. 15 from which one deduces $\Lambda_{\text{UE}} \sim 10$ GeV, and for a large range of R it dominates over hadronisation. Furthermore pileup (multiple pp collisions in a given beam crossing) is expected to add up to an extra 100 GeV of soft "junk" per unit rapidity.

All of this implies that it is important to understand in more detail how jets are affected by "low-p_t" noise that is roughly uniformly distributed in rapidity. Two things can

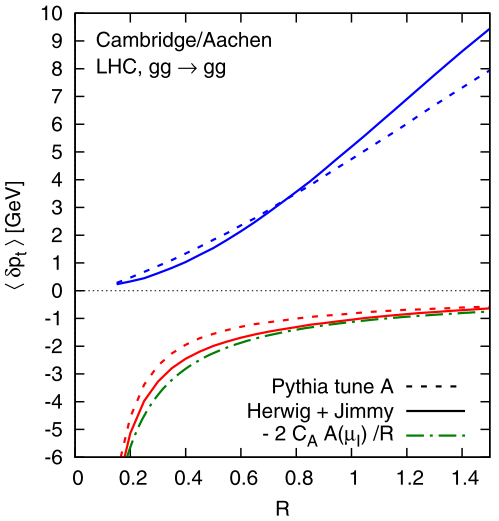

Fig. 15 Similar to Fig. 14, but for just one algorithm, at the LHC (pp, $\sqrt{s} = 14$ TeV) rather than the Tevatron, and for $gg \to gg$ collisions (rather than $qq \to qq$). Taken from [150]

[25] Later we will talk of transverse momentum ρ per unit area on the rapidity–azimuth plane; $\Lambda_{\text{UE}} = 2\pi\rho_{\text{UE}}$.

happen: firstly, the soft junk can end up in the jet—to study this it is useful to refer to the "jet area" [41], a measure of the extent of the region in rapidity and azimuth over which a jet captures UE or pileup; secondly, the presence of the UE (and pileup) can modify the way non-UE particles get clustered into jets, a process named back-reaction in [41].

4.4.1 Jet areas

A jet's "area" is a way of measuring its susceptibility to contamination from soft radiation. Two definitions were proposed for it in [41] and the results quoted here are all taken from there. The *passive* area is a measure of the jet's susceptibility to pointlike radiation. One introduces a "ghost" particle, $g(y,\phi)$ with infinitely low transverse momentum and situated at some rapidity and azimuth y,ϕ, and then defines the area for jet J in terms of the region in y,ϕ over which the ghost is clustered with the jet:

$$a(J) \equiv \int dy\, d\phi f(g(y,\phi), J),$$
$$f(g,J) = \begin{cases} 1, & g \in J, \\ 0, & g \notin J. \end{cases} \tag{45}$$

For an infrared safe algorithm J itself is of course unaffected by the addition of the infinitely soft particle g. If J consists of a single (hard) particle then its passive area is πR^2 for all algorithms.

An alternative definition of area is the *active* area, which measures a jet's susceptibility to diffuse radiation. Here one imagines a large number of very soft ghost particles, uniformly distributed in rapidity and azimuth (with some optional randomness). One can define a jet's active area for a given ensemble $\{g_i\}$ of ghost particles,

$$A\big(J \,\big|\, \{g_i\}\big) = \frac{\mathcal{N}_g(J)}{\nu_g}, \tag{46}$$

where $\mathcal{N}_g(J)$ is the number that end up in the jet and ν_g their number density in y,ϕ. One then often considers the average active area, an average over many ghost ensembles

$$A(J) = \lim_{\nu_g\to\infty} \big\langle A\big(J \,\big|\, \{g_i\}\big)\big\rangle_g, \tag{47}$$

taken in the limit of many ghost particles (with fixed infinitesimal total p_t per unit area).[26] A key difference between the passive and active areas, is that in the latter, with many ghosts, the ghosts can cluster not only with the real event particles but also with other ghosts and this modifies the result for the area.

Given that one usually imagines the UE and pileup as being fairly diffuse (and UE/pileup particles can cluster between themselves), it is the active area that is probably the most natural measure of sensitivity to the UE or pileup. However, there are two reasons why it is useful to consider both passive and active areas. Firstly, the UE is actually somewhere in between diffuse and pointlike and a full understanding of UE contamination benefits from considering both limits. Secondly, of the two, the passive area is often simpler to treat analytically.

Let us illustrate these points for the case of a jet that has just one, hard particle (1PJ). As mentioned above, the passive area is πR^2. This statement holds for all jet algorithms. The average active area and its standard deviation over ghost ensembles are given in Table 4. For one algorithm, anti-k_t, the active area is identical to the passive area and $A(J\,|\,\{g_i\})$ is independent of the particular ghost ensemble. This can be seen as advantageous, insofar as it implies that the contamination of an anti-k_t jet will be independent of the detailed structure of the UE or pileup.

SISCone also has the property that its active area is independent of the ghost ensemble, but the actual value is much smaller than for the passive area (a consequence of the split–merge step which eats away from the main jet). This is good insofar as it means less overall sensitivity to noise, but bad because the exact amount of contamination will depend on the details of just how pointlike the UE or pileup is (a feature that therefore needs to be well tuned in Monte Carlo programs).

The k_t and C/A algorithms are unlike the other two in that $A(J\,|\,\{g_i\})$ depends significantly on the exact set of ghosts, as indicated by the standard deviations in Table 4, which are about one third of the average area. The non-zero standard deviation arises because ghosts tend to cluster between themselves before clustering with the hard particle, and slight shifts in the layout of the ghosts lead to significant differences in the final clustering. This implies an extra source of fluctuations from UE and pileup contamination: one has not only the intrinsic fluctuations in the amount of p_t in a given event's UE/pileup, but also a fluctuation in how much of the UE/pileup the jet actually captures. The consequent (moderate) worsening of the kinematic resolution of the jets seems to be an inevitable feature of jet algorithms with a QCD-motivated hierarchical clustering sequence: the algorithm is trying to assign meaningful QCD substructure to the jet, and the absence of such substructure in the UE/pileup induces a degree of randomness in the outcome of the clustering (this is related also to the irregularity of the jet boundaries in Fig. 7).

The above results hold for 1-particle jets (1PJ). Real jets are more complex because QCD branching gives them substructure. To a first approximation, one can examine what

[26] These two areas are strictly speaking both "scalar" areas. Passive and active areas also come in "4-vector" variants, which take into account the ghosts' full impact on a jet's 4-vector. Though useful for subtracting pileup and other noise, most of their features are quite similar to those of scalar areas, so we shall not discuss them separately in this section.

Table 4 The average active area $A(1\text{PJ})$, (47), for an isolated one-particle jet in various jet algorithms and its standard deviation $\Sigma(1\text{PJ})$ over ghost ensembles. Results are also given for the area of jets that are purely composed of ghosts (GJ), in the cases where this makes sense (in SISCone the result depends critically on the distribution of ghosts, while for anti-k_t the distribution of ghost-jet areas has two peaks, one at 0, the other at πR^2)

Algorithm	k_t	C/A	SISCone	anti-k_t
$\frac{A(1\text{PJ})\pm\Sigma(1\text{PJ})}{\pi R^2}$	0.812 ± 0.277	0.814 ± 0.261	$\frac{1}{4} \pm 0$	1 ± 0
$\frac{A(\text{GJ})\pm\Sigma(\text{GJ})}{\pi R^2}$	0.554 ± 0.174	0.551 ± 0.176	–	–

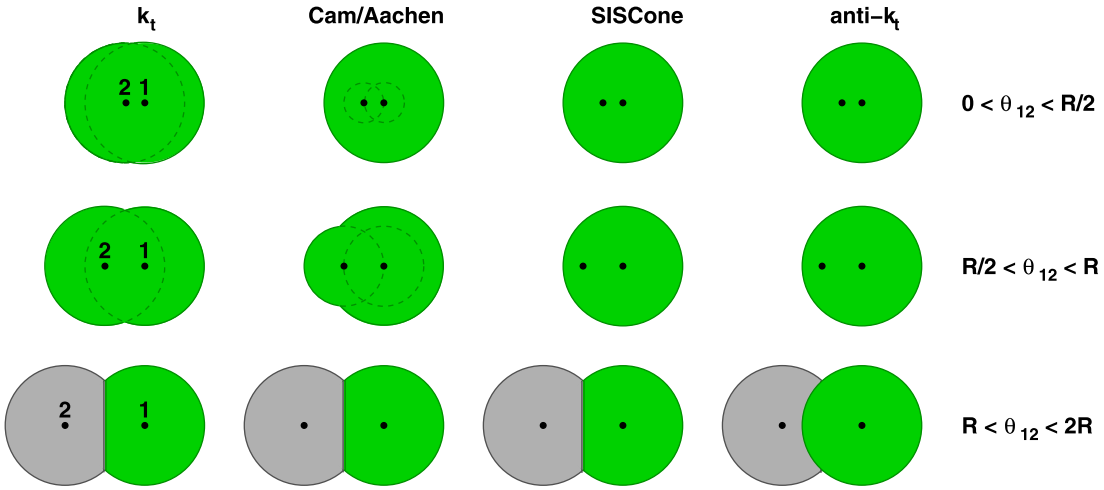

Fig. 16 Schematic representation of the passive area of a jet containing one hard particle "*1*" and a softer one "*2*", $a_{\text{JA},R}(\theta_{12})$, for various separations between them and for the usual 4 jet algorithms. Different *shadings* represent distinct jets. Figure adapted from [41]

happens if one adds a single soft gluon at an angle θ with respect to the jet axis. This gives a modified jet area, e.g. $a_{\text{JA},R}(\theta)$ in the passive case, illustrated in Fig. 16. After integration over the (soft, collinear) QCD branching matrix element one obtains

$$\langle a_{\text{JA},R}\rangle = \pi R^2 + d_{\text{JA},R}\frac{C_1}{\pi b_0}\ln\frac{\alpha_s(Q_0)}{\alpha_s(Rp_{tJ})}, \tag{48}$$

where the anomalous dimension (i.e. the p_t-dependent rightmost term) stems from the integration over the energy of the soft gluon, and its coefficient is given by

$$d_{\text{JA},R} = \int_0^{2R}\frac{d\theta}{\theta}\big(a_{\text{JA},R}(\theta) - \pi R^2\big). \tag{49}$$

In (48) $b_0 = \frac{11C_A - 2n_f}{12\pi}$ and C_1 is the colour factor of the hard particle in the jet (C_F or C_A). The scale Q_0 is a non-perturbative cutoff scale, introduced by hand, and which is necessary because jet areas are not IR safe (except in the case of anti-k_t). The physically natural value for Q_0 will depend on the characteristics of the UE/pileup: given an amount of transverse momentum ρ per unit area, one expects Q_0 to be $\mathcal{O}(\rho R^3)$.[27]

Formulae analogous to (48, 49) hold for the active area ($\pi R^2 \to A(1\text{PJ})$, $d \to D$), and also for the standard deviations $\sigma_{\text{JA},R}$ of the passive area,

$$\big\langle\sigma^2_{\text{JA},R}\big\rangle = s^2_{\text{JA},R}\frac{C_1}{\pi b_0}\ln\frac{\alpha_s(Q_0)}{\alpha_s(Rp_{t1})},$$
$$s^2_{\text{JA},R} = \int_0^{2R}\frac{d\theta}{\theta}\big(a_{\text{JA},R}(\theta) - \pi R^2\big)^2 \tag{50}$$

and the active area

$$\big\langle\Sigma^2_{\text{JA},R}\big\rangle = \Sigma^2_{\text{JA},R}(1\text{PJ}) + S^2_{\text{JA},R}\frac{C_1}{\pi b_0}\ln\frac{\alpha_s(Q_0)}{\alpha_s(Rp_{t1})}. \tag{51}$$

The various coefficients are all summarised in Table 5, while in Fig. 17 the resulting predictions are compared to jet areas measured in Herwig Monte Carlo simulations (with Q_0 fitted on a case-by-case basis). One sees how k_t has

[27] That is: a transverse momentum with respect to the beam $\mathcal{O}(\rho R^2)$, which translates to a transverse momentum with respect to the jet $\mathcal{O}(\rho R^3)$, it being the latter that corresponds to Q_0 in (48) etc.

Table 5 A summary of main area results for our four jet algorithms: the passive (a) and active (A) areas for 1-particle jets (1PJ), the magnitude of the passive/active area fluctuations (σ, Σ), followed by the coefficients of the respective anomalous dimensions (d, D; s, S), in the presence of perturbative QCD radiation. All results are normalised to πR^2, and rounded to two decimal figures. For algorithms other than anti-k_t, active-area results hold only in the small-R limit, though finite-R corrections are small

	a(1PJ)	A(1PJ)	σ(1PJ)	Σ(1PJ)	d	D	s	S
k_t	1	0.81	0	0.28	0.56	0.52	0.45	0.41
Cam/Aachen	1	0.81	0	0.26	0.08	0.08	0.24	0.19
SISCone	1	1/4	0	0	−0.06	0.12	0.09	0.07
anti-k_t	1	1	0	0	0	0	0	0

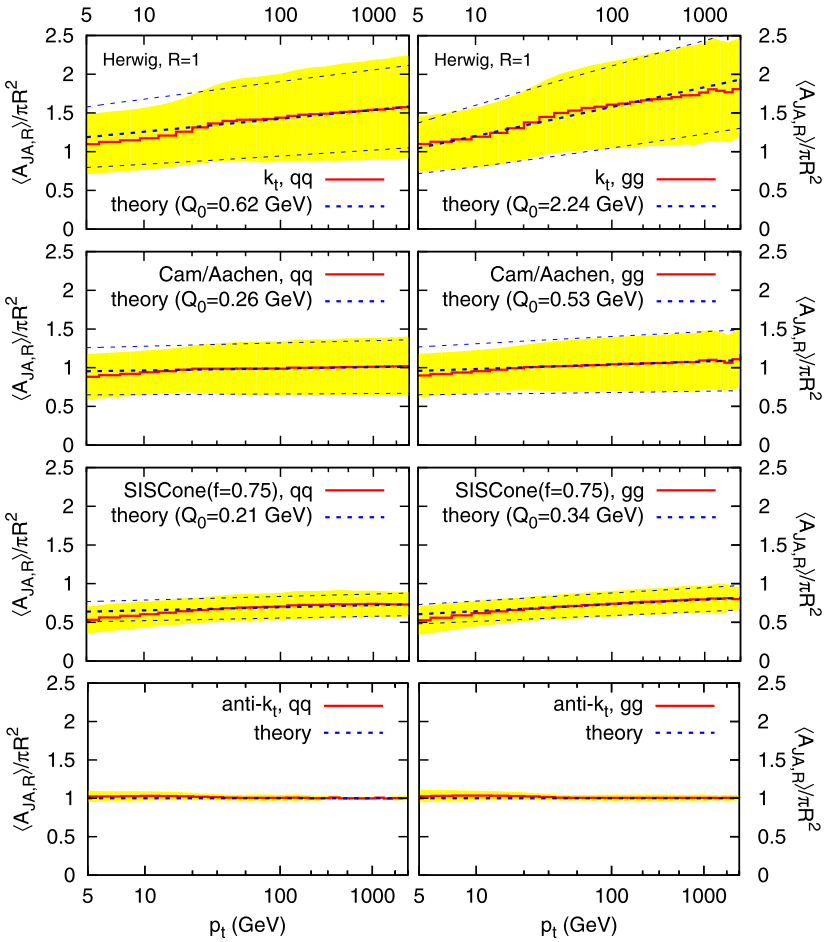

Fig. 17 Average active area and standard deviation (*solid lines* and band) in simulated Herwig 6.5 events (default UE) compared to analytical expectations (*dashed lines*) with a fitted Q_0 value; shown separately for four algorithms and for $qq \to qq$ and $gg \to gg$ events. Adapted from [37, 41]

a fairly large area, large fluctuations and strong p_t dependence, C/A an area $\sim\pi R^2$ with moderate fluctuations and little p_t dependence, SISCone an area smaller than πR^2 (but still larger than $\pi R^2/4$), small fluctuations and moderate p_t dependence and, finally, anti-k_t an area very close to πR^2, with almost no fluctuations or p_t dependence. A corollary of the k_t algorithm's strong p_t dependence is that is that if one increases the UE/pileup density ρ, the jet area will *shrink*, a consequence of the presence of $\alpha_s(Q_0)$ in (48), with $Q_0 \sim \rho R^3$.

A final comment concerns the relation between passive and active areas. They differ in sparse events because there is an ambiguity in how one assigns "empty" parts of the event to the jets—the two kinds of area simply consist of different prescriptions for doing this. In very dense events, where the jet boundaries are well delimited by the event's particles, the passive and active areas become identical (as should any other sensible definition of area).

4.4.2 *Back reaction*

Suppose you have an event with particles numbered 1–100, and in which numbers 1–10 end up in jet a. Now immerse that event in a soft background with *finite* p_t. The back-

ground will add its own particles to the jet, but it can also alter the behaviour of the clustering with respect to the original particles. So maybe only particles 1–9 would end up in jet a, or maybe jet a would additionally contain particle 11. This is back reaction.

The study of back reaction bears similarities to that of jet areas: in particular one can study it with pointlike noise, or with diffuse noise. The former can be dealt with analytically, whereas the latter is tractable only numerically.

Full details are given in [41], but the basic analytical result is that the average net change in a jet's p_t due to back reaction in the presence of diffuse noise has an asymptotic behaviour of the form

$$\left\langle \Delta p_{t,\mathrm{JA},R}^{BR} \right\rangle \simeq \mathcal{B}_{\mathrm{JA},R}\rho \cdot \frac{C_1}{\pi b_0} \ln \frac{\alpha_s(\rho R^3)}{\alpha_s(p_{t1}R)} + \mathcal{O}(\alpha_s \rho), \qquad (52)$$

where the coefficients are $\mathcal{B}_{k_t,R} \simeq \mathcal{B}_{\mathrm{C/A},R} \simeq -0.10\pi R^2$ and $\mathcal{B}_{\mathrm{SISCone},R} = \mathcal{B}_{\text{anti-}k_t,R} = 0$. In practice, given the small size of the $\mathcal{B}$ coefficients (and the fact that the $\frac{C_1}{\pi b_0} \ln \frac{\alpha_s(\rho R^3)}{\alpha_s(p_{t1}R)}$ factor is often $\mathcal{O}(1)$), the term of order $\alpha_s\rho$ is usually as important as the formally leading term. Both terms are generally small compared to the direct contamination of the jet from UE/pileup noise, $\mathcal{O}(\rho \cdot \pi R^2)$.

The concrete situation for the various algorithms is illustrated in Fig. 18, which shows the distribution of back reaction for a high-p_t jet immersed in pileup ($\rho \sim 15$ GeV). In about 1% of events one has a back reaction of order of ρ, except for anti-k_t, whose back reaction is far more suppressed. Figure 18 confirms that back reaction is a modest effect compared to the direct contamination of a jet from background noise. Essentially it is relevant only when trying to determine a jet's energy to very high precision, or in the presence of extreme noise (as in heavy-ion collisions).

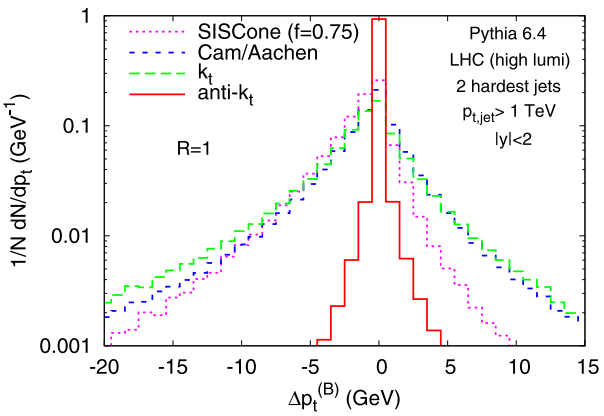

Fig. 18 The distribution of back reaction for high-p_t jets ($p_t > 1$ TeV) immersed in pileup corresponding to high-luminosity LHC running ($\rho \sim 15$ GeV per unit area). Simulated with Pythia 6.4 and shown for 4 algorithms

4.5 Summary

We have seen a number of results here. Let us summarise them:

- Most jet algorithms will cluster a pair of particles if they are within R of each other; SISCone reaches out to $2R$ (somewhat less in real events) if the two particles are of similar hardness.
- At small R, a jet's p_t is reduced relative to a parton's by an amount $\sim\alpha_s p_t \ln 1/R$. With $R = 0.4$, that is of order 5% for a quark, 10% for a gluon. The mean squared jet mass goes as $\alpha_s R^2 p_t^2$.
- Hadronisation reduces a quark jet's p_t by an amount ~ 0.5 GeV$/R$ at small R (roughly double this for a gluon jet), with modest differences between algorithms.
- The underlying event and pileup induce contaminations proportional to $\sim R^2$. Because the intrinsic energy scale associated with the underlying event (p_t per unit rapidity of 10–15 GeV at the LHC) is an order of magnitude larger than that from hadronisation (and pileup is yet another order of magnitude larger), one should devote special effort to understanding different jet algorithms' susceptibility to them. This can be done via the concept of jet areas. The k_t algorithm has the largest jet area (with noticeable p_t dependence and fluctuations), SISCone the smallest, and anti-k_t has the most stable jet area, nearly always πR^2.
- The UE (and pileup) modifies how an event's original particles get clustered into jets—this is back reaction. Its impact is an order of magnitude smaller than the direct contamination, but can be relevant for precision studies. It is essentially zero for the anti-k_t algorithm.

The differing impact of various physical effects across algorithms and as a function of R might seem like a source of considerable complication in jet finding, and in some ways it is. However, it can also be used to our advantage. One example is in studies like top-mass measurements that are in part limited by physics-modelling systematics. If one uses multiple jet definitions with different sensitivities to UE/pileup, gluon radiation and hadronisation, and then finds that the final Monte Carlo-corrected top mass is independent of the choice of jet definition, then this provides a powerful cross check of the physics modelling within the Monte Carlo generator. And, in the next section, we shall see how our understanding of jets can help guide the choice of "optimal" jet definitions for various reconstruction tasks.

5 Using jets

So far at hadron colliders, jets have mostly been used as fixed objects—universal, if imperfect proxies for partons. Generally, experiments have settled on one or two main jet

definitions for nearly all their analyses: for example at CDF the Midpoint algorithms with $R = 0.7$ for most inclusive-jet studies,[28] and JetClu with $R = 0.4$ for top-quark physics and for searches.

Such a strategy was probably not too far from optimal at the Tevatron, where most of the physics being looked at is in a modest range of scales, from a few tens of GeV to a few hundred, and pileup is present, but not overwhelming.

The LHC, in contrast, will cover a broader range of scales from a few tens of GeV to a few TeV, events with multiple simultaneous scales will be common (e.g. EW bosons and top quarks with $p_t \gg m$) and pileup will range from almost none to 20–30 simultaneous pp interactions in each bunch crossing. This begs the question: could analyses benefit from more flexible jet finding?

The work examined below tries to examine this question by concentrating on two characteristic types of analysis—standard mass reconstructions, with attention also to the issue of pileup; and the task of identifying highly boosted massive particles. Our discussion will be restricted to studies at "particle level" (also referred to as hadron level) and will not go into detector-specific effects. For a discussion of the latter, see for example [16, 137, 186].

5.1 Choosing an algorithm and a radius

Which jet algorithm is "best"? This is a widespread question, and a natural follow-on question is "which R should one use"? This question cannot be answered in isolation. It inevitably goes with the issue of what one wants to use the jet algorithm for.

The most reliable way of answering the question is to carry out a detailed study of the process one is interested in, with many jet algorithms, and many R values for each. Then one may devise some "quality measure" and establish which algorithm optimises it. This can be a big job (4 algorithms, maybe $10R$ values) and is seldom done in a systematic way. In what follows we'll see how even crude analytical estimates can give guidance on the question, and then examine some Monte Carlo studies.

5.1.1 Analytical study

In a QCD measurement like that of the inclusive jet spectrum, one will compare data to a perturbative QCD prediction. At moderate p_t, one of the largest ambiguities in the comparison comes from non-perturbative effects (since perturbative effects are calculable to some accuracy), often comparable with PDF and experimental uncertainties.

Table 6 R values that minimise the two non-perturbative contributions in various circumstances for Tevatron and LHC running, based on (53), with $2\mathcal{M}\mathcal{A}(\mu_I)/\pi = 0.19$ GeV and $\Lambda_{\rm UE} = 4$ GeV (10 GeV) at the Tevatron (LHC)

	quark jets	gluon jets
Tevatron	0.56	0.73
LHC (14 TeV)	0.41	0.54

Therefore one might want to choose an algorithm and R value that minimise hadronisation and UE contributions. One can choose to ignore the relatively modest differences between algorithms, and just take the analytic formulae of Sects. 4.3, 4.4. From these, one deduces a value of R that minimises the squared sum of hadronisation and UE pieces [150],

$$R = \sqrt{2}\left(\frac{2C_i\mathcal{M}\mathcal{A}(\mu_I)}{\pi\Lambda_{\rm UE}}\right)^{1/3}, \tag{53}$$

where only the leading R terms have been used, C_i is the appropriate colour factor (C_F, C_A) for quark/gluon jets, and we have assumed a jet area of πR^2 for simplicity The resulting numerical R values are given in Table 6.[29]

If one uses jets for kinematic reconstruction, the considerations are different: when trying to identify a mass peak, for example, it is of little consolation that one can calculate the perturbative degradation of the peak if that degradation in any case causes the peak to disappear under the background. A *very* crude estimate of what goes on can be had by assuming that fluctuations in a jet's momentum due to perturbative radiation, hadronisation and UE are each proportional to their average effect. Adding the squared averages in quadrature gives Fig. 19 (left) and the minimum provides an idea of the optimal R (as before, ignore differences between algorithms), and illustrates how the main relevant interplay is between perturbative radiation and the UE. The right-hand plot shows how the resulting optimal R varies with p_t: gluon jets and high p_t jets prefer larger R values (because of the greater relative importance of perturbative radiation), while one needs smaller R values at the LHC than at the Tevatron (the former has more UE).

While Fig. 19 is useful for understanding general trends (notably the need for large R at high p_t), it is not quantitatively reliable: the fluctuations in a jet's kinematics and the mean energy-loss due to gluon radiation are for example *not* proportional to each other; also, for $R \sim 1$, the $\alpha_s p_t \ln R$ approximation for perturbative energy loss is in itself poor since it neglects terms of $\mathcal{O}(\alpha_s p_t)$; finally, for simplicity,

[28] Though in recent years they also studied the k_t algorithm with three R values [1, 79], and this probably played a key role in convincing the LHC experiments that the k_t algorithm is viable.

[29] In practice, an additional issue is that perturbative uncertainties from missing higher-order contribution may also depend on R. The interplay between this and non-perturbative uncertainties has not been studied.

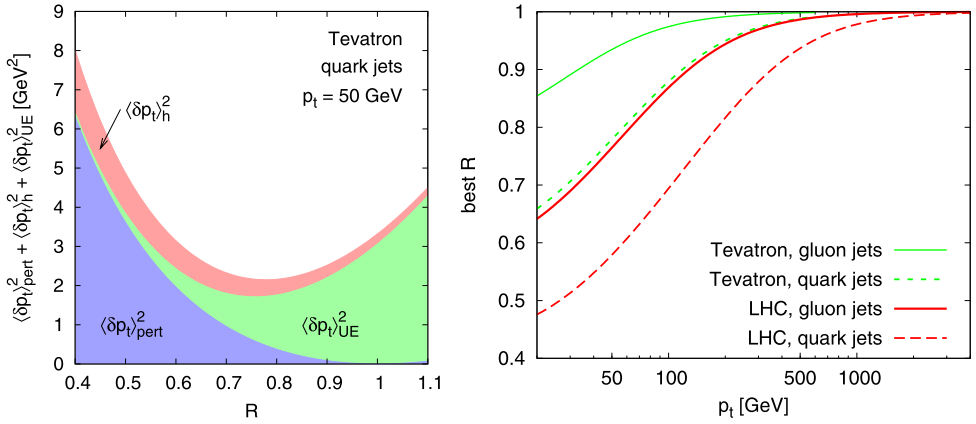

Fig. 19 *Left*: sum of the squares of the mean shifts of a jet's momentum due to perturbative gluon radiation, hadronisation and the UE, as a function of R for $p_t \sim 50$ GeV quark jets at the Tevatron; *right*: the resulting crude estimate for the "best" R as a function of jet p_t, for quark and gluon jets at the Tevatron and LHC (14 TeV). These values are to be taken as indicative of general trends rather than reliable estimates of the best R. The plots use the same parameters as Table 6 and the perturbative contribution is taken in the small-R limit. Taken from [150]

it has been obtained neglecting differences between algorithms and this is not entirely legitimate.

5.1.2 Numerical studies

Given that a complete analytic treatment is not yet available, one can use Monte Carlo event simulation to examine the optimisation of the choice of jet definition.

Historically the approach taken to studying the quality of jet definitions has been to take hard partons in a Monte Carlo, let them shower and hadronise, and then see how closely the reconstructed hadron-level jets match the original partons (see for example [187]). This procedure has the drawback that it is conceptually impossible to extend it to advanced Monte Carlo tools like MC@NLO [54], because the "original parton" is no longer identifiable. Furthermore it leads to several distinct quality measures: whether the number of jets is equal to the number of "partons", the angular distance between the jets and the partons, and the p_t difference between the jets and the partons. It is then often not clear which of these measures is most representative of the algorithm's usefulness in a real physics analysis.

The most robust way of proceeding would be, for each possible experimental study, to carry out a full signal and background analysis with a wide variety of jet definitions and then see which provides the best signal to background (or root-background) ratio. As well as being a major undertaking, this can have subtleties: for example, optimal cuts in an analysis may depend on the jet definition and so may need to be reoptimised for each new jet definition.

An approach taken in [93, 96, 188, 189] attempts to carry out a simplified version of this procedure. It takes a physical process, for example the production of a narrow Z' that decays to $q\bar{q}$, or a $t\bar{t}$ event ($t \to$ hadrons) and attempts to reconstruct the massive object. The "better" the reconstructed mass peak, the better the jet algorithm. This ignores issues like how the jet algorithm performs with respect to background events (which was however additionally studied in [93]), but is well-defined (no reference to partons) and avoids the appearance of multiple quality measures (angular dispersion, energy dispersion, etc.). Note: the physical process itself need not necessarily be realistic—e.g. it is highly unlikely that there exists an as-yet undiscovered, hadronically decaying Z' with mass 100 GeV. But it still serves as a useful stand-in for a generic $q\bar{q}$ resonance, whose mass scale can easily be varied.

Quantifying the quality of the mass peak is, as it turns out, a complex issue. Two properties that matter are the position of the mass peak (how close it is to the mass scale of the particle being reconstructed) and its width. The position matters, for example, when trying to accurately reconstruct the mass of a hadronically decaying resonance. The width matters in terms of being able to identify clear signal peaks over a smooth background. In this section we will concentrate of the width. That the width is not trivial to determine is evident from Fig. 20. It is tempting to measure the peak quality by fitting a Gaussian. However, the fit is poor; the results of the fit depend on the choice of fit-window; and then it is not clear which parameters of the Gaussian would serve as the quality measure: the normalisation? The width? Some combination of the two? The approach of [96, 188, 189] is to avoid the fit-function and instead to find the width of the smallest window that contains a specified fraction z of the events, $Q^w_{f=z}$. A sharper (i.e. better) peak corresponds to a lower $Q^w_{f=z}$ value. There is still some arbitrariness in this, for example the choice of the fraction of events z (defined with respect to all events before cuts). However z is easily

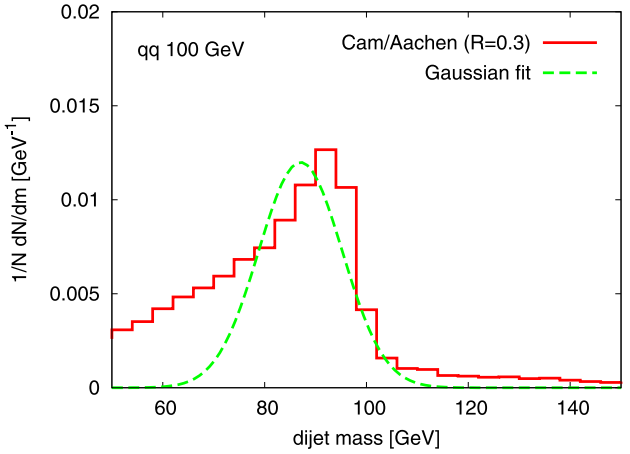

Fig. 20 Distribution of the reconstructed invariant mass of a 100 GeV $q\bar{q}$ system for the C/A algorithm with $R = 0.3$, simulated with Pythia 6.4, together with a Gaussian fit

varied to check the robustness of the procedure and one can also examine other quality measures.[30]

Figure 21 illustrates the procedure for a 100 GeV $q\bar{q}$ resonance and a 2 TeV gg resonance, examining three jet definitions (the use of $z = 0.12$ corresponds to taking about 25% of events after cuts).[31] One sees how better peaks have lower values for $Q^w_{f=z}$, together with the extent of the differences between algorithms, and the relevance of the choice of R.

The full R-dependence of the quality measure is shown for 5 algorithms in Fig. 22, for the same two physics cases. The minimum of each curve indicates the best R for that particular algorithm, while the differences between the curves are illustrative of the different behaviour of the various algorithms. In particular, one sees the preference for larger R in the 2 TeV gg case. This is in accord with the expectations discussed in Sect. 5.1.1: the larger the importance of perturbative gluon radiation, the larger the preferred R value. The optimal R as a function of mass scale, for the different algorithms and for the $q\bar{q}$ and gg cases, is illustrated in Fig. 23. The overall trend is not unlike the rough analytical estimate, Fig. 19 (right), but the details differ: for example the full result does not show as rapid an R dependence, and it is not clear to which extent the optimal R saturates at the highest scales in Fig. 23.

[30] One alternative is to fix the window width to be x GeV, place the window so as to maximise the number of events that it contains, and then use the inverse fraction of contained events $Q^{1/f}_{w=x}$ as the quality measure. A better peak concentrates more events in a given window, giving a lower result for $Q^{1/f}_{w=x}$.

[31] This and other figures in this subsection are all taken from [96], to which the reader is referred for full details. In the dijet case, a mass is reconstructed from the two hardest jets, with a cut $|\Delta y| < 1$ on the rapidity interval between the two jets (because in studies with background, such a cut greatly reduces the background).

Figure 22 shows that even at the optimal R there are differences between algorithms. The origin of these differences has not been analysed in full detail, but can almost certainly be traced back to the very different area properties of the various algorithms: k_t fares worst because its larger area allows more UE into the jet, causing enhanced fluctuations of the kinematics from event to event; meanwhile SISCone, with its small area, fares well, as does the filtered version of the C/A algorithm, which resolves each jet on an angular scale $R/2$ and takes just the two hardest subjets (cf. Sect. 2.2.6). Reference [95] has shown that additional modifications of the filtering procedure ("trimming") and tuning of its parameters can yield yet further improvements, as does noise "subtraction", discussed in Sect. 5.2.

A key question in examining results such as those in Figs. 21 and 22 is how much the differences between algorithms (and R-values) matter: from this information an experiment can then decide whether it is worthwhile investing in the calibration of multiple jet definitions (or in the inherent flexibility that allows easy use of any jet definition). One way of making such an estimate is to assume that the peak is being reconstructed in the context of a search with significant background. If one can assume that the amount of background basically scales as the width of the window that comes out of the $Q^w_{f=z}$ quality measure, then the significance $S/\sqrt{B}$ of any signal will just be inversely proportional to $\sqrt{Q^w_{f=z}}$. One can then define a measure ρ_L, which is the extra factor in luminosity that is needed to see the signal with given significance when using one jet definition (JD) relative to another.

Results for ρ_L are given in Fig. 24. One sees that the impact of the jet algorithm choice is greatest at large mass scales (not surprising perhaps, given that large scales prefer large R, where the area-sensitivity matters particularly). That figure also illustrates how, at large mass scales, especially for gluon jets (as discussed first in [189]), standard choices of $R \sim 0.5$ are extremely poor—requiring up to twice as much luminosity to see a mass peak above a background. This conclusion is relatively robust: Fig. 24 actually has results for two different quality measures, which agree remarkably well (the solid line derives from $Q^w_{f=z}$, discussed above, while the dashed line stems from an alternative measure, cf. footnote 30, or [96] for full details).

A reader who wishes to examine these quality measures further is encouraged to consult a web-tool [190], which provides access to over 100,000 plots, two different quality measures and z values, with histograms for a wide range of jet definitions and mass scales as well as summary plots of the quality measures and resulting ρ_L values.

Three comments are due concerning the above discussion. Firstly, it applies directly only to simple dijet events. There have also been studies with multi-jet events from top-quark decays, cf. the two bottom rows of Fig. 24, as well

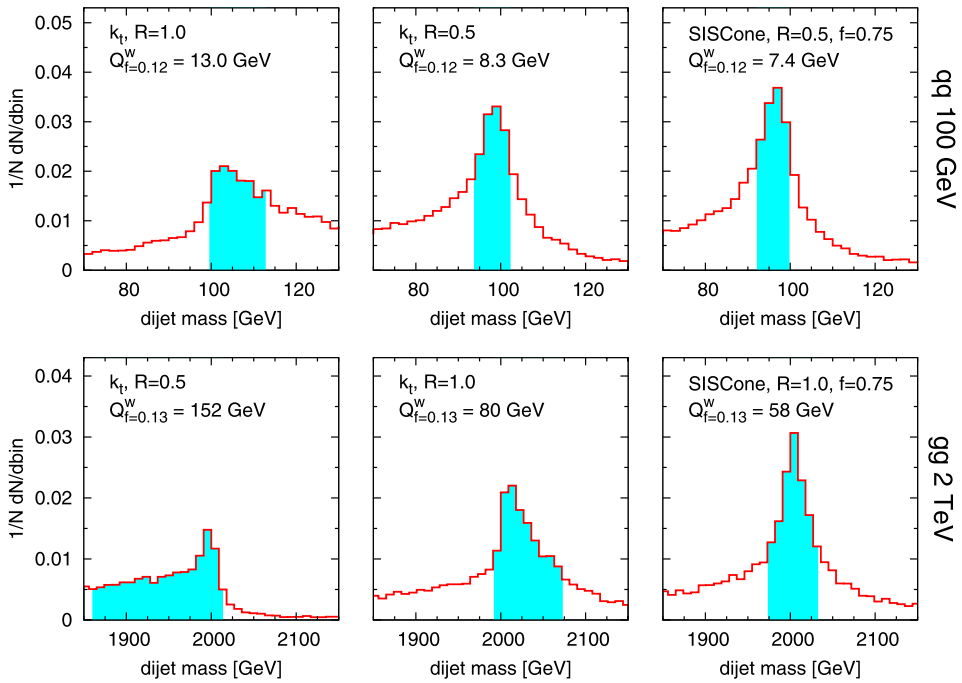

Fig. 21 Illustrative dijet invariant mass distributions for two processes (above: $q\bar{q}$ case at $M = 100$ GeV; below: gg case at $M = 2$ TeV), comparing three jet definitions for each process. The *shaded bands* indicate the regions used when obtaining the Q_z^w quality measure. Note that different values of R have been used for the $q\bar{q}$ and gg cases

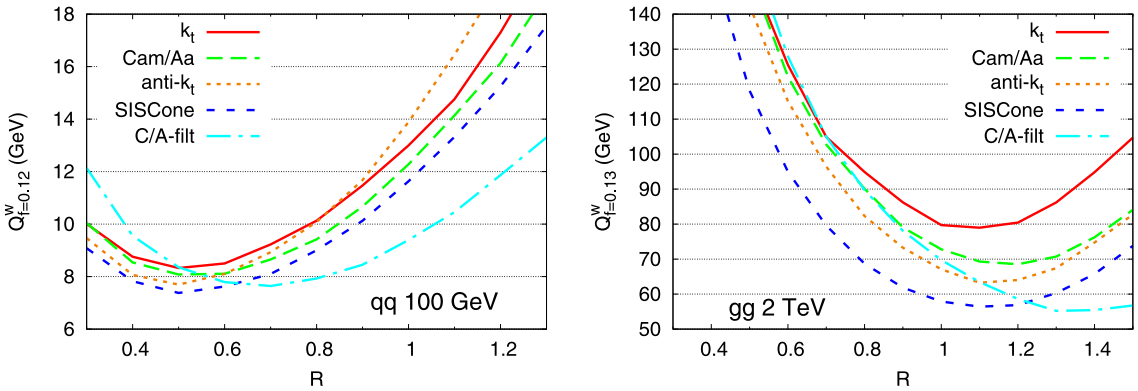

Fig. 22 The quality measure $Q^w_{f=z}$, for different jet algorithms as a function of R, for the 100 GeV $q\bar{q}$ case (*left*) and 2 TeV gg (*right*)

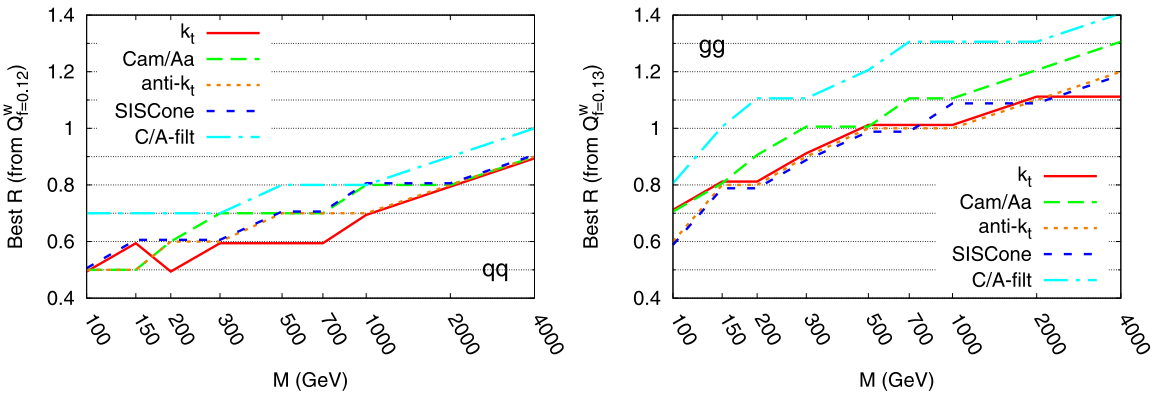

Fig. 23 The optimal value for R as a function of the mass of the $q\bar{q}/gg$ system (*left*/*right*), as determined from the $Q^w_{f=z}$ quality measure for various jet algorithms. Note that the exact results for the optimal R depend a little on the choice of quality measure, however the observed trends do not

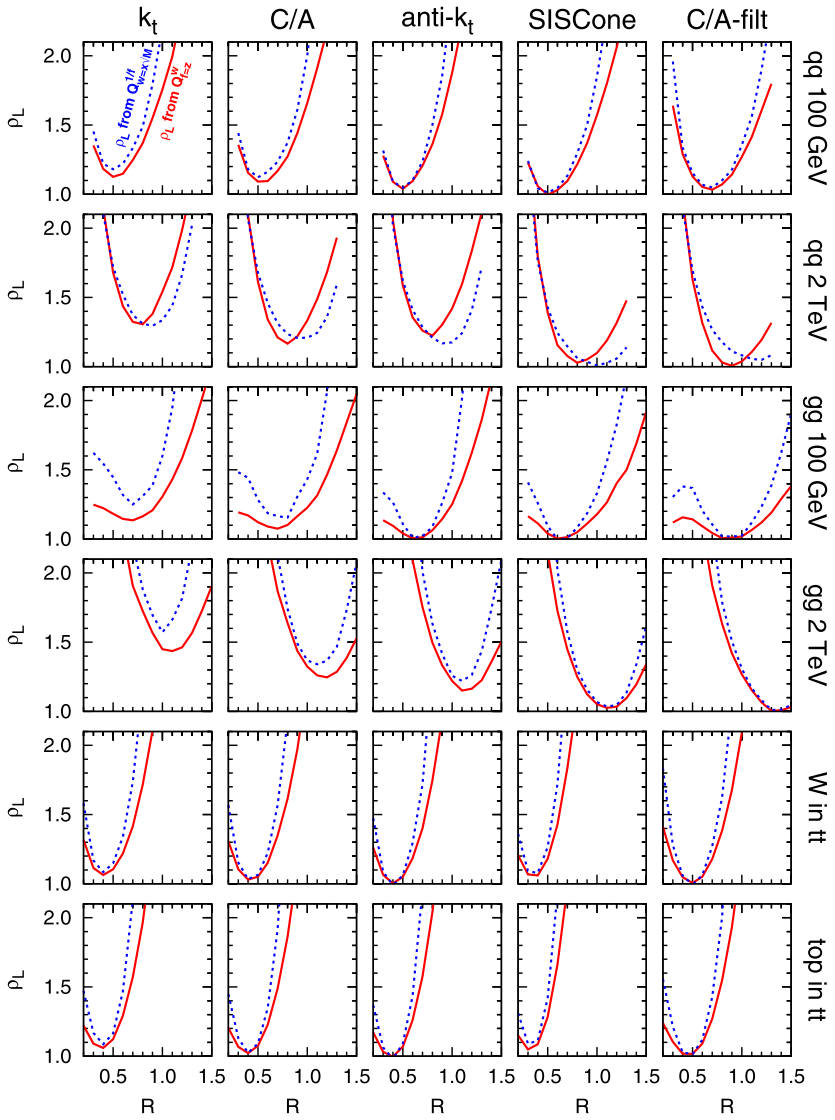

Fig. 24 For each process (one per row) this plot shows the extra factor in luminosity, ρ_L, required in order to obtain the same significance as with the best jet definition, as a function of R. The (*red*) *solid line* corresponds to the estimate of ρ_L based on the minimal width $Q^{w}_{f=z}$, while the (*blue*) *dotted line* corresponds to that based on the maximal fraction $Q^{1/f}_{w=1.25\sqrt{M}}$ (cf. footnote 30)

as an extensive analysis in [191]. What emerges from these studies is that the best choices in dijet events (where SISCone works very well) may not be optimal in multi-jet cases. For example, in [191] SISCone had more difficulty resolving all relevant jets, while in Fig. 24 the acceptable range of R is somewhat narrower for SISCone than for other algorithms. A related point is that in multi-jet events the conclusion about the need for larger R at high scales is likely to conflict with the need to resolve the multiple jets. These are important issues and call for further study.

A second comment is that [96, 188, 189] did not carry out any detailed tests of how the presence of realistic background events affects the relation between mass scale and optimal R. However, the analysis to be described below, [93], did include a study with background events, and confirms that at high masses large-R values are preferred (though the cuts and other details differ somewhat from those in [96]).

The final comment concerns the relation between the results here and those in Table 6. Here we have seen that for high masses, large R values are preferred, whereas Table 6 showed that in order to minimise non-perturbative corrections one should use smaller R values. These results are not in contradiction. In the case of Table 6, we had in mind observables such as the inclusive jet spectrum, where the effects of perturbative radiation just shift the distribution slightly, in a way that is accounted for within the NLO QCD predictions to which one compares experimental data (as long as R is not so small that the perturbative expansion breaks down). Therefore our aim was simply to minimise the poorly controlled non-perturbative contributions, leading to a preference for small R values. In the discussion in this section we considered the reconstruction of a hadronically decaying resonance. Perturbative radiation loss deforms the peak making it less visible above a smooth background. Though we could calculate that deformation pertur-

Table 7 Percentage improvement in the number of events from a resonance X that have been reconstructed in the mass window $m_X \pm 25$ GeV, comparing a fixed-R algorithm at its best R (first number in brackets) with the variable-R algorithm (the second number in brackets, ρ/GeV, sets the jet radius as $R(p_t) = \rho/p_t$). Results taken from [93]

Algorithm	500 GeV	1 TeV	2 TeV	3 TeV
anti-k_t → anti-k_t VR	18% (0.9, 200)	14% (1.0, 450)	10% (1.2, 1000)	8% (1.3, 1500)
C/A → C/A VR	17% (0.9, 175)	14% (1.0, 400)	7% (1.2, 1000)	9% (1.3, 1500)

batively, our ultimate aim is to make the peak more visible and so a larger R value, which retains more perturbative radiation, becomes preferable.

Variable R One should be aware that there may also be benefits to be had by moving away from the use of a single R value even when studying a single mass scale. For example, one might choose to adapt R according to the amount of noise (UE, pileup) in each given event. Alternatively, other kinematic variables, like the total transverse energy in the event [192] or the rapidity separation between the leading jets, can also be correlated with the optimal R choice on an event-by-event basis.

This last point was studied recently by Krohn, Thaler and Wang (KRT) [93] with a variable-R jet algorithm (cf. Sect. 2.2.6). Their R value is actually not directly a function of the rapidity difference, Δy, between the two hardest jets, but rather scales as $1/p_{t,\mathrm{jet}}$, which for two hard jets stemming from a resonance of given fixed mass translates to a rapidity dependence $R \sim \cosh\frac{\Delta y}{2}$. This was motivated on the grounds that jets from a resonance decay emit gluons on an angular scale that is independent of whether the jets are transverse or along the beam direction; in the centre-of-mass frame of the resonance, for two partons at rapidity $y/2$, separated by an angle $\theta_{ij} \ll 1$, the boost-invariant angular distance ΔR_{ij} is given by $\theta_{ij}\cosh\frac{y}{2}$. Hence the scaling used for the jet radius.[32]

Table 7 illustrates the improvements in signal reconstruction that are obtained with this approach as compared to fixed-R algorithms. The benefit is at the level of tens of percent. This is similar in magnitude to the improvement seen above by optimising the choice of algorithm, or optimising a fixed R as compared to a standard $R = 0.5$ or $R = 0.7$ choice.

The KRT analysis was performed using the two leading jets reconstructed from all particles with $|\eta| < 3$. This means that significant numbers of events involve two leading jets with large rapidity separations. In this respect, the KRT analysis differs from that discussed above [96], which only studied events in which the leading jet pair was separated by $|\Delta y| < 1$. With the latter requirement, since $\cosh\frac{\Delta y}{2}$ would be close to 1, one might expect the p_t-dependent variable-R choice to have a more modest impact.

KRT also studied jet performance for resonance reconstruction that includes a dijet background. Here too they found improvements with a variable R choice (and again at the level of about 10–15%), but only if they supplemented their analysis with a "jet quality" cut which requires that the energy be deposited centrally within the jet. The corresponding fixed-R analysis confirmed the need for large R values at high mass scales.

5.2 Pileup subtraction

The LHC will collide protons with an unprecedented instantaneous luminosity of up to 10^{34} cm^{-2} s^{-1} and a bunch spacing of 25 ns, corresponding to 0.25 mb^{-1} per bunch crossing. While this high luminosity is essential for many searches of rare new physics processes at high-energy scales, it also complicates analyses, because at each bunch crossing there will be of the order of 20 minimum-bias pp interactions, which pollute any interesting hard events with many soft particles. The beams at LHC will have a longitudinal spread, and it may be possible experimentally to associate each charged particle with a distinct primary vertex that corresponds to a single pp interaction and so eliminate some fraction of the soft contamination. However, for neutral particles this is not possible, and many jet measurements are in any case expected to be carried out with calorimeter-cell or cluster information, for which there is not sufficient angular resolution to reconstruct the original primary vertex. Therefore kinematic measurements for jets will be adversely affected by pileup (PU), with resolution and absolute energy measurements suffering significantly.

The impact of PU is illustrated in the upper row of Fig. 25, which shows histograms for the same 2 TeV gg resonance used above, but now with varying degrees of pileup: none, low-luminosity LHC running (0.05 mb^{-1} per bunch crossing) and high-luminosity running (0.25 mb^{-1} per bunch crossing). The degradation of the peak and its shift to higher masses are clearly evident here. While the shift is perhaps not overly consequential (it could be corrected for by comparing to MC simulation of the pileup), the loss of resolution is a serious issue.

[32] The optimal R choice should of course depend also on initial state radiation and the underlying event, and further studies might benefit by taking into account this information too.

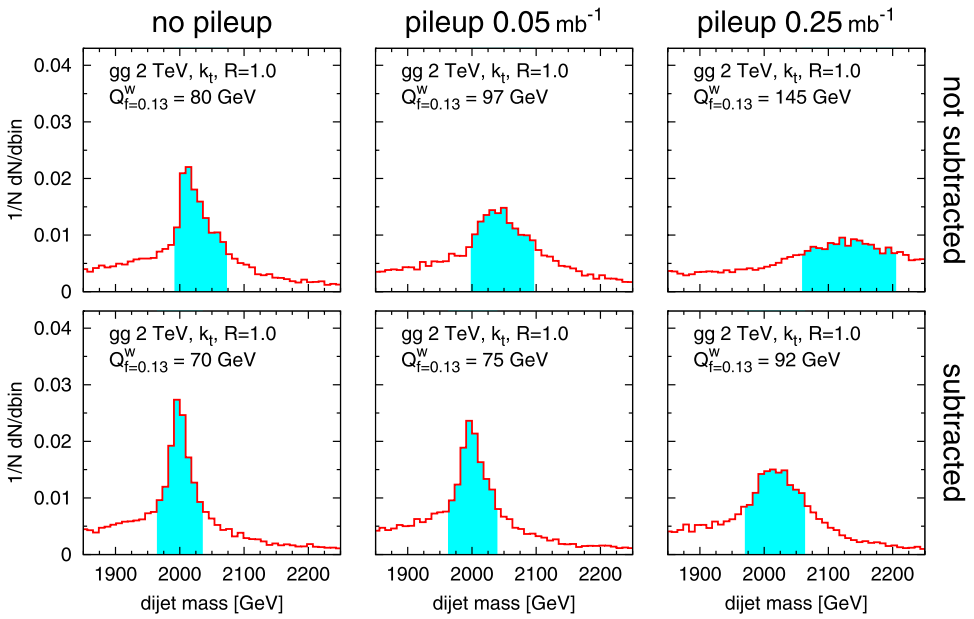

Fig. 25 Invariant mass distributions for the 2 TeV gg process of Sect. 5.1.2, for the k_t algorithm with $R = 1$, shown with no pileup (*left*), low pileup (*middle*) and high pileup (*right*), without subtraction (*upper row*) and with pileup subtraction as outlined in [193] (*lower row*). The *shaded bands* indicate the region used to calculate the $Q^w_{f=z}$ quality measure in each case. Figure taken from [96]

Both the Tevatron and LHC experiments have examined the question of pileup. Some approaches to limiting its impact are based on average correction procedures, for example the requirement that final measured distributions should be independent of luminosity [1], or a correction to each jet given by some constant times the number of primary interaction vertices (minus one) [194]. These approaches have the advantage of being simple, but their averaged nature limits the extent to which they can restore resolution lost through pileup. Other approaches involve event-dependent corrections that are applied to calorimeter towers either before or during the clustering [195, 196]. These can give better restoration of resolution than average-based methods. One drawback that they have is that they are tightly linked to the specific experimental setup (for example calorimeter cell size), and require ad-hoc transverse-momentum thresholds to distinguish pileup from hard jets. Additionally they are sometimes tied to specific (legacy) jet algorithms, and so may not always be readily applied to more modern jet algorithms.

The above issues triggered the development of an experiment-independent pileup subtraction approach in [193]. The essential observation is that pileup roughly modifies a jet's p_t as follows:

$$\Delta p_t = A\rho \pm \sigma\sqrt{A} + \Delta p_t^B, \tag{54}$$

where A is the jet's area (after addition of the pileup), ρ is the mean amount of transverse momentum per unit area that has been added to the event by pileup; σ measures the fluctuations of the pileup from point-to-point within the event (defined as the standard deviation of the distribution of pileup across many squares of area 1); and Δp_t^B is the net change in transverse momentum due to back reaction. Fluctuations in the jet p_t arise because A varies from jet-to-jet, ρ from event-to-event, because the pileup density fluctuates from place to place within an event (the σ term) and because of back reaction. The approach of [193] involves first running the jet algorithm, estimating ρ and then subtracting the $A\rho$ term from each jet. This leaves just the $\sigma\sqrt{A}$ piece and the back-reaction term and should significantly reduce both the fluctuations and the mean offset in jet energy.[33]

The estimation of ρ (without using detector-specific information, such as the origin of tracks) is non-trivial because one must decide what part of the event belongs to the hard event and which part comes from pileup. Ideally one wants to do this without introducing any explicit threshold to distinguish the two, given that the natural threshold would vary significantly from event to event. One observation of [193] is that this can be done using the jets themselves. Figure 26a shows a scatter plot of jet p_t versus jet area for a single Monte Carlo event and one sees a clear correlation from nearly all the jets. Figure 26b shows p_t/A for each jet as a function of rapidity for the same event and one sees that the p_t/A results cluster around a value that is fairly independent of rapidity (it is still unclear just how true this will actually be at the LHC). These two features led to the proposal to take the distribution of p_t/A for all jets in an event, up to some maximum rapidity, and to then use its median (robust with respect to outliers, i.e. hard jets) as an estimate

[33] One might eliminate the back reaction too if one could subtract the PU before running the jet-finder—subtracting PU directly at particle level leads, however, to negative momenta, with consequent non-trivial issues within many jet-algorithms.

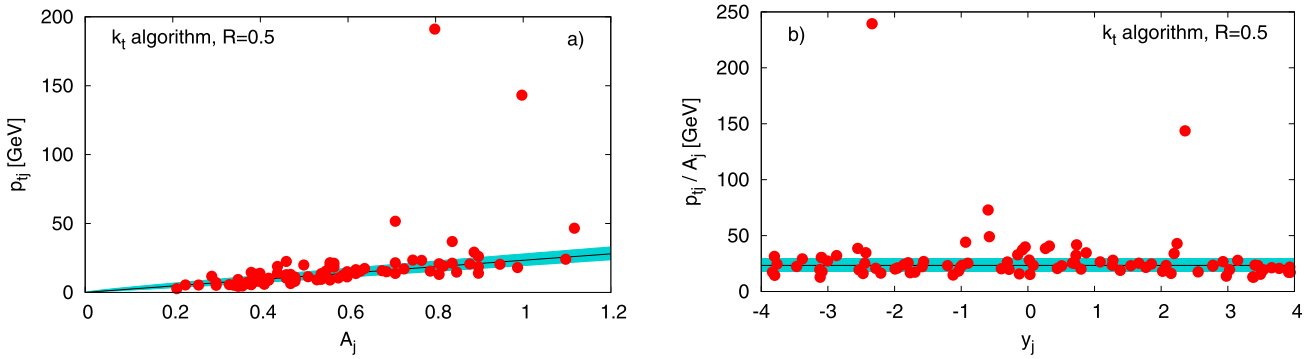

Fig. 26 (**a**) Scatter plot of the jet transverse momentum p_{tj} versus its area A_j, for an LHC dijet event with a pileup of 22 minimum-bias interactions (simulated with the default tune of Pythia 6.325 [114]). The *line* and *band* are given by $\rho A_j \pm \sigma\sqrt{A_j}$. (**b**) The ratio p_{tj}/A_j as a function of the rapidity, y_j, for the same event; the *line* and *band* are given by $\rho \pm \sigma/\sqrt{\langle A\rangle}$. Taken from [193]

of ρ.[34] That estimate gives the black line in Fig. 26, while the band's width is controlled by the value of σ obtained from examining the width of the p_t/A distribution.

With ρ estimated in this fashion, one can correct each jet by an amount:

$$p_{tj}^{\mu} \to p_{tj}^{\mu} - \rho A_j^{\mu}, \tag{55}$$

where A_j^{μ} is the jet's 4-vector area. This approach was used to obtain the lower row of Fig. 25, illustrating the substantial gain in peak quality that is to be had with the method (as well as nearly correct reconstruction of peak position). In this specific case there is even an improvement in the peak quality in the case without pileup, a consequence of the fact that the above method also subtracts UE.

One comment is that pileup subtraction does not completely eliminate the effect of pileup. In the area-based approach just described, this is because of the last two terms on the RHS of (54) are still present after subtraction. Nevertheless it reduces the impact of pileup sufficiently that conclusions about optimal jet definitions drawn from Fig. 24 in the absence of pileup also hold with pileup. This is important, because it means that analyses that use data taken at different luminosities can successfully use a common jet algorithm, independently of the pileup.

Subtraction in heavy-ion collisions The techniques described above have the potential to be useful also in heavy-ion (HI) jet finding, where the problem is to identify jets given the large soft background of particles that results from the hot dense matter that is formed in a heavy-ion collision. This is of interest in the heavy-ion community (see for example the review [23]) because the modification of jets as they traverse the hot dense medium may provide insight into the nature of the medium.

The proposal for area-based pileup subtraction [193] also included an application to the HI case and it has been investigated by the STAR collaboration at RHIC in a first preliminary measurement of jet-cross sections in Au Au gold collisions at $\sqrt{S_{NN}} = 200$ GeV [24].

The value of ρ in the heavy-ion case is up to an order of magnitude larger than in high-luminosity pp running. This places particularly stringent constraints on the accuracy that is required in the subtraction and has spurred various ongoing investigations. Given the similarities between HI and high-pileup pp jet finding, it is to be expected that these investigations will be beneficial in both environments.

Among the issues that are being considered is that of how to estimate ρ without recourse to the whole event, given that there is significant rapidity dependence (and even azimuth dependence in some cases) in the production of soft particles, both in HI and pp collisions (the event in Fig. 26b is a little unusual in its degree of rapidity-independence). Other issues are those of minimising systematic residual shifts from back reaction (for which the anti-k_t algorithm is beneficial) and reducing the impact of point-to-point fluctuations in the noise (in this respect C/A filtering seems to offer a promising avenue).

5.3 Substructure

A key feature of the LHC is that it will be the first collider to probe scales that are significantly above the EW scale. This is what will allow the LHC to investigate the nature of electroweak symmetry breaking and explore new territory in the search for particles and phenomena beyond those of the standard model.

[34] One technical detail is that only certain jet algorithms, essentially k_t and C/A, are suitable for estimating ρ, while the subtraction itself can be performed for any algorithm. When trying to optimise the subtraction there are also issues with the choice of the correct R value in the JD used to estimate ρ, with $R \sim 0.5$–0.6 being a generally reasonably choice.

The importance of physics at transverse momenta $p_t \gg m_Z$ has implications for the structure of the final state because at high transverse momenta, "signature" particles, W's, Z's, Higgs bosons and top quarks, have very collimated decays (due to their relativistic boost). Standard approaches for identifying these particles (i.e. recombining different jets) fail because all the decay products end up in a single jet.

The work so far on identifying hadronic decays of boosted heavy particles has fallen into two broad classes: particles with two-pronged decays (the EW bosons), and those with three-pronged decays (top quarks). In each case, the mass of the jet is one indicator of its origin (as discussed recently for example in [197–201]). However, even for massless partons, QCD branching generates a significant fraction of jets with large masses (or equivalently with 2- or 3-pronged substructure): assuming a given jet p_t, the leading-order (fixed-coupling) differential QCD jet-mass distribution goes as

$$\frac{1}{n}\frac{dn}{dM^2} \sim \frac{1}{M^2}\frac{\alpha_s C_i}{\pi}\left(\ln\frac{R^2 p_t^2}{M^2} + \mathcal{O}(1)\right) \tag{56}$$

(see [151, 152] for more detailed analytic expressions, or [153, 155] for corresponding resummed results in e^+e^- collisions) and the logarithm can in part compensate the smallness of α_s, especially at larger p_t. Two main questions that need to be answered are then: how can one reduce the background of QCD jets of a given mass, and how can one get the best resolution on jet mass so as to be able to use a small jet-mass window in selecting candidate heavy particles?

5.3.1 Two-pronged decays

The first detailed discussion of advanced jet techniques for two-pronged decays, over 15 years ago, was given by Seymour in [202] in the context of a search for a heavy Higgs boson decaying to WW with one W decaying leptonically, the other hadronically. He mainly considered the issue of mass resolution and investigated two approaches. One method involved the (inclusive) k_t algorithm, with $R = 1$, in which the clustering sequence for the hardest jet was essentially undone by one step, so as to resolve the jet into the two subjets from the W decay. The resulting separation of the subjets could then be used to set a smaller R for a second run of the k_t algorithm, which helped improve the mass resolution. Another method involved the use of a cone algorithm with quite small R, $\sim$0.25 in order to directly identify the two subjets. This small R was needed in order to robustly resolve the two subjets, but that then caused it to lose significant gluon radiation from the $W \to q\bar{q}$ system, giving worse mass resolution than the k_t algorithm. The basic observation was therefore that the k_t algorithm's intrinsic internal information on substructure allowed one to be more flexible in the compromise between identifying substructure and capturing the bulk of the relevant radiation.

The next development on the subject was made by Butterworth, Cox and Forshaw [203] who examined WW scattering, again with one leptonically and one hadronically decaying W. They observed that the distribution of k_t distance, d_{ij} (8), between the two W subjets was close to the W mass in W decays, but tended to have lower values in generic massive jets. This allowed them to obtain a substantial reduction in the background. The same idea was used later for electroweak-boson reconstruction in the context of a SUSY search [204]. The tool associated with this technique is often referred to as "Y-splitter".

It is worthwhile looking at some simple analytic results that relate to the techniques of [203] and [202]. For a quasi-collinear splitting into two objects i and j, the total mass is $m^2 \simeq p_{ti}\,p_{tj}\,\Delta R_{ij}^2$. Labelling i and j such that $p_{tj} < p_{ti}$ and defining $z = p_{tj}/p_t$ ($p_t = p_{ti} + p_{tj}$), then

$$m^2 \simeq z(1-z)p_t^2\Delta R_{ij}^2, \tag{57}$$

$$d_{ij} = z^2 p_t^2 \Delta R_{ij}^2 \simeq \frac{z}{(1-z)}m^2. \tag{58}$$

Electroweak bosons decay with a fairly uniform distribution in z (exactly uniform for a Higgs boson), whereas a QCD splitting has a soft divergence, e.g.

$$P_{gq} \propto \frac{1+(1-z)^2}{z}. \tag{59}$$

This means that for a fixed mass window, the background will have lower d_{ij} values than the signal. Indeed, the logarithm in (56) comes from the integral over the $1/z$ divergence in (59), with lower limit $z \gtrsim m^2/p_t^2R^2$. If one places a cut on d_{ij}, or analogously on z, then one eliminates that logarithm, thus reducing the QCD background (one can even calculate, analytically, what the optimal cut is for given signals and backgrounds).

A second set of observations concerns mass resolution. Firstly, with a small cone of size $R \ll \Delta R_{ij}$ used to reconstruct the two prongs of a colour-singlet $q\bar{q}$ state, then there will be an average loss of (squared) mass, and correspondingly of mass resolution, dominated by a contribution from perturbative gluon radiation,

$$\langle\delta m^2\rangle \simeq 2m^2 \cdot \frac{\alpha_s L_q}{\pi}\left(\ln\frac{R}{\Delta R_{ij}} + \mathcal{O}(1)\right), \quad R \ll \Delta R_{ij}, \tag{60}$$

with $L_q \simeq C_F$ as given in (30). If instead a single jet is used to reconstruct the whole $q\bar{q}$ system, then one can show that most of the perturbative radiation from the $q\bar{q}$ system will be contained in the jet. However there may then be significant contamination from the UE and pileup,

$$\langle\delta m^2\rangle \simeq \rho p_t \frac{\pi R^4}{2}, \tag{61}$$

for a circular jet (cf. (44), with $\rho \equiv \Lambda_{\rm UE}/2\pi$), with an additional contribution coming also from perturbative radiation from the beam. Even though the above two equations represent major oversimplifications of the full dynamics, one can understand the task of optimising mass resolution as one of minimising both types of contribution (in analogy with Sect. 5.1.1).

This understanding provided the backdrop to a two-pronged subjet technique given in [94], used there for a high-p_t Higgs boson search in association with a back-to-back high-p_t vector boson. The approach involved the Cambridge/Aachen algorithm, because its sequential recombination in increasing angular distance is ideally suited to dealing with problems that involve multiple or unknown angular scales. The basic procedure that was used to identify a $H \to b\bar{b}$ decay went as follows:

1. Break a C/A jet j into two subjets by undoing its last stage of clustering. Label the two subjets j_1, j_2 such that $m_{j_1} > m_{j_2}$.
2. If there was a significant mass drop (MD), $m_{j_1} < \mu m_j$, and the splitting is not too asymmetric, $y = \frac{\min(p_{tj_1}^2, p_{tj_2}^2)}{m_j^2} \Delta R_{j_1,j_2}^2 > y_{\rm cut}$, then deem j to be the heavy-particle neighbourhood and exit the loop (μ was taken to be 0.67 and $y_{\rm cut} = 0.09$). Note that $y \simeq \min(p_{tj_1}, p_{tj_2})/\max(p_{tj_1}, p_{tj_2})$.[35]
3. Otherwise redefine j to be equal to j_1 and go back to step 1.

The search for a mass-drop, step 2, served to identify the point in the decomposition that involved significant hard substructure and, in the context of a Higgs-boson search, one can verify that the two subjets at that stage both have a b-tag. The cut on $y \simeq z/(1-z)$ allows one to kill the logarithm for (fake b-tag) QCD backgrounds in (56). By virtue of angular ordering [84–88], the two C/A subjets produced at that stage, each with opening angle equal to $\Delta R_{j_1,j_2}$, should contain nearly all the perturbative radiation from the $b\bar{b}$ system (i.e. (60) is close to zero). They still tend to include too much contamination from the UE however, so one can then apply a filtering technique in which the two subjets are reexamined on a smaller angular scale $R_{\rm filt}$ and only the three hardest components (i.e. $b\bar{b}g$) were retained. This essentially reduces the coefficient of the UE contamination in (61). The value used for $R_{\rm filt}$ was specific to the jet, $R_{\rm filt} = \min(0.3, R_{b\bar{b}}/2)$, though this could perhaps be further optimised.

A comparison of different jet algorithms for the ZH search channel for $m_H = 115$ GeV, with $Z \to e^+e^-, \mu^+\mu^-$ for $p_{tH}, p_{tZ} > 200$ GeV (and other cuts detailed in [94]) is shown in Table 8. The C/A algorithm with the mass-drop and filtering (MD-F) is clearly the best both at extracting the signal and limiting the background. The k_t algorithm fares poorly mainly because of its poor mass resolution (its larger area and fluctuations, cf. Sect. 4.4, make it intrinsically worse than the C/A algorithm, and it is shown without any filtering). SISCone does quite well on the reconstruction of the signal, mainly because of its particularly low sensitivity to UE contamination, but does poorly on the background rejection because it fails to correlate the b tagging with the subjet momentum structure, as does anti-k_t. It is probably fair to say that the defects of the algorithms could to some extent be resolved with refinements such as the use of jet finding with multiple R values. However it is only in the C/A algorithm that the use of multiple R values fits in naturally within the context of a single run of the jet finder, and the C/A algorithm provides an internal representation of the jet structure that makes it particularly easy to establish the right R values.

Table 8 Cross section for signal (σ_S) and the Z + jets background (σ_B) in the leptonic Z channel of HZ production at a 14 TeV LHC, for $200 < p_{TZ}/\text{GeV} < 600$ and $110 < m_J/\text{GeV} < 125$, with perfect b-tagging; the C/A algorithm uses the procedure outlined in the text; the k_t algorithm uses the first step of decomposition to identify two subjets with a cut on y_{ij} as for C/A; SISCone and anti-k_t do not use any subjet analysis, but each require two b-tags within the jet. In each case R has been chosen to give near optimal significance with that algorithm

Jet definition	σ_S/fb	σ_B/fb	$\sigma_S/\sqrt{\sigma_B \cdot \text{fb}}$
C/A, $R = 1.2$, MD-F	0.57	0.51	0.80
k_t, $R = 1.0$, $y_{\rm cut}$	0.19	0.74	0.22
SISCone, $R = 0.8$	0.49	1.33	0.42
anti-k_t, $R = 0.8$	0.22	1.06	0.21

For completeness, Fig. 27 shows the results of the Monte Carlo simulation (particle-level) of the boosted $pp \to HV$ Higgs-boson search, illustrating how this becomes a relevant search channel at the LHC (and one that provides clean access to the product of Hbb and ZZH, WWH couplings). Subsequent to the writing of the original version of this review, ATLAS confirmed that results similar to those of [94] are obtained when accounting for detector effects [205]. Related methods were also examined for a $t\bar{t}H$ search [206] and for Higgs-boson production in new physics events [207].

5.3.2 *Three-pronged decays*

Three-pronged decays have been studied mainly in the context of top decays.[36] This is motivated in part because

[35] This $y_{\rm cut}$ is related to, but not the same as, that used to calculate the splitting scale in [203, 204], which use a dimensionful $d_{\rm cut}$.

[36] Though there has also recently been work on the three-pronged hadronic decay of a neutralino in an R-parity violating SUSY scenario [208].

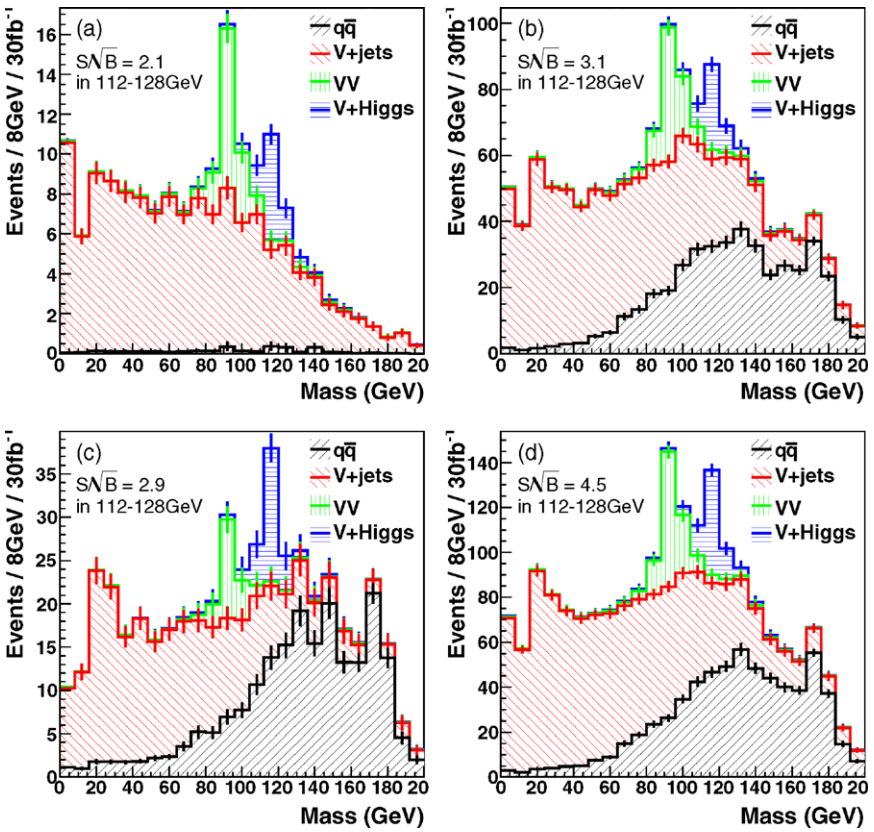

Fig. 27 Signal and background for a 115 GeV SM Higgs in the $pp \to VH$ channels, with $H \to b\bar{b}$, simulated using Herwig 6.5 and Jimmy 4.31 (an ATLAS tune), C/A MD-F with $R = 1.2$ and $p_t > 200$ GeV, for 30 fb^{-1}. The b tag efficiency is assumed to be 60% and a fake-tag probability of 2% is used. The $q\bar{q}$ sample includes dijets and $t\bar{t}$. The vector boson selections are (**a**) two leptons, (**b**) missing energy and (**c**) lepton plus missing energy, while (**d**) shows the sum of all three channels (see [94] for details). The errors reflect the statistical uncertainty on the simulated samples, and correspond to integrated luminosities >30 fb^{-1}

high-mass $t\bar{t}$ resonances are a feature of many new physics scenarios (see for example [197, 209–212] and references therein).

The use of subjet structure in identifying hadronically decaying tops is a much more recent topics than for EW bosons, having developed mainly in the last two years. However many of the ideas are directly inspired from the two-pronged case. Aside from examining the jet-mass (whose distribution is calculated in detail at leading order in [151, 152]), techniques that have been investigated include subjet-decomposition with the k_t algorithm [213, 214], C/A subjet techniques [192] and pruning [97, 98]. Among the discriminating variables that are used, there are d_{ij} type variables [214, 215], z-type variables [97, 98, 192, 206, 213] and event-shape variables [151, 152, 213] (in both cases, a spherocity-like variable in the plane transverse to the jet), constraints on a W-subjet mass [192, 213] as well as other interjet correlation variables (a helicity angle θ_h in [192]). Most of the work has been geared to quite high-p_t boosted tops in the simple environment of a resonance decaying to $t\bar{b}t$, though one study has also been carried out of moderately boosted top-tagging in the busy environment of $pp \to t\bar{t}H$ [206].

A summary of results for top-tagging efficiencies and fake rates in the various high-p_t methods is given in Table 9. What emerges from this is that the C/A-based approach of [192] seems to offer good efficiencies and very good QCD-jet rejection, with the best signal significance and signal-to-background ratio ("better than b-tagging at high p_t"). Compared to the C/A-based method of [94] for Higgs decays, particularly relevant differences are that it avoids any reference to mass drops (thus simplifying the method), and introduces a minimal distance between subjects, which needs to be adjusted with the jet p_t. Its signal efficiency and fake-tag rates are shown as a function of transverse momentum in Fig. 28 (left). The decrease in efficiencies at high transverse momenta is simply a consequence of the inclusion of finite calorimeter tower sizes (0.1×0.1), and could perhaps be alleviated experimentally with the use of tracking and electromagnetic calorimetry, both of which have finer angular resolution. In tests by CMS [216] of a variant of the method, the efficiency instead saturates near 45% at high-p_t, while it is the fake rate that progressively degrades.

One important point in top-tagging is that to obtain the best tagging at high transverse momenta, one should use an R value that scales as $1/p_t$, because the top-quark decay is mostly contained in a cone of width of order 2–3 times m/p_t. Using a jet-opening angle that is much larger than this will lead to considerable degradation in mass resolution, not only because of UE contamination (as in the colour-singlet two-body decay case), but also because the top quark,

Table 9 Efficiencies for reconstructing top quarks with $p_t \sim 1$ TeV and the fraction of normal QCD jets that get a fake "top-tag". Shown for the various tagging methods that quoted numbers easily amenable to interpretation in this manner (numbers in brackets are for alternative sets of cuts). Insofar as results involve different detector and resolution assumptions, Monte Carlo generator choices, as well as slightly different p_t cuts, the comparison should be considered indicative rather than precise. Furthermore the results of the various methods have different dependences on the transverse momenta being studied

	Method	Efficiency	Fake fraction
(from [213])	just jet mass	50%	10%
ATLAS [214, 215]	3, 4 k_t subjets, d_{cut}	45% (85%)	5%(15%)
Thaler and Wang [213]	2, 3 k_t subjets, z_{cut} + shape	40%	5%
Kaplan et al. [192]	3, 4 C/A subjets, $z_{\text{cut}} + \theta_h$	40%	1%
Ellis et al. [97, 98]	Pruning	15%	0.05%
CMS [216]	variant of [192]	45%	3%

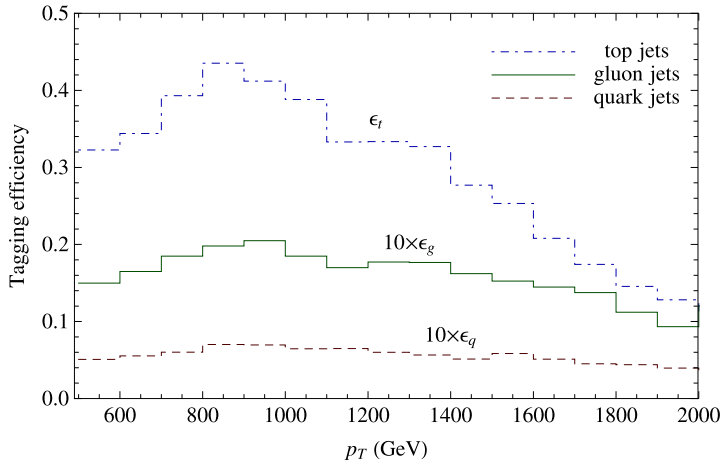

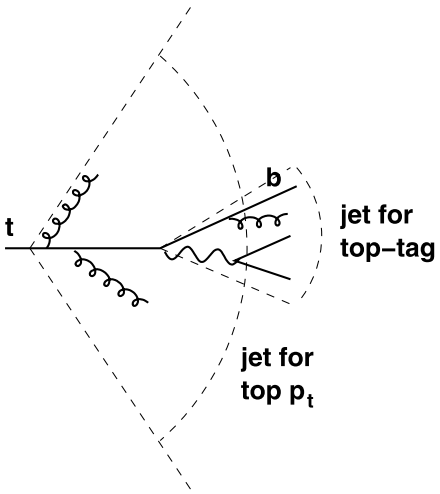

Fig. 28 *Left*: signal efficiency for boosted top ID, ϵ_t, and fake-tag rates for quark and gluon jets (ϵ_q, ϵ_g, both multiplied by 10 for visibility) for the Kaplan et al. C/A-based top-tagger, as a function of jet p_t (reproduced from [192]). *Right*: the use of two jet sizes for top reconstruction: the inner cone, of order a few times m/p_t, includes the top decay products, but excludes radiation from the top quark itself (dead-cone). To capture that radiation and reconstruct the correct top p_t, one should use the outer cone

a coloured object, itself radiates gluons, which will tend to increase the jet mass. The C/A-based approach of [192] is to some extent able to find the right R automatically for a given top-decay, and this is part of its strength.

Finding the top quark is only half the task however: one must also establish its momentum. Barely any of the gluons emitted from a fast-moving top quark are contained in the small jet used to identify the top—this is the dead-cone phenomenon for radiation from a massive quark. To capture them one should instead use a jet with large opening angle, as one would for a high-p_t light quark [96], cf. Sect. 5.1. This is essential if one is to obtain good mass resolution on a $t\bar{t}$ resonance and is summarised in Fig. 28 (right).

Thus, when studying highly boosted tops, one needs to examine the event on two angular scales: quite small $R \sim 3m_t/p_t$ to tag the top-decay structure, and large $R \sim 1$ to reconstruct the top-quark momentum before the top started emitting gluons.

5.4 Summary

It is probably fair to say that the question of how best to use jets is still in its infancy. Nevertheless, some clear results have emerged from the above discussion.

- There will not be a single "best" jet definition (i.e. R and jet-algorithm) at the LHC. What is optimal will depend on what one wants to measure. The trade-off will be between resolving separate jets (not really discussed here), capturing their perturbative radiation and limiting UE contamination, and depends on the momentum scale of an event, the number of jets, and so forth. In particular, kinematic reconstructions prefer larger R values at high p_t and for gluon jets (even $R \gtrsim 1$), because of the increased importance of capturing perturbative emission from the jets.
- Monte Carlo studies of dijet resonances confirm this picture. They also indicate that among the different algorithms, k_t is worst and SISCone and Cambridge/Aachen

with filtering are best (cf. Fig. 24). This is in accord with expectations based on their areas, i.e. their sensitivity to the UE, and is most relevant at high scales. Differences between algorithms, expressed as the extra luminosity needed to obtain a given (toy) signal significance, are at the level of a few tens of percent.

Furthermore, it seems that event-dependent choices for the R value can lead to additional improvements of a similar order of magnitude.

- Pileup is a major issue, and significantly degrades kinematic reconstructions, even at high momentum scales. One can devise tools to measure the amount of pileup event-by-event and to subtract it jet-by-jet. This leads to a noticeable improvement in kinematic reconstruction quality, though it does not quite restore it to the level of the no-pileup case.
- At the LHC's highest momentum scales, electroweak-scale particles appear to be light. Their decays are collimated into single jets. Sequential-recombination jet algorithms provide a clean way of resolving the consequent substructure, and the most flexible seems to be Cambridge/Aachen, again with filtering to reduce UE contamination.

There are many remaining open questions. Among them: how to reconcile the need for large R at high p_t with the task of resolving complex multi-jet events; how this connects with the use of substructure is resolving highly boosted decays; how to calculate the optimal R analytically, perhaps using the resulting information event-by-event; how to choose the parameters of filtering and how this ties in with possible improvements in pileup subtraction; and how all of this works in full physics studies, including realistic backgrounds and detector effects. It is to be hoped that future work will cast light on these questions.

6 Conclusions

This review has covered a range of developments in the practical and theoretical aspects of jet finding over the past few years. These are steps on the way to a fully developed science of the use of jets, "jetography".

One important development is that LHC now has access to a range of fast, infrared- and collinear-safe algorithms, together with methods that allow any of the algorithms to be used in a high-luminosity LHC environment. IRC safety is essential if the LHC is to benefit maximally from the huge predictive effort that is ongoing within the QCD theory community. Practicality is a necessary condition for the algorithms to be used in an experimental context.

A number of these advances have been taken up by the LHC experiments. For example both ATLAS and CMS incorporate FastJet within their software frameworks. At the time of writing (v2 of the arXiv version of this report), all 4 LHC experiments have seen first collisions at a centre-of-mass energy of $\sqrt{s} = 900$ GeV and it appears that both ATLAS and CMS have used the anti-k_t algorithm for finding jets in this initial data. These are welcome developments given the importance of IRC safety for straightforward comparisons with perturbative QCD predictions and for the use of perturbative methods in generally thinking about jets.

The second main development is that theoretical work has started on the question of how best to use jets in an LHC-type environment. This is an important question because the LHC spans two orders of magnitude in jet energy and has substantial (and variable) pileup, and no single jet definition will work optimally for the whole range of LHC phenomena.

Progress has been outlined here (Sect. 4) on our analytical understanding of how jets behave, and in Sect. 5 we have seen a handful of examples that benefited significantly from the use of the "right" jet-finding approach. Currently these two aspects of work on jets are connected qualitatively: the understanding of Sect. 4 helped to interpret the results and inspire some of the methods of Sect. 5. However a rigorous, quantitative link is still missing, and Sect. 5 in any case covered only a small fraction of the possible use-cases for jets. This highlights a clear path for future work: that of bringing our analytical tools to bear on the full range of uses of jets at the LHC, so as to identify optimal jet-finding solutions across the board.

Acknowledgements My initial interest in the subject of jet finding owes much to talks, exchanges, arguments, comments, encouragement by/with/from Jon Butterworth, Günther Dissertori, Joey Huston, Mike Seymour, Markus Wobisch, as well as many others. The bulk of my direct involvement in the subject has been in collaboration with Matteo Cacciari and Gregory Soyez and they have done a lot to transform the subject—without their ideas, determination and enthusiasm, the advances that I've been involved with would not have happened. Many others have contributed, both as collaborators, Andrea Banfi, Jon Butterworth, Adam Davison, John Ellis, Mrinal Dasgupta, Lorenzo Magnea, Are Raklev, Juan Rojo, Mathieu Rubin, Sebastian Sapeta, Giulia Zanderighi; and in terms of more informal exchanges: Timothy Chan, Olivier Devillers (both from the field of computational geometry) as well as Patrick Aurenche, Siegmund Brandt, Tancredi Carli, Pierre-Antoine Delsart, Yuri Dokshitzer, Steve Ellis, David d'Enterria, Michel Fontannaz, Peter Jacobs, Thomas Kluge, David Kosower, Bruce Knuteson, Peter Loch, Michelangelo Mangano, Arthur Moraes, Andreas Oehler, Klaus Rabbertz, Christof Roland, Philipp Schieferdecker, Torbjörn Sjöstrand, Peter Skands, George Sterman, Brock Tweedie, Monica Vazquez Acosta. I am also grateful to David Kosower and an anonymous reviewer for their detailed comments on this manuscript, and to Florent Fayette and Adam Falkowski for pointing out ambiguities and typographical errors.

References

1. A. Abulencia et al. (CDF II Collab.), Measurement of the inclusive jet cross section using the $k(t)$ algorithm in p anti-p collisions at $\sqrt{s} = 1.96$-TeV. Phys. Rev. Lett. **96**, 122001 (2006). hep-ex/0512062

2. V.M. Abazov et al. (D0 Collaboration), Measurement of the inclusive jet cross-section in $p\bar{p}$ collisions at $s^{1/2} = 1.96$-TeV. Phys. Rev. Lett. **101**, 062001 (2008). arXiv:0802.2400 [hep-ex]
3. C. Adloff et al. (H1 Collaboration), Measurement of inclusive jet cross-sections in photoproduction at HERA. Eur. Phys. J. C **29**, 497 (2003). arXiv:hep-ex/0302034
4. J. Breitweg et al. (ZEUS Collaboration), High $E(T)$ inclusive jet cross-sections in photoproduction at HERA. Eur. Phys. J. C **4**, 591 (1998). arXiv:hep-ex/9802012
5. S.M. Wang (CDF Collaboration, and D0 Collaboration), Search for supersymmetry at the Tevatron. arXiv:0705.2896 [hep-ex]
6. V.M. Abazov et al. (D0 Collaboration), Measurement of the top quark mass in final states with two leptons. Phys. Rev. D **80**, 092006 (2009). arXiv:0904.3195 [hep-ex]
7. T. Aaltonen et al. (The CDF Collaboration), Measurement of the top quark mass and $p\bar{p} \to t\bar{t}$ cross section in the all-hadronic mode with the CDFII detector. arXiv:1002.0365 [hep-ex]
8. F.D. Aaron et al. (H1 Collaboration), Jet production in ep collisions at high Q^2 and determination of α_s. Eur. Phys. J. C **65**, 363 (2010). arXiv:0904.3870 [hep-ex]
9. S. Chekanov et al. (ZEUS Collaboration), Inclusive jet cross sections in the Breit frame in neutral current deep inelastic scattering at HERA and determination of alpha(s). Phys. Lett. B **547**, 164 (2002). arXiv:hep-ex/0208037
10. J. Abdallah et al. (DELPHI Collaboration), Measurement of the energy dependence of hadronic jet rates and the strong coupling alpha(s) from the four-jet rate with the DELPHI detector at LEP. Eur. Phys. J. C **38**, 413 (2005). arXiv:hep-ex/0410071
11. G. Abbiendi et al. (OPAL Collaboration), Measurement of the strong coupling alpha(s) from four-jet observables in $e^+ e^-$ annihilation. Eur. Phys. J. C **47**, 295 (2006). arXiv:hep-ex/0601048
12. A. Heister et al. (ALEPH Collaboration), Measurements of the strong coupling constant and the QCD colour factors using four-jet observables from hadronic Z decays. Eur. Phys. J. C **27**, 1 (2003)
13. S. Catani, F. Krauss, R. Kuhn, B.R. Webber, QCD matrix elements + parton showers. J. High Energy Phys. **0111**, 063 (2001). arXiv:hep-ph/0109231
14. J. Alwall et al., Comparative study of various algorithms for the merging of parton showers and matrix elements in hadronic collisions. Eur. Phys. J. C **53**, 473 (2008). arXiv:0706.2569 [hep-ph]
15. G. Sterman, S. Weinberg, Jets from quantum chromodynamics. Phys. Rev. Lett. **39**, 1436 (1977)
16. G. Aad et al. (The ATLAS Collaboration), Expected performance of the ATLAS experiment—detector, trigger and physics. arXiv:0901.0512 [hep-ex]
17. G.L. Bayatian et al. (CMS Collaboration), CMS physics: Technical design report. CMS-TDR-008-1
18. J.M. Campbell, J.W. Huston, W.J. Stirling, Hard interactions of quarks and gluons: A primer for LHC physics. Rep. Prog. Phys. **70**, 89 (2007). arXiv:hep-ph/0611148
19. K. Hatakeyama, High et jet production. arXiv:0911.1580 [hep-ex]
20. Z.J. Ajaltouni et al., Proceedings of the workshop: HERA and the LHC workshop series on the implications of HERA for LHC physics. arXiv:0903.3861 [hep-ph]
21. G.C. Blazey et al., Run II jet physics. hep-ex/0005012
22. S.D. Ellis, J. Huston, K. Hatakeyama, P. Loch, M. Tonnesmann, Jets in hadron-hadron collisions. Prog. Part. Nucl. Phys. **60**, 484 (2008). arXiv:0712.2447 [hep-ph]
23. D. d'Enterria, Jet quenching in QCD matter: from RHIC to LHC. arXiv:0902.2488 [nucl-ex]
24. S. Salur (STAR Collaboration), First Direct Measurement of Jets in $\sqrt{s_{NN}} = 200$ GeV Heavy Ion Collisions by STAR. arXiv:0809.1609 [nucl-ex]
25. J.E. Huth et al., Toward a standardization of jet definitions. FNAL-C-90-249-E, published in the proceedings of the 1990 Summer Study on High Energy Physics, Research Directions for the Decade, Snowmass, Colorado, June 25–July 13, 1990
26. S.D. Ellis, Z. Kunszt, D.E. Soper, The one jet inclusive cross-section at order α_s^3. 1. Gluons only. Phys. Rev. D **40**, 2188 (1989)
27. S. Catani, Y.L. Dokshitzer, M. Olsson, G. Turnock, B.R. Webber, New clustering algorithm for multi—jet cross-sections in $e^+ e^-$ annihilation. Phys. Lett. B **269**, 432 (1991)
28. S. Catani, Y.L. Dokshitzer, M.H. Seymour, B.R. Webber, Longitudinally invariant $K(t)$ clustering algorithms for hadron hadron collisions. Nucl. Phys. B **406**, 187 (1993)
29. S.D. Ellis, D.E. Soper, Successive combination jet algorithm for hadron collisions. Phys. Rev. D **48**, 3160 (1993). hep-ph/9305266
30. Y.L. Dokshitzer, G.D. Leder, S. Moretti, B.R. Webber, Better jet clustering algorithms. J. High Energy Phys. **9708**, 001 (1997). hep-ph/9707323
31. M. Wobisch, T. Wengler, Hadronization corrections to jet cross sections in deep-inelastic. arXiv:hep-ph/9907280
32. M. Wobisch, Measurement and QCD analysis of jet cross sections in deep-inelastic positron proton collisions at $\sqrt{s} =$ 300-GeV. DESY-THESIS-2000-049
33. S.D. Ellis, Private communication to the OPAL Collaboration
34. D.E. Soper, H.-C. Yang, Private communication to the OPAL Collaboration
35. L.A. del Pozo, University of Cambridge Ph.D. thesis, RALT–002 (1993)
36. R. Akers et al. (OPAL Collaboration), QCD studies using a cone based jet finding algorithm for $e^+ e^-$ collisions at LEP. Z. Phys. C **63**, 197 (1994)
37. M. Cacciari, G.P. Salam, G. Soyez, The anti-k_t jet clustering algorithm. J. High Energy Phys. **0804**, 063 (2008). arXiv:0802.1189 [hep-ph]
38. C. Buttar et al., Standard Model Handles and Candles Working Group: Tools and Jets Summary Report. arXiv:0803.0678 [hep-ph]
39. G. Arnison et al. (UA1 Collaboration), Hadronic jet production at the cern proton–anti-proton collider. Phys. Lett. B **132**, 214 (1983)
40. F. Abe et al. (CDF Collaboration), The Topology of three jet events in $\bar{p}p$ collisions at $\sqrt{s} = 1.8$ TeV. Phys. Rev. D **45**, 1448 (1992)
41. M. Cacciari, G.P. Salam, G. Soyez, The catchment area of jets. J. High Energy Phys. **0804**, 005 (2008). arXiv:0802.1188 [hep-ph]
42. M.H. Seymour, C. Tevlin, A comparison of two different jet algorithms for the top mass reconstruction at the LHC. J. High Energy Phys. **0611**, 052 (2006). arXiv:hep-ph/0609100
43. M.H. Seymour, Jet shapes in hadron collisions: Higher orders, resummation and hadronization. Nucl. Phys. B **513**, 269 (1998). hep-ph/9707338
44. G.P. Salam, G. Soyez, A practical Seedless Infrared-Safe Cone jet algorithm. J. High Energy Phys. **0705**, 086 (2007). arXiv:0704.0292 [hep-ph]
45. M. Cacciari, G.P. Salam, G. Soyez, http://fastjet.fr/
46. P.A. Delsart, K. Geerlins, J. Huston, http://www.pa.msu.edu/~huston/SpartyJet/SpartyJet.html
47. T. Aaltonen et al. (CDF Collaboration), Measurement of the cross section for W-boson production in association with jets in $p\bar{p}$ collisions at $\sqrt{s} = 1.96$TeV. Phys. Rev. D **77**, 011108 (2008). arXiv:0711.4044 [hep-ex]
48. J. Campbell, R.K. Ellis, Next-to-leading order corrections to $W + 2$ jet and $Z + 2$ jet production at hadron colliders. Phys. Rev. D **65**, 113007 (2002). hep-ph/0202176

49. Z. Nagy, Three-jet cross sections in hadron hadron collisions at next-to-leading order. Phys. Rev. Lett. **88**, 122003 (2002). hep-ph/0110315
50. Z. Nagy, Next-to-leading order calculation of three-jet observables in hadron hadron collision. Phys. Rev. D **68**, 094002 (2003). hep-ph/0307268
51. C.F. Berger et al., Precise predictions for $W+3$ jet production at hadron colliders. arXiv:0902.2760 [hep-ph]
52. R.K. Ellis, K. Melnikov, G. Zanderighi, Generalized unitarity at work: first NLO QCD results for hadronic $W+3$ jet production. arXiv:0901.4101 [hep-ph]
53. R.K. Ellis, K. Melnikov, G. Zanderighi, $W+3$ jet production at the Tevatron. arXiv:0906.1445 [hep-ph]
54. S. Frixione, B.R. Webber, Matching NLO QCD computations and parton shower simulations. J. High Energy Phys. **0206**, 029 (2002). arXiv:hep-ph/0204244
55. P. Nason, G. Ridolfi, A positive-weight next-to-leading-order Monte Carlo for Z pair hadroproduction. J. High Energy Phys. **0608**, 077 (2006). arXiv:hep-ph/0606275
56. S.D. Ellis, J. Huston, M. Tonnesmann, On building better cone jet algorithms, in *Proc. of the APS/DPF/DPB Summer Study on the Future of Particle Physics (Snowmass 2001)*, ed. by N. Graf, p. P513. hep-ph/0111434
57. M.G. Albrow et al. (TeV4LHC QCD Working Group), Tevatron-for-LHC report of the QCD working group. arXiv:hep-ph/0610012
58. S. Moretti, L. Lonnblad, T. Sjostrand, New and old jet clustering algorithms for electron positron events. J. High Energy Phys. **9808**, 001 (1998). arXiv:hep-ph/9804296
59. T. Sjostrand, The lund Monte Carlo for $e^+ e^-$ jet physics. Comput. Phys. Commun. **28**, 229 (1983)
60. J. Dorfan, A cluster algorithm for the study of jets in high-energy physics. Z. Phys. C **7**, 349 (1981)
61. H.J. Daum, H. Meyer, J. Burger, A cluster algorithm for jet studies. Z. Phys. C **8**, 167 (1981)
62. K. Lanius, H.E. Roloff, H. Schiller, Selection of jets in multihadron final states produced by $e^+ e^-$ annihilation. Z. Phys. C **8**, 251 (1981)
63. A. Backer, Normicity, a general jet measure. Z. Phys. C **12**, 161 (1982)
64. W. Bartel et al. (JADE Collaboration), Experimental studies on multi-jet production in $e^+ e^-$ annihilation at petra energies. Z. Phys. C **33**, 23 (1986)
65. S. Bethke et al. (JADE Collaboration), Experimental investigation of the energy dependence of the strong coupling strength. Phys. Lett. B **213**, 235 (1988)
66. N. Brown, W.J. Stirling, Jet cross-sections at leading double logarithm in $e^+ e^-$ annihilation. Phys. Lett. B **252**, 657 (1990)
67. S. Catani, Jet topology and new jet counting algorithms. CERN-TH-6281-91, in *Erice 1991, Proceedings, QCD at 200-TeV*, p. 21
68. G. Leder, Jet fractions in $e^+ e^-$ annihilation. Nucl. Phys. B **497**, 334 (1997). hep-ph/9610552
69. A. Banfi, G.P. Salam, G. Zanderighi, Principles of general final-state resummation and automated implementation. J. High Energy Phys. **0503**, 073 (2005). arXiv:hep-ph/0407286
70. G. Dissertori, M. Schmelling, An improved theoretical prediction for the two jet rate in $e^+ e^-$ annihilation. Phys. Lett. B **361**, 167 (1995)
71. A. Banfi, G.P. Salam, G. Zanderighi, Semi-numerical resummation of event shapes. J. High Energy Phys. **0201**, 018 (2002). arXiv:hep-ph/0112156
72. S. Catani, B.R. Webber, Y.L. Dokshitzer, F. Fiorani, Average multiplicities in two and three jet $e^+ e^-$ annihilation events. Nucl. Phys. B **383**, 419 (1992)
73. S. Chekanov et al. (ZEUS Collaboration), Substructure dependence of jet cross sections at HERA and determination of alpha(s). Nucl. Phys. B **700**, 3 (2004). arXiv:hep-ex/0405065
74. S. Catani, Y.L. Dokshitzer, B.R. Webber, The K-perpendicular clustering algorithm for jets in deep inelastic scattering and hadron collisions. Phys. Lett. B **285**, 291 (1992)
75. M. Seymour, http://hepwww.rl.ac.uk/theory/seymour/ktclus/
76. J.M. Butterworth, J.P. Couchman, B.E. Cox, B.M. Waugh, KtJet: A C++ implementation of the $K(T)$ clustering algorithm. Comput. Phys. Commun. **153**, 85 (2003). hep-ph/0210022; http://hepforge.cedar.ac.uk/ktjet/
77. V.M. Abazov et al. (D0 Collaboration), The inclusive jet cross-section in p anti-p collisions at $\sqrt{s} = 1.8$-TeV using the $k(T)$ algorithm. Phys. Lett. B **525**, 211 (2002). hep-ex/0109041
78. V.M. Abazov et al. (D0 Collaboration), Subjet multiplicity of gluon and quark jets reconstructed with the k_T algorithm in $p\bar{p}$ collisions. Phys. Rev. D **65**, 052008 (2002). hep-ex/0108054
79. A. Abulencia et al. (CDF—Run II Collaboration), Measurement of the inclusive jet cross section using the k_{T} algorithm in $p\overline{p}$ collisions at $\sqrt{s} = 1.96$ TeV with the CDF II detector. Phys. Rev. D **75**, 092006 (2007). Erratum-ibid. D **75**, 119901 (2007). arXiv:hep-ex/0701051
80. S. Chekanov et al. (ZEUS Collaboration), Three- and four-jet final states in photoproduction at HERA. Nucl. Phys. B **792**, 1 (2008). arXiv:0707.3749 [hep-ex]
81. J. Breitweg et al. (ZEUS Collaboration), Dijet cross-sections in photoproduction at HERA. Eur. Phys. J. C **1**, 109 (1998). arXiv:hep-ex/9710018
82. A. Aktas et al. (H1 Collaboration), Measurement of inclusive jet production in deep-inelastic scattering at high Q^2 and determination of the strong coupling. Phys. Lett. B **653**, 134 (2007). arXiv:0706.3722 [hep-ex]
83. S. Chekanov et al. (ZEUS Collaboration), Jet-radius dependence of inclusive-jet cross sections in deep inelastic scattering at HERA. Phys. Lett. B **649**, 12 (2007). arXiv:hep-ex/0701039
84. V.S. Fadin, Double logarithmic asymptotics of the cross-sections of $e^+ e^-$ annihilation into quarks and gluons. Yad. Fiz. **37**, 408 (1983) (in Russian)
85. B.I. Ermolaev, V.S. Fadin, Log-log asymptotic form of exclusive cross-sections in quantum chromodynamics. JETP Lett. **33**, 269 (1981) [Pisma Z. Eksp. Teor. Fiz. **33**, 285 (1981)]
86. A.H. Mueller, On the multiplicity of hadrons in QCD jets. Phys. Lett. B **104**, 161 (1981)
87. Y.L. Dokshitzer, V.S. Fadin, V.A. Khoze, Double logs of perturbative QCD for parton jets and soft hadron spectra. Z. Phys. C **15**, 325 (1982)
88. A. Bassetto, M. Ciafaloni, G. Marchesini, Jet structure and infrared sensitive quantities in perturbative QCD. Phys. Rep. **100**, 201 (1983)
89. A.T. Pierce, B.R. Webber, Comparisons of new jet clustering algorithms for hadron hadron collisions. Phys. Rev. D **59**, 034014 (1999). arXiv:hep-ph/9807532
90. A. Banfi, G.P. Salam, G. Zanderighi, Infrared safe definition of jet flavour. Eur. Phys. J. C **47**, 113 (2006). arXiv:hep-ph/0601139
91. A. Banfi, G.P. Salam, G. Zanderighi, Accurate QCD predictions for heavy-quark jets at the Tevatron and LHC. J. High Energy Phys. **0707**, 026 (2007). arXiv:0704.2999 [hep-ph]
92. S. Hoeche, F. Krauss, S. Schumann, F. Siegert, QCD matrix elements and truncated showers. arXiv:0903.1219 [hep-ph]
93. D. Krohn, J. Thaler, L.T. Wang, Jets with variable R. arXiv:0903.0392 [hep-ph]
94. J.M. Butterworth, A.R. Davison, M. Rubin, G.P. Salam, Jet substructure as a new Higgs search channel at the LHC. Phys. Rev. Lett. **100**, 242001 (2008). arXiv:0802.2470 [hep-ph]
95. D. Krohn, J. Thaler, L.T. Wang, Jet trimming. arXiv:0912.1342 [hep-ph]

96. M. Cacciari, J. Rojo, G.P. Salam, G. Soyez, Quantifying the performance of jet definitions for kinematic reconstruction at the LHC. J. High Energy Phys. **0812**, 032 (2008). arXiv:0810.1304 [hep-ph]
97. S.D. Ellis, C.K. Vermilion, J.R. Walsh, Techniques for improved heavy particle searches with jet substructure. arXiv:0903.5081 [hep-ph]
98. S.D. Ellis, C.K. Vermilion, J.R. Walsh, Recombination algorithms and jet substructure: pruning as a tool for heavy particle searches. arXiv:0912.0033 [hep-ph]
99. L. Lonnblad, Ariadne version 4: a program for simulation of QCD cascades implementing the color dipole model. Comput. Phys. Commun. **71**, 15 (1992)
100. L. Lonnblad, Arclus: a new jet clustering algorithm inspired by the color dipole model. Z. Phys. C **58**, 471 (1993)
101. S. Chekanov, A new jet algorithm based on the k-means clustering for the reconstruction of heavy states from jets. hep-ph/0512027
102. H. Steinhaus, Sur la division des corp materiels en parties. Bull. Acad. Polon. Sci. **1**, 801 (1956)
103. L. Angelini et al., Jet analysis by deterministic annealing. Phys. Lett. B **545**, 315 (2002). hep-ph/0207032
104. L. Angelini et al., Deterministic annealing as a jet clustering algorithm in hadronic collisions. Phys. Lett. B **601**, 56 (2004). hep-ph/0407214
105. D.Y. Grigoriev, E. Jankowski, F.V. Tkachov, Towards a standard jet definition. Phys. Rev. Lett. **91**, 061801 (2003). hep-ph/0301185
106. D.Y. Grigoriev, E. Jankowski, F.V. Tkachov, Optimal jet finder. Comput. Phys. Commun. **155**, 42 (2003). hep-ph/0301226
107. I. Volobouev, http://projects.hepforge.org/fftjet/
108. I. Volobouev, FFTJet: a package for multiresolution particle jet reconstruction in the Fourier domain. arXiv:0907.0270 [hep-ex]
109. C.F. Berger et al., Snowmass 2001: Jet energy flow project, in *Proc. of the APS/DPF/DPB Summer Study on the Future of Particle Physics (Snowmass 2001)*, ed. by N. Graf, Snowmass, Colorado, 30 Jun–21 Jul 2001, pp. P512. arXiv:hep-ph/0202207
110. Y.S. Lai, B.A. Cole, Jet reconstruction in hadronic collisions by Gaussian filtering. arXiv:0806.1499 [nucl-ex]
111. T. Sjostrand, S. Mrenna, P. Skands, `Pythia` 6.4 physics and manual. J. High Energy Phys. **0605**, 026 (2006). arXiv:hep-ph/0603175
112. G. Marchesini, B.R. Webber, G. Abbiendi, I.G. Knowles, M.H. Seymour, L. Stanco, HERWIG: A Monte Carlo event generator for simulating hadron emission reactions with interfering gluons. Version 5.1–April 1991. Comput. Phys. Commun. **67**, 465 (1992)
113. G. Corcella et al., HERWIG 6: An event generator for hadron emission reactions with interfering gluons (including supersymmetric processes). J. High Energy Phys. **0101**, 010 (2001). hep-ph/0011363
114. T. Sjostrand, L. Lonnblad, S. Mrenna, P. Skands, PYTHIA 6.3: Physics and manual. arXiv:hep-ph/0308153
115. I.P. Lokhtin, A.M. Snigirev, A model of jet quenching in ultra-relativistic heavy ion collisions and high-$p(T)$ hadron spectra at RHIC. Eur. Phys. J. C **45**, 211 (2006). arXiv:hep-ph/0506189
116. I.P. Lokhtin, A.M. Snigirev, Simulation of jet quenching at RHIC and LHC. arXiv:hep-ph/0612109
117. C. Adler et al. (STAR Collaboration), Multiplicity distribution and spectra of negatively charged hadrons in Au Au collisions at $\sqrt{s_{NN}} = 130$-GeV. Phys. Rev. Lett. **87**, 112303 (2001). arXiv:nucl-ex/0106004
118. M.R. Anderberg, *Cluster Analysis for Applications*. Probability and Mathematical Statistics, vol. 19 (Academic Press, San Diego, 1973)
119. D. Eppstein, Fast hierarchical clustering and other applications of dynamic closest pairs. J. Exp. Algorithmics **5**, 1–23 (2000). cs.DS/9912014
120. J. Cardinal, D. Eppstein, Lazy algorithms for dynamic closest pair with arbitrary distance measures. Tech. Rep. 502, Univ. Libre de Bruxelles (2003)
121. M. Cacciari, G.P. Salam, Dispelling the N^3 myth for the $k(t)$ jet-finder. Phys. Lett. B **641**, 57 (2006). arXiv:hep-ph/0512210
122. G.L. Dirichlet, Uber die Reduktion der positiven quadratischen Formen mit drei unbestimmten ganzen Zahlen. J. Reine Angew. Math. **40**, 209 (1850)
123. G. Voronoi, Nouvelles applications des paramètres continus à la théorie des formes quadratiques. J. Reine Angew. Math. **133**, 97 (1908)
124. F. Aurenhammer, Voronoi diagrams—a survey of a fundamental geometric data structure. ACM Comput. Surv. **23**, 345 (1991)
125. A. Okabe, B. Boots, K. Sugihara, S.N. Chiu, *Spatial Tessellations—Concepts and Applications of Voronoi Diagrams*, 2nd edn. (Wiley, New York, 2000)
126. S. Fortune, A sweepline algorithm for Voronoi diagrams, in *Proceedings of the Second Annual Symposium on Computational Geometry*, p. 312 (1986)
127. O. Devillers, S. Meiser, M. Teillaud, Fully dynamic Delaunay triangulation in logarithmic expected time per operation. Comput. Geom.: Theory Appl. **2**, 55 (1992)
128. O. Devillers, On deletion in Delaunay triangulation. arXiv:cs.CG/9907023
129. A. Fabri et al., On the design of CGAL a computational geometry algorithms library. Softw. Pract. Exp. **30**, 1167 (2000)
130. J.-D. Boissonnat et al., Triangulations in CGAL. Comput. Geom. **22**, 5 (2001)
131. M. Cacciari, G.P. Salam, Jet clustering in particle physics, via a dynamic nearest neighbour graph implemented with CGAL. LPTHE-06-02, Unpublished note
132. T.M. Chan, Closest-point problems simpli on the RAM, in *Proc. 13rd ACM-SIAM Sympos. on Discrete Algorithms* (2002)
133. E.D. Demaine, J.S.B. Mitchell, J. O'Rourke, The Open Problems Project (problem 63). http://maven.smith.edu/~orourke/TOPP/P63.html
134. I. Volobouev, Presentation at MC4LHC meeting, CERN, July 2006
135. T. Sjöstrand, Private communication (2009)
136. S. Brandt, H.D. Dahmen, Axes and scalar measures of two-jet and three-jet events. Z. Phys. C **1**, 61 (1979)
137. The CMS Collaboration, Performance of jet algorithms in CMS. CMS-PAS-JME-07-03 (March 2008). http://cms.cern.ch/iCMS/jsp/openfile.jsp?tp=draft&files=AN2008_002_v3.pdf
138. B. Abbott, M. Bhattacharjee, D. Elvira, F. Nang, H. Weerts (for the D0 Collaboration), Fixed cone jet definitions in D0 and R(sep). FERMILAB-PUB-97-242-E
139. T. Aaltonen et al. (CDF Collaboration), Measurement of the inclusive jet cross section at the fermilab tevatron p-pbar collider using a cone-based jet algorithm. Phys. Rev. D **78**, 052006 (2008). arXiv:0807.2204 [hep-ex]
140. M. Furman, Study of a nonleading QCD correction to hadron calorimeter reactions. Nucl. Phys. B **197**, 413 (1982)
141. F. Aversa, P. Chiappetta, M. Greco, J.P. Guillet, QCD corrections to parton-parton scattering processes. Nucl. Phys. B **327**, 105 (1989)
142. F. Aversa, P. Chiappetta, M. Greco, J.P. Guillet, Jet production in hadronic collisions to $O(\alpha_s^3)$. Z. Phys. C **46**, 253 (1990)
143. J.P. Guillet, One jet $O(\alpha_s^3)$ cross-section: Mass dependence. Z. Phys. C **51**, 587 (1991)
144. B. Jager, M. Stratmann, W. Vogelsang, Single-inclusive jet production in polarized p p collisions at $O(\alpha_s^3)$. Phys. Rev. D **70**, 034010 (2004). arXiv:hep-ph/0404057

145. D. de Florian, W. Vogelsang, Resummed cross section for jet production at hadron colliders. Phys. Rev. D **76**, 074031 (2007). arXiv:0704.1677 [hep-ph]
146. N. Kidonakis, G. Sterman, Resummation for QCD hard scattering. Nucl. Phys. B **505**, 321 (1997). arXiv:hep-ph/9705234
147. N. Kidonakis, G. Oderda, G. Sterman, Threshold resummation for dijet cross sections. Nucl. Phys. B **525**, 299 (1998). arXiv:hep-ph/9801268
148. N. Kidonakis, G. Oderda, G. Sterman, Evolution of color exchange in QCD hard scattering. Nucl. Phys. B **531**, 365 (1998). arXiv:hep-ph/9803241
149. N. Kidonakis, J.F. Owens, Effects of higher-order threshold corrections in high-$E(T)$ jet production. Phys. Rev. D **63**, 054019 (2001.) arXiv:hep-ph/0007268
150. M. Dasgupta, L. Magnea, G.P. Salam, Non-perturbative QCD effects in jets at hadron colliders. J. High Energy Phys. **0802**, 055 (2008). arXiv:0712.3014 [hep-ph]
151. L.G. Almeida, S.J. Lee, G. Perez, G. Sterman, I. Sung, J. Virzi, Substructure of high-p_T Jets at the LHC. arXiv:0807.0234 [hep-ph]
152. L.G. Almeida, S.J. Lee, G. Perez, I. Sung, J. Virzi, Top jets at the LHC. arXiv:0810.0934 [hep-ph]
153. S. Catani, L. Trentadue, G. Turnock, B.R. Webber, Resummation of large logarithms in $e^+ e^-$ event shape distributions. Nucl. Phys. B **407**, 3 (1993)
154. S.J. Burby, E.W.N. Glover, Resumming the Light Hemisphere Mass and Narrow Jet Broadening distributions in e^+e^- annihilation. J. High Energy Phys. **0104**, 029 (2001). arXiv:hep-ph/0101226
155. M. Dasgupta, G.P. Salam, Resummation of non-global QCD observables. Phys. Lett. B **512**, 323 (2001). arXiv:hep-ph/0104277
156. M. Dasgupta, G.P. Salam, Resummed event-shape variables in DIS. J. High Energy Phys. **0208**, 032 (2002). arXiv:hep-ph/0208073
157. G. Oderda, G. Sterman, Energy and color flow in dijet rapidity gaps. Phys. Rev. Lett. **81**, 3591 (1998). arXiv:hep-ph/9806530
158. C.F. Berger, T. Kucs, G. Sterman, Energy flow in interjet radiation. Phys. Rev. D **65**, 094031 (2002). arXiv:hep-ph/0110004
159. R.B. Appleby, M.H. Seymour, Non-global logarithms in inter-jet energy flow with kt clustering requirement. J. High Energy Phys. **0212**, 063 (2002). arXiv:hep-ph/0211426
160. Y. Delenda, R. Appleby, M. Dasgupta, A. Banfi, On QCD resummation with $k(t)$ clustering. J. High Energy Phys. **0612**, 044 (2006). arXiv:hep-ph/0610242
161. M. Dasgupta, G.P. Salam, Accounting for coherence in interjet $E(t)$ flow: A case study. J. High Energy Phys. **0203**, 017 (2002). arXiv:hep-ph/0203009
162. A. Banfi, G. Marchesini, G. Smye, Away-from-jet energy flow. J. High Energy Phys. **0208**, 006 (2002). arXiv:hep-ph/0206076
163. A. Banfi, G.P. Salam, G. Zanderighi, Semi-numerical resummation of event shapes. J. High Energy Phys. **0201**, 018 (2002). hep-ph/0112156
164. S. Catani, Y.L. Dokshitzer, B.R. Webber, Average number of jets in deep inelastic scattering. Phys. Lett. B **322**, 263 (1994)
165. J.R. Forshaw, M.H. Seymour, Subjet rates in hadron collider jets. J. High Energy Phys. **9909**, 009 (1999). arXiv:hep-ph/9908307
166. W. Ochs, R.P. Ramos, Particle multiplicity in jets and sub-jets with jet axis from color current. Phys. Rev. D **78**, 034010 (2008). arXiv:0807.1082 [hep-ph]
167. G.P. Korchemsky, G. Sterman, Nonperturbative corrections in resummed cross-sections. Nucl. Phys. B **437**, 415 (1995). arXiv:hep-ph/9411211
168. Y.L. Dokshitzer, B.R. Webber, Calculation of power corrections to hadronic event shapes. Phys. Lett. B **352**, 451 (1995). arXiv:hep-ph/9504219
169. R. Akhoury, V.I. Zakharov, On the universality of the leading, $1/Q$ power corrections in QCD. Phys. Lett. B **357**, 646 (1995). arXiv:hep-ph/9504248
170. P. Ball, M. Beneke, V.M. Braun, Resummation of $(\beta_0\alpha_s)^n$ corrections in QCD: Techniques and applications to the tau hadronic width and the heavy quark pole mass. Nucl. Phys. B **452**, 563 (1995). arXiv:hep-ph/9502300
171. Y.L. Dokshitzer, G. Marchesini, B.R. Webber, Dispersive approach to power-behaved contributions in QCD hard processes. Nucl. Phys. B **469**, 93 (1996). arXiv:hep-ph/9512336
172. E. Gardi, Dressed gluon exponentiation. Nucl. Phys. B **622**, 365 (2002). arXiv:hep-ph/0108222
173. M. Beneke, Renormalons. Phys. Rep. **317**, 1 (1999). arXiv:hep-ph/9807443
174. A. Aktas et al. (H1 Collaboration), Measurement of event shape variables in deep-inelastic scattering at HERA. Eur. Phys. J. C **46**, 343 (2006). arXiv:hep-ex/0512014
175. S. Chekanov et al. (ZEUS Collaboration), Event shapes in deep inelastic scattering at HERA. Nucl. Phys. B **767**, 1 (2007). arXiv:hep-ex/0604032
176. M.L. Mangano, Hard scattering in high-energy QCD. arXiv:hep-ph/9911256
177. J.M. Butterworth, J.R. Forshaw, M.H. Seymour, Multiparton interactions in photoproduction at HERA. Z. Phys. C **72**, 637 (1996). arXiv:hep-ph/9601371
178. M. Dasgupta, G.P. Salam, Event shapes in e^+ e^- annihilation and deep inelastic scattering. J. Phys. G **30**, R143 (2004). arXiv:hep-ph/0312283
179. Y.L. Dokshitzer, A. Lucenti, G. Marchesini, G.P. Salam, Universality of $1/Q$ corrections to jet-shape observables rescued. Nucl. Phys. B **511**, 396 (1998). Erratum-ibid. B **593**, 729 (2001). arXiv:hep-ph/9707532
180. Y.L. Dokshitzer, A. Lucenti, G. Marchesini, G.P. Salam, On the universality of the Milan factor for $1/Q$ power corrections to jet shapes. J. High Energy Phys. **9805**, 003 (1998). arXiv:hep-ph/9802381
181. M. Dasgupta, B.R. Webber, Two-loop enhancement factor for $1/Q$ corrections to event shapes in deep inelastic scattering. J. High Energy Phys. **9810**, 001 (1998). arXiv:hep-ph/9809247
182. M. Dasgupta, L. Magnea, G. Smye, Universality of $1/Q$ corrections revisited. J. High Energy Phys. **9911**, 025 (1999). arXiv:hep-ph/9911316
183. G.E. Smye, On the $1/Q$ correction to the C-parameter at two loops. J. High Energy Phys. **0105**, 005 (2001). arXiv:hep-ph/0101323
184. M. Dasgupta, Y. Delenda, On the universality of hadronisation corrections to QCD jets. arXiv:0903.2187 [hep-ph]
185. ZEUS Collaboration, ZEUS-prel-09-16, http://www-zeus.desy.de/public_results/functiondb.php?id=ZEUS-prel-09-016
186. M. Campanelli, K. Geerlings, J. Huston, in *Standard Model Handles and Candles Working Group: Tools and Jets Summary Report*. arXiv:0803.0678 [hep-ph]
187. D. Benedetti et al., in *Les Houches Physics at TeV Colliders 2005, Standard Model, QCD, EW, and Higgs Working Group: Summary Report*. arXiv:hep-ph/0604120
188. M. Cacciari, J. Rojo, G.P. Salam, G. Soyez, in *Standard Model Handles and Candles Working Group: Tools and Jets Summary Report*. arXiv:0803.0678 [hep-ph]
189. V. Büge, M. Heinrich, B. Klein, K. Rabbertz, in *Standard Model Handles and Candles Working Group: Tools and Jets Summary Report*. arXiv:0803.0678 [hep-ph]
190. M. Cacciari, J. Rojo, G.P. Salam, G. Soyez, http://quality.fastjet.fr
191. M.M. Nojiri, M. Takeuchi, Study of the top reconstruction in top-partner events at the LHC. J. High Energy Phys. **0810**, 025 (2008). arXiv:0802.4142 [hep-ph]

192. D.E. Kaplan, K. Rehermann, M.D. Schwartz, B. Tweedie, Top tagging: a method for identifying boosted hadronically decaying top quarks. Phys. Rev. Lett. **101**, 142001 (2008). arXiv:0806.0848 [hep-ph]
193. M. Cacciari, G.P. Salam, Pileup subtraction using jet areas. Phys. Lett. B **659**, 119 (2008). arXiv:0707.1378 [hep-ph]
194. A. Abulencia et al. (CDF Run II Collaboration), Measurement of the inclusive jet cross section in $p\bar{p}$ interactions at $\sqrt{s} =$ 1.96-TeV using a cone-based jet algorithm. Phys. Rev. D **74**, 071103 (2006). arXiv:hep-ex/0512020
195. O.L. Kodolova et al., Study of $\gamma +$ Jet Channel in Heavy ion Collisions with CMS. CMS NOTE-1998/063. V. Gavrilov, A. Oulianov, O. Kodolova and I. Vardanian, Jet reconstruction with Pileup subtraction. CMS RN 2003/004
196. S.L. Blyth et al., A cone jet-finding algorithm for heavy-ion collisions at LHC energies. J. Phys. G **34**, 271 (2007). arXiv:nucl-ex/0609023
197. A.L. Fitzpatrick, J. Kaplan, L. Randall, L.T. Wang, Searching for the Kaluza–Klein graviton in bulk RS models. J. High Energy Phys. **0709**, 013 (2007). arXiv:hep-ph/0701150
198. W. Skiba, D. Tucker-Smith, Using jet mass to discover vector quarks at the LHC. Phys. Rev. D **75**, 115010 (2007). arXiv:hep-ph/0701247
199. B. Holdom, t' at the LHC: The physics of discovery. J. High Energy Phys. **0703**, 063 (2007). arXiv:hep-ph/0702037
200. B. Holdom, The heavy quark search at the LHC. J. High Energy Phys. **0708**, 069 (2007). arXiv:0705.1736 [hep-ph]
201. K. Agashe et al., LHC signals for warped electroweak neutral gauge bosons. Phys. Rev. D **76**, 115015 (2007). arXiv:0709.0007 [hep-ph]
202. M.H. Seymour, Searches for new particles using cone and cluster jet algorithms: a comparative study. Z. Phys. C **62**, 127 (1994)
203. J.M. Butterworth, B.E. Cox, J.R. Forshaw, $W\,W$ scattering at the LHC. Phys. Rev. D **65**, 096014 (2002). arXiv:hep-ph/0201098
204. J.M. Butterworth, J.R. Ellis, A.R. Raklev, Reconstructing sparticle mass spectra using hadronic decays. J. High Energy Phys. **0705**, 033 (2007). arXiv:hep-ph/0702150
205. ATLAS Collaboration, ATLAS sensitivity to the standard model Higgs in the HW and HZ channels at high transverse momenta. ATL-PHYS-PUB-2009-088
206. T. Plehn, G.P. Salam, M. Spannowsky, Fat jets for a light Higgs. arXiv:0910.5472 [hep-ph]
207. G.D. Kribs, A. Martin, T.S. Roy, M. Spannowsky, Discovering the Higgs boson in new physics events using jet substructure. arXiv:0912.4731 [hep-ph]
208. J.M. Butterworth, J.R. Ellis, A.R. Raklev, G.P. Salam, Discovering baryon-number violating neutralino decays at the LHC. arXiv:0906.0728 [hep-ph]
209. K. Agashe, A. Belyaev, T. Krupovnickas, G. Perez, J. Virzi, LHC signals from warped extra dimensions. Phys. Rev. D **77**, 015003 (2008). arXiv:hep-ph/0612015
210. B. Lillie, L. Randall, L.T. Wang, The bulk RS KK-gluon at the LHC. J. High Energy Phys. **0709**, 074 (2007). arXiv:hep-ph/0701166
211. R. Frederix, F. Maltoni, Top pair invariant mass distribution: a window on new physics. J. High Energy Phys. **0901**, 047 (2009). arXiv:0712.2355 [hep-ph]
212. U. Baur, L.H. Orr, Searching for t-bar t resonances at the large hadron collider. Phys. Rev. D **77**, 114001 (2008). arXiv:0803.1160 [hep-ph]
213. J. Thaler, L.T. Wang, Strategies to identify boosted tops. J. High Energy Phys. **0807**, 092 (2008). arXiv:0806.0023 [hep-ph]
214. G. Brooijmans, High pT hadronic top quark identification, Part I: Jet Mass and YSplitter. ATLAS note, ATL-COM-PHYS-2008-001
215. ATLAS Collaboration, Reconstruction of high mass tt resonances in the lepton + jets channel. ATL-PHYS-PUB-2009-081
216. CMS Collaboration, A Cambridge–Aachen (C–A) based jet algorithm for boosted top-jet tagging. CMS-PAS-JME-09-001